AFRL-AFOSR-UK-TR-2014-0052

Cross-Layer Resource Allocation for Wireless Visual Sensor Networks and Mobile Ad Hoc Networks

Lisimachos P. Kondi

UNIVERSITY OF IOANNINA RESEARCH COMMITTEE
UNIVERSITY OF IOANNINA CAMPUS
IOANNINA, 45110 GREECE

EOARD Grant 12-0001

Report Date: October 2014

Final Report for 19 October 2011 to 18 October 2014

Distribution Statement A: Approved for public release distribution is unlimited.

Air Force Research Laboratory
Air Force Office of Scientific Research
European Office of Aerospace Research and Development
Unit 4515 Box 14, APO AE 09421

REPORT DOCUMENTATION PAGE

Form Approved OMB No. 0704-0188

1. REPORT DATE *(DD-MM-YYYY)*	**2. REPORT TYPE**	**3. DATES COVERED** *(From – To)*
18 October 2014	Final Report	19 October 2011 – 18 October 2014

4. TITLE AND SUBTITLE

Cross-Layer Resource Allocation for Wireless Visual Sensor Networks and Mobile Ad Hoc Networks

5a. CONTRACT NUMBER

FA8655-12-1-0001

5b. GRANT NUMBER

Grant 12-0001

5c. PROGRAM ELEMENT NUMBER

61102F

6. AUTHOR(S)

Prof Lisimachos P. Kondi

5d. PROJECT NUMBER

5d. TASK NUMBER

5e. WORK UNIT NUMBER

7. PERFORMING ORGANIZATION NAME(S) AND ADDRESS(ES)
UNIVERSITY OF IOANNINA RESEARCH COMMITTEE
UNIVERSITY OF IOANNINA CAMPUS
IOANNINA, 45110 GREECE

8. PERFORMING ORGANIZATION REPORT NUMBER

N/A

9. SPONSORING/MONITORING AGENCY NAME(S) AND ADDRESS(ES)

EOARD
Unit 4515
APO AE 09421-4515

10. SPONSOR/MONITOR'S ACRONYM(S)

AFRL/AFOSR/IOE (EOARD)

11. SPONSOR/MONITOR'S REPORT NUMBER(S)

AFRL-AFOSR-UK-TR-2014-0052

12. DISTRIBUTION/AVAILABILITY STATEMENT

Distribution A: Approved for public release; distribution is unlimited.

13. SUPPLEMENTARY NOTES

14. ABSTRACT

In the context of this project, we worked on the development of a cross-layer resource management system over single hop and multihop Direct-Sequence Code Division Multiple Access (DS-CDMA) Visual Sensor Networks (VSNs). The target was the optimal determination and allocation of the source and channel coding rates and the power levels among the nodes of the considered network. For the efficient allocation of the nodes' transmission parameters, we applied various distortion-related criteria, drawing inspiration from game theory as well, and investigated fairness and efficiency under different perspectives for each of them. Computational intelligence optimization algorithms and reinforcement learning techniques were applied in order to solve the resulting optimization problems. All the solutions provided by the examined schemes were Pareto-optimal and thus, the choice about the most fair and efficient scheme is problem-dependent. Some of the approaches that were taken into account for further improving the end-to-end video distortion of a wireless multiple-access VSN included the time scheduling of transmitting nodes for interference mitigation, the optimal Instantaneous Decoding Refresh (IDR) frame placement during encoding, the content-based node prioritization, and the weighted bi-objective optimization for measuring the trade-off between video quality and consumed transmission power. The evaluation of all proposed approaches showed that enhanced end-to-end video quality can be achieved, by keeping power consumption at reasonable levels, when compared to the case of assigning equal values to the transmission parameters of all nodes constituting the network.

15. SUBJECT TERMS

EOARD, Nano particles, Photo-Acoustic Sensors

16. SECURITY CLASSIFICATION OF:			**17. LIMITATION OF ABSTRACT**	**18, NUMBER OF PAGES**	**19a. NAME OF RESPONSIBLE PERSON**
a. REPORT	**b. ABSTRACT**	**c. THIS PAGE**			James H Lawton, PhD
UNCLAS	UNCLAS	UNCLAS	SAR	112	**19b. TELEPHONE NUMBER** *(Include area code)* (703)696-5999

Grant Number: FA8655-12-1-0001

Cross-Layer Resource Allocation for Wireless Visual Sensor Networks and Mobile Ad Hoc Networks

Principal Investigator: Lisimachos P. Kondi

Period of Performance: October 19, 2011 to October 18, 2014

Contents

1 Abstract **4**

2 Summary **4**

3 Introduction **7**

4 Methods, Assumptions and Procedures **14**

4.1 A Study on Visual Sensor Network Cross-Layer Resource Allocation Using Quality-Based Criteria and Metaheuristic Optimization Algorithms 14

4.1.1 Wireless VSN 14

4.1.2 Optimization Criteria 18

4.1.3 Employed Optimization Algorithms 21

4.2 Game-Theoretic Solutions through Intelligent Optimization for Efficient Resource Management in Wireless Visual Sensor Networks 26

4.2.1 Background Information 26

4.2.2 Nash Bargaining Solution 27

4.3 Geometric Bargaining Approach for Optimizing Resource Allocation in Wireless Visual Sensor Networks 29

4.3.1 Game-Theory Basics 29

4.3.2 Kalai-Smorodinsky Bargaining Solution 30

4.3.3 Geometric Approach 30

4.3.4 Performance Evaluation 32

4.4 Fairness Issues in Resource Allocation Schemes for Wireless Visual Sensor Networks 34

4.5 Distortion-Aware Joint Scheduling and Resource Allocation for Wireless Video Transmission 36

4.6 Resource Allocation in Visual Sensor Networks Using a Reinforcement Learning Framework 37

4.7 Priority-Based Cross-Layer Optimization for Multihop DS-CDMA Visual Sensor Networks 40

4.8 Power-Aware QoS Enhancement in Multihop DS-CDMA Visual Sensor Networks . 43

4.9 A No-Reference Bitstream-Based Perceptual Model for Video Quality Estimation of Videos Affected by Coding Artifacts and Packet Losses 45

5 Results and Discussion **46**

5.1 A Study on Visual Sensor Network Cross-Layer Resource Allocation Using Quality-Based Criteria and Metaheuristic Optimization Algorithms 46

5.2 Game-Theoretic Solutions through Intelligent Optimization for Efficient Resource Management in Wireless Visual Sensor Networks 58

5.3 Geometric Bargaining Approach for Optimizing Resource Allocation in Wireless Visual Sensor Networks 76

5.4 Fairness Issues in Resource Allocation Schemes for Wireless Visual Sensor Networks 81

5.5 Distortion-Aware Joint Scheduling and Resource Allocation for Wireless Video Transmission 86

5.6 Resource Allocation in Visual Sensor Networks Using a Reinforcement Learning Framework 88

5.7 Priority-Based Cross-Layer Optimization for Multihop DS-CDMA Visual Sensor Networks 92

5.8 Power-Aware QoS Enhancement in Multihop DS-CDMA Visual Sensor Networks . 94

5.9 A No-Reference Bitstream-Based Perceptual Model for Video Quality Estimation of Videos Affected by Coding Artifacts and Packet Losses 100

6 Conclusions **102**

1 Abstract

In the context of this project, we worked on the development of a cross-layer resource management system over single hop and multihop Direct-Sequence Code Division Multiple Access (DS-CDMA) Visual Sensor Networks (VSNs). The target was the optimal determination and allocation of the source and channel coding rates and the power levels among the nodes of the considered network. For the efficient allocation of the nodes' transmission parameters, we applied various distortion-related criteria, drawing inspiration from game theory as well, and investigated fairness and efficiency under different perspectives for each of them. Computational intelligence optimization algorithms and reinforcement learning techniques were applied in order to solve the resulting optimization problems. All the solutions provided by the examined schemes were Pareto-optimal and thus, the choice about the most fair and efficient scheme is problem-dependent. Some of the approaches that were taken into account for further improving the end-to-end video distortion of a wireless multiple-access VSN included the time scheduling of transmitting nodes for interference mitigation, the optimal Instantaneous Decoding Refresh (IDR) frame placement during encoding, the content-based node prioritization, and the weighted bi-objective optimization for measuring the tradeoff between video quality and consumed transmission power. The evaluation of all proposed approaches showed that enhanced end-to-end video quality can be achieved, by keeping power consumption at reasonable levels, when compared to the case of assigning equal values to the transmission parameters of all nodes constituting the network.

2 Summary

Initially, in this work we considered two quality-based optimization criteria aiming at video distortion minimization. The first one, called the Minimized Average Distortion (MAD), minimizes the overall average video distortion of the network, neglecting fairness among the nodes. The second criterion, called the Minimized Maximum Distortion (MMD), minimizes the maximum distortion among all nodes of the network, promoting a rather unbiased treatment of the nodes. We employed the Particle Swarm Optimization (PSO) algorithm, while for comparison reasons, the performance of PSO was compared to that of the deterministic Active-Set (AS) algorithm. In addition, motivated by the promising performance of hybrid algorithms that combine population-based approaches with deterministic schemes, we also considered a hybrid algorithm that combines PSO with AS, denoted as HPSOAS (Hybrid PSO-AS). This work led to a publication in the Applied Soft Computing (ASOC) journal [1].

In addition, we developed optimization criteria based on the Nash Bargaining Solution (NBS). The objective was to ameliorate the quality of the videos received by the Centralized Control Unit (CCU) from each node, taking into account the fact that different nodes image videos with varying amounts of motion. Since the simultaneous maximization of the video qualities of all nodes is not possible, we employed the NBS in order to pinpoint one of the infinite Pareto-optimal solutions, based on the stipulation that the solution should satisfy four fairness axioms. Specifically, this solution promises fairness for all nodes, taking into account the amounts of motion in the videos they capture. In particular, we introduced two versions of the NBS that differ in the definition of the bargaining powers. The first variant (NNBS) treats equally each individual node of the VSN, while the second variant (CNBS) provides equal treatment to each class of nodes. The PSO algorithm was applied to the problem indicated by the NBS, under a cooperative game-theoretical perspective, and its performance was compared with the performance of three deterministic optimization methods, which were used as benchmarks, such as AS, Interior-Point (IP) and Trust-Region-Reflective (TRR). This work led to a publication in the Signal Processing: Image Communication (SPIC) journal [2].

Moreover, we applied the Kalai-Smorodinsky Bargaining Solution (KSBS) to non-convex utility spaces, in order to find a fair utility allocation resulting from the optimal determination of the nodes' transmission parameters. The KSBS was derived geometrically, directly from the graphical representations of the nodes' utility sets. In addition, we emphasized on the reliable evaluation of the KSBS performance, in the quality and resource domains. We applied a metric that captures both performance and fairness aspects for the KSBS evaluation in the quality domain, and we calculated the total consumed power relatively with the total utility gain for the KSBS evaluation in the resource domain. The performance of the KSBS criterion was examined in comparison with the NBS criterion. The KSBS results were also compared with results using two alternative schemes that maximize the total system utility achieved by all nodes of the network. The first scheme calculates an *unweighted* version of the total system utility and is called the Maximize Total Utility (MTU) criterion, while the second scheme calculates a *weighted* version of the overall system utility, and is called the weighted Maximize Total Utility (w.MTU). This work led to a publication in the Circuits and Systems for Video Technology (CSVT) journal [3].

In fact, all of the aforementioned criteria were able to provide a Pareto–optimal solution, meaning that there is no other solution that is simultaneously preferred by all nodes. Thus, it is not clear which scheme results in the best resource allocation for the whole network. To handle the resulting tradeoffs, we examined four metrics that investigate fairness and efficiency under different perspectives. Specifically, we applied a metric that considers both fairness and performance issues, and another metric that measures the "equality" of a resource allocation (equal utilities for the nodes). The third metric computes the total system utility, while the last metric computes the total power consumption of the nodes. This work led to a publication presented at the SPIE-IS&T Electronic Imaging conference [4].

Since the performance of DS-CDMA based systems highly depend on the interference caused by multiple transmissions, interference reduction may result by using time scheduling of the transmitting nodes and by allocating accordingly the nodes' transmission parameters. A study on the intra-cell scheduling and resource allocation for wireless video transmission in a hybrid DS-CDMA over a Time Division Multiple Access (TDMA) network, examined the scenario, where a subset of the network nodes are able to simultaneously transmit (at the same time slot). The key issue was to jointly select the subset of the nodes for transmission per time slot, and to allocate the available resources so that a function of the end–to–end video distortion of each node over a time frame is minimized. Therefore, we formulated the scheduling and the resource allocation as a joint end–to–end video quality–driven optimization problem, by implementing an approach, which considered the optimality of the solution over a specific number of time slots (time frame). This study resulted in a publication presented at the European SIgnal Processing COnference (EUSIPCO) [5].

Additionally, in an effort to ameliorate further the quality of the videos transmitted by the nodes, we dealt with the optimal IDR-frame placement during the encoding process, based on the motion level included in each video sequence, jointly with adjustment of the nodes' transmission parameters. Three optimization criteria that optimize a different objective function of the video qualities of the nodes (MAD, NBS, MTU) were used and the resulting optimization problems were tackled using a Reinforcement Learning (RL) strategy that promises efficient exploration and exploitation of the parameters' space. This work led to a publication presented at the Digital Signal Processing (DSP) conference [6].

Furthermore, we also worked on the extension of the cross-layer resource management scheme to the case of multihop VSNs. Multihop is required when the distance from the node (camera) to the CCU is so great that one-hop communication is not possible and an intermediate node is required in order to relay the data. Two priority-based criteria that allocate the resources with respect to the motion level of the recorded video scenes were proposed and compared. The w.NBS criterion maximizes the distortion–related Nash product, by using motion–based bargaining powers, while the Minimization of the Weighted Aggregation of Distortions (MWAD) criterion minimizes the weighted aggregation of the expected end–to–end video distortions, by using motion–based weights. Also, for the sake of comparison, an NBS-based scheme that considers equal bargaining powers for all nodes (e.NBS) was also explored. This work led to a publication presented at the International Conference on Image Processing (ICIP) [7].

In the same context of a multihop DS-CDMA VSN, we proposed a joint optimization scheme that allocates the available resources among the nodes with respect to the imposed constraints, in order to achieve the best possible video quality at the receiver, while consuming the least possible transmission power. Accordingly, we formulated a weighted bi-objective optimization problem and studied the tradeoff between video quality and consumed transmission power. In this bi–objective problem formulation, we used weighting factors that regulate the tradeoff between these two objectives. Furthermore, we defined different weights for the aggregation function of the video distortion of the source nodes that achieve to favor specific nodes according to the assigned weights. This research resulted in a publication presented at the Digital Signal Processing (DSP) conference [8].

Another topic that triggered our interest was that of Video Quality Assessment (VQA), without using the original video as a reference. Specifically, we proposed a No-Reference (NR) model for estimating the quality of H.264/Advanced Video Coding (AVC) video sequences, affected by both compression artifacts and packet losses. A large number of quality-relevant features were extracted from the impaired bitstream, without the need of decoding it first. The feature observations were given as input to the Least Absolute Shrinkage and Selection Operator (LASSO) regression method, in order for the latter to indicate those features that have the strongest effects towards video quality, and produce video quality estimates, at the same time. This study resulted in a publication, which will be presented at the SPIE-IS&T Electronic Imaging conference [9].

3 Introduction

Wireless sensor networks have constituted a very active research topic in computer science and telecommunications over the past few years. Initially, such networks were mainly concerned with the transmission of unidimensional signals (e.g., temperature, sound etc). Nowadays, their applications have been expanded to the transmission of visual data, such as images or videos. This type of wireless sensor network that conveys visual data is the well-known Visual Sensor Network (VSN).

In VSNs, each node is equipped with a camera for imaging different fields of view and detecting events of interest. VSNs support a plethora of applications, ranging from security and teleconference systems to environmental monitoring. In our research, we considered a Direct-Sequence Code Division Multiple Access (DS-CDMA) VSN, where the sensor nodes record scenes with varying motion levels, which is a common approach in real-time VSN applications. All the nodes of the network communicate directly with a Centralized Control Unit (CCU) and they exchange information in order to achieve the ideal tradeoff between the transmitted video quality and energy consumption.

Each sensor node has a bit rate that can be used for both source coding and channel coding, while it also has an amount of power necessary for sensing, processing, and transmission of the captured data. Hence, the source coding rate, channel coding rate, and power constitute the transmission parameters of each node. Naturally, each node compresses the captured data at a different source coding rate, according to the detected amount of motion in each scene. Thus, channel coding rate shall be different for each node. Under a total bit rate constraint, a higher source coding rate results in a lower channel coding rate, and vice versa. Consequently, higher levels of power are required for data transmission due to the lower protection from channel errors. On one hand, transmission power should be adequately high to permit data transmission and maintain the quality of the video reception, while on the other hand, it needs to be adequately low in order to prolong battery lifetime, keep interference at low levels among nodes, and efficiently exploit channel capacity, resulting in high system Quality of Service (QoS).

We proposed a cross-layer multi-node optimization design that accounts for the overall system performance through all network layers. Particularly, this scheme is responsible for the optimal determination of the source coding rates, channel coding rates, and power levels, at the application layer, data link layer, and physical layer, respectively. The layer collaboration is coordinated by the CCU, which undertakes to communicate with all nodes in order to request changes in transmission parameters, according to their unique, content-aware needs for resources. Figure 1 gives an insight of a wireless VSN with two diverse video priorities.

In order to optimally and jointly allocate system resources to all nodes, we considered two quality-based optimization criteria aiming at video distortion minimization. The first one, called the Minimized Average Distortion (MAD), minimizes the overall average video distortion of the network, neglecting fairness among the nodes. The second criterion, called the Minimized Maximum Distortion (MMD), minimizes the maximum distortion among all nodes of the network, promoting a rather unbiased treatment of the nodes. For both criteria, we required that the total

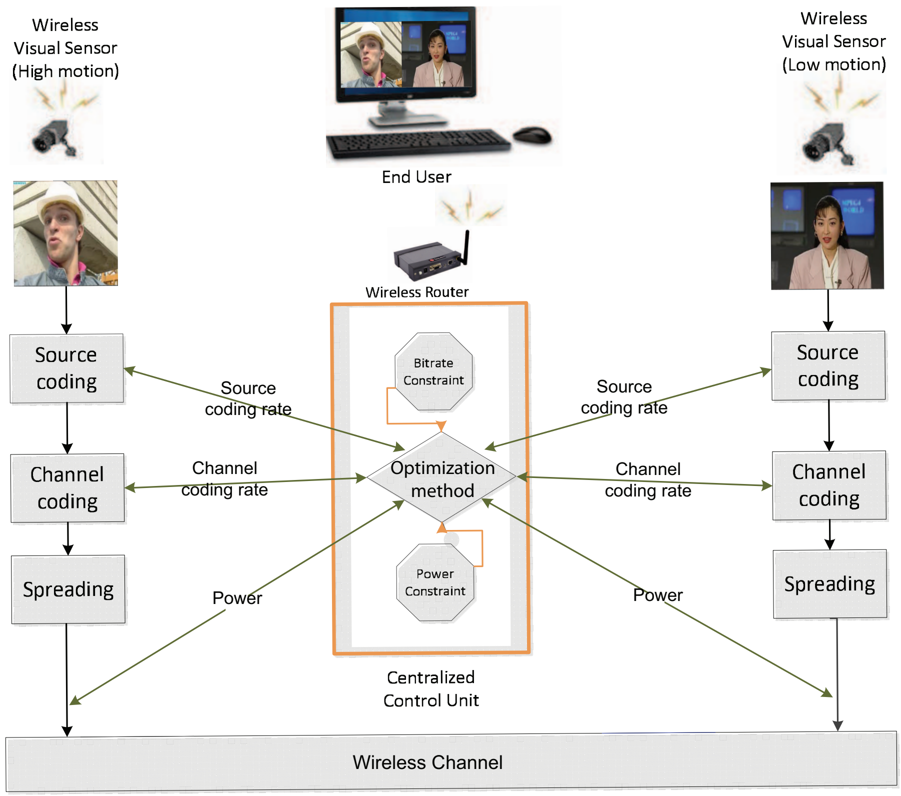

Figure 1: A wireless VSN with two diverse video priorities.

bit rate is identical for all nodes.

Additionally, we applied cooperative game theory, by using the Nash Bargaining Solution (NBS). The objective was to ameliorate the quality of the videos received by the CCU from each node, taking into account the fact that different nodes image videos with varying amounts of motion. Since the simultaneous maximization of the video qualities of all nodes is not possible, we employed the NBS in order to pinpoint one of the infinite Pareto-optimal solutions, based on the stipulation that the solution should satisfy four fairness axioms. Specifically, this solution promises fairness for all nodes, taking into account the amounts of motion in the videos they capture.

Driven by the fact that in a considered game, users' collaboration promotes improved outcomes favorable for all players participating in the game, for the NBS, we took careful treatment to the optimal setting of the disagreement point (dp), which is the vector of minimum utilities that each node expects by joining the game, without cooperating with the other nodes. Particularly, the disagreement point was set by the system designer, after experimentation on various values, in order to find that value that behaves equally fairly to each node and do not favor more some specific nodes. Therefore, it did not correspond to the Nash equilibrium.

Furthermore, we introduced two versions of the NBS that differ in the definition of the bargaining powers. The first variant (NNBS) treats equally each individual node of the VSN, while the second variant (CNBS) provides equal treatment to each class of nodes. The proposed optimization schemes can be used for any wireless VSN with a centralized topology that uses DS-CDMA for data transmission. They keep low computational complexity, especially after the assumption of node clustering, based on the amounts of the detected motion in the videos recorded by the nodes. Given this assumption, fewer parameters need to be estimated and thus, less time is required for their computation. Additionally, the specific schemes not only provide Pareto-optimal solutions, but also guarantee fairness for all nodes of the VSN, as their fairness axioms state. Practically, these schemes were tested for diverse parameter settings, while the results from both NBS approaches were assessed in comparison with the results from the MAD and MMD criteria.

In the same context of game theory, we applied the Kalai-Smorodinsky Bargaining Solution (KSBS) to non-convex utility spaces, in order to find a fair utility allocation resulting from the optimal determination of the nodes' transmission parameters, considering a number of assumptions and constraints. The KSBS results were compared with the NBS results, as well as with the results using two alternative schemes that maximize the total system utility achieved by all nodes of the network. The first scheme calculates an *unweighted* version of the total system utility and is called the Maximize Total Utility (MTU) criterion [10]. Additionally, the second scheme we compared with the KSBS results calculates a *weighted* version of the overall system utility, and is called the *weighted* Maximize Total Utility (w.MTU) [11]. Moreover, we engaged in an effort to reliably evaluate the KSBS performance, in the quality and resource domains. For the KSBS performance evaluation in the quality domain, we employed the Performance to Fairness (PF) metric [12], while in the resource domain, we estimated the total power consumption, cumulatively for all nodes.

More emphasis on the fairness and efficiency evaluation of the employed resource allocation schemes was given in [4]. Since an ideal scheme offers high amounts of total utility cumulatively for all nodes, behaves equally fairly to all of them by assigning similar utilities, and also consumes low amounts of power for all nodes, for the results evaluation obtained from all optimization schemes, we investigated four different fairness notions. Firstly, we applied the PF metric that captures both performance and fairness issues, assuming that the total utility varies per scheme. Secondly, we computed the Jain's fairness index [13] in order to investigate the "equality" of the resource allocations achieved by each considered scheme. Thirdly, we calculated the overall gained utility cumulatively for all nodes and fourthly, we measured the total power required by all nodes of each considered scheme.

All of the aforementioned criteria (MAD, MMD, NNBS, CNBS, KSBS, MTU, w.MTU) were applied to mixed-integer optimization problems. We considered continuous (and bounded) power levels; the source coding rates retained discrete values, since channel coding rates could take values only within a finite discrete set [14]. Clearly, allowing power levels to take values from a continuous set offers flexibility to the CCU to perform better management of the nodes' transmission parameters, achieving in this way better end-to-end video quality for each node. In particular, for all schemes except from the KSBS, we employed the Particle Swarm Optimization (PSO) algorithm [15], which is a computational intelligence approach that draws inspiration from social dynamics. The KSBS was derived geometrically, by following an innovative approach, directly from the graphical representations of the nodes' utility sets.

In [1], for comparison reasons, the performance of PSO was compared to that of the deterministic Active-Set (AS) algorithm [16, 17, 18]. In addition, motivated by the promising performance of hybrid algorithms that combine population-based approaches with deterministic schemes (often called *memetic algorithms*) [19], we also considered a hybrid algorithm that combines PSO with AS. The new algorithm, henceforth denoted as HPSOAS (Hybrid PSO-AS), aims at exploiting the benefits of both PSO and AS, thereby increasing efficiency. Similarly, in [2] the performance of PSO was compared with the performance of two more deterministic optimization methods, which were used as benchmarks, such as Interior-Point (IP) [20, 21] and Trust-Region-Reflective (TRR) [22, 23], besides AS.

A major issue in multi-access wireless VSNs, such as DS-CDMA, is the interference among the transmitting nodes. Namely, each node's transmission causes interference to the other nodes' video transmissions, resulting in video quality degradation at the receiver. In most cases, due to the different rate-distortion characteristics of each recorded video, each node has different resource requirements. In order to reduce the effects of the interference caused by the simultaneous video transmissions of the neighboring visual sensors, we need to establish a joint network resource allocation aiming at the enhancement of the global video quality. Another key challenge in DS-CDMA systems is to restrict the number of codes that are used for spreading. Even if the spreading codes used are orthogonal to each other, transmissions from one node cause interference to the other nodes. Hence, using scheduling helps reduce the number of required spreading codes and, consequently, helps reduce interference.

In our published work in [5], we focused on achieving high end-to-end video quality on a hybrid DS-CDMA Time Division Multiple Access (TDMA) network. To this end, we needed to reduce the effects of the interference caused by the simultaneous transmissions of the neighboring nodes. Therefore, we formulated the scheduling and the resource allocation as a joint end-to-end video quality-driven optimization problem. We implemented an approach, which considers the optimality of the solution over a specific number of time slots (time frame).

Whereas joint source and channel coding, as well as energy consumption minimization have been the main objectives in wireless VSN research [24, 25, 26, 27, 28], a literature review demonstrates that little evidence is available for the investigation of efficient coding techniques by applying adaptive Group of Pictures (GoP) length, at the same time. This latter approach aims at the enhancement of video resiliency to channel errors during wireless transmissions. The works presented in [29] and [30] proposed GoP structures adaptive to video content, without addressing resource allocation issues, at the same time.

The H.264/AVC video coding standard defines three frame types for video coding: intra frames (IDR, I), predictive frames (P) and bidirectionally predictive frames (B). Intra frames are coded without reference to other frames, while the difference between P-frames and B-frames is the number of reference frames they are allowed to use for coding. An Instantaneous Decoding Refresh (IDR) frame is a regular I-frame with the constraint that pictures appearing after it in the bitstream cannot use the pictures appearing before it as references. A GoP, which is a group of successive pictures within a coded video stream, always begins with an IDR-frame, and therefore the propagation of any errors within the GoP structure is stopped by the next IDR-frame.

The aim of our published work in [6] was twofold. Firstly, it studied the cross-layer resource allocation problem among the nodes of a wireless VSN and secondly, it dealt with the optimal IDR-frame placement during the encoding process, based on the motion level included in each video sequence. Due to the high problem's dimensionality of this work, the use of the brute-force search algorithm was rather impractical. Hence, this work abandoned the traditional Exhaustive Search (ES) algorithm [24, 25], and enjoyed the benefits of other innovative optimization methods extracted from the area of Reinforcement Learning (RL) [31].

A significant contribution of the work in [6] was the incorporation of an RL scheme in the resource allocation problem, which allowed the controller to make optimal decisions in unknown environments with very large or continuous state spaces. Specifically, in [6] we used the tabular SARSA algorithm, which is a model-free on-policy algorithm that belongs in the family of Temporal Difference (TD) algorithms [31]. The resource allocation problem of that work was modeled appropriately as a Markov Decision Process (MDP) [32]. The particular approach exploits the received raw experience, discovering the optimal combination of the nodes' transmission parameters in a more efficient way. Roughly speaking, SARSA constructs a map that allows us to explore the best parameters with the minimum effort, starting from any randomly selected parameters' combination. Last but not least, the specific RL approach gives the opportunity for the proposed scheme to be used in an online mode.

Since the transmission range of a sensor is limited, the recorded video sequences may need to be transmitted using relay nodes until they reach the CCU via a multihop path. An example of a two-hop wireless VSN is depicted in Fig. 2. In addition, a node's transmissions cause interference to other transmitting nodes within its transmission range, leading to degradation of the quality of the received videos. Moreover, the nodes may record scenes with different amounts of motion, so their resource requirements are different. Due to all these factors, resources (transmission power, source coding rate, channel coding rate) have to be optimally allocated using a quality-aware joint strategy, in order to maintain the end-to-end distortion at a low level for all nodes.

Our work presented in [7] proposed a cross–layer optimization scheme across the physical, network and application layer to achieve optimal video transmission over multihop DS–CDMA wireless VSNs. It moved beyond the state-of-the-art, since along with the problem of efficiently allocating the transmission power, we appropriately assigned the source coding rate and the channel coding rate to each visual sensor, while at the same time we determined the transmission power and the channel coding rate for each relay node. Furthermore, the optimization was quality-driven, i.e., the objective was to optimize a function of the received video qualities for each visual sensor, as opposed to optimizing network parameters such as bit error rate, throughput, etc. We introduced a novel priority-based criterion, which aims at minimizing the weighted aggregation of the expected end-to-end distortion of all videos. The weights were defined with the purpose of assigning a different priority to the transmitted video of each source node. The priorities reflected the requirements for the delivered video quality, namely the higher the priority of a source node, the higher its requirement for video quality.

Instead of explicitly optimizing network-related parameters, such as bit error rate or throughput, the work in [8] analyzed an optimization scheme, which intended to maximize the delivered video quality in terms of Peak Signal-to-Noise Ratio (PSNR), under the network's power con-

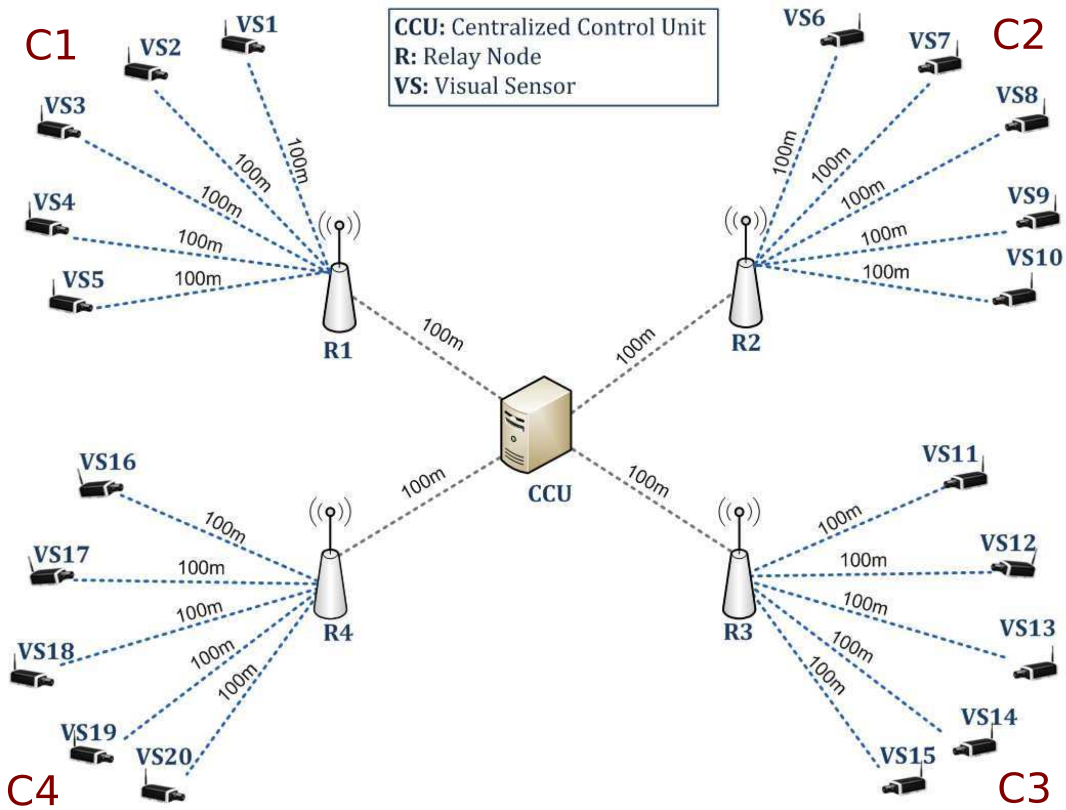

Figure 2: Example of a wireless VSN topology with two hops.

straints. Particularly, the network resources (transmission power, source and channel coding rates) had to be optimally allocated to the source and relay nodes using a quality-aware strategy, in order to maintain the end-to-end distortion at a low level for all source nodes. Moreover, power control was dictated by the battery-powered sensors.

The paper in [8] built on the concept introduced in our previous work [7] and moved beyond by jointly considering the end-to-end video quality enhancement, along with the power control. For the assignment of the available resources, a compromise between two aspects was essential: on the one hand, the power consumption had to be minimized in order to prolong the wireless VSN's lifespan and simultaneously reduce the interference among the transmitted signals; on the other hand, the distortion of the delivered video sequences had to be minimized as well, so that the QoS requirements of an application are satisfied. Therefore, we proposed a bi-objective method that jointly allocates the transmission power to the source and relay nodes, the source coding rates to the source nodes, and the channel coding rates to all nodes.

As video communications become increasingly popular, Video Quality Assessment (VQA) gains more and more the attention of the researchers. It is generally admitted that the human observer is the most reliable source for VQA. However, the collection of video subjective scores implicates a series of constraints. In subjective quality assessment tests, a number of human subjects are required to rate the video quality of the presented content. Such tests have to be carefully designed and performed and require a significant number of viewers available to perform the specific task [33]. An alternative approach to subjective tests is crowdsourcing, where the testing procedure is conducted through the Internet. By following this method, one can access a wider range of evaluators, while keeping the financial cost low and obtaining results similar to those of lab-based subjective tests. Even in such a case, these tests are time-consuming and cannot be used in real-time applications.

In order to avoid subjective VQA tests, many modern methods for perceptual quality assessment have been developed and can be grouped into three categories. Full-Reference (FR) methods have access to both the original and impaired videos, and they are mostly suitable for offline applications, due to their dependence on the original video. Reduced-Reference (RR) methods use only partial information from the original video, which is transmitted to the receiver either using an ancillary channel or by watermarking. However, the cost of maintaining an ancillary channel may be high, while such methods may be unable to meet the requirements of quality estimation in the event of a failure in information delivery. No-Reference (NR) methods have access only to the impaired video, and thus, they are the most broadly applicable in real-time applications, though quality estimation with limited available input information can be challenging.

In general, degradation of perceptual video quality can incur due to lossy video encoding and transmission losses. Lossy encoding methods are applied to video sequences in order to reduce the bit rate required for storage and/or transmission, while network congestion may result in packet losses with visible impairments on the decoded video. Therefore, there is the need for the development of a perceptual video quality model able to estimate possible video degradations due to both sources of distortion.

The work presented in [9] moved beyond the works existing in the literature and proposed a NR model for predicting the quality of H.264/AVC video sequences, affected by both compression artifacts and packet losses. The concept of this article was based on the extraction of a large set of quality-relevant features from the impaired bitstream. The extracted features represented virtually all of the relevant features proposed in the literature, aiming at capturing the impact of various distortion types on perceptual quality. The proposed set of features as a whole was never used before and even some features were firstly proposed in [9]. The feature observations were given as input to the Least Absolute Shrinkage and Selection Operator (LASSO) regression method, in order for the latter to indicate those features that have the strongest effects towards video quality. To the best of our knowledge, LASSO regression was applied for the first time to evaluate the significance of the features in building a NR model, as well as to produce video quality predictions. Our proposed method was validated with Mean Opinion Score (MOS), the Structural Similarity Index (SSIM) [34], and the Video Quality Metric (VQM) [35].

4 Methods, Assumptions and Procedures

4.1 A Study on Visual Sensor Network Cross-Layer Resource Allocation Using Quality-Based Criteria and Metaheuristic Optimization Algorithms

4.1.1 Wireless VSN

1) Video Compression

Video compression is essential in communications due to limitations in the bandwidth of the communication channel. Different video sequences have different bit rate requirements for their compression. Generally, these requirements depend on the amount of motion in the video sequence. Clearly, video sequences with less motion can be source encoded at a lower bit rate while still maintaining good perceptual quality. On the other hand, video sequences that contain intense motion activity shall be compressed at a higher bit rate in order to avoid significant degradation of the video quality.

Thus, assuming that the total bit rate is fixed, if a node needs a higher source coding rate, a lower percentage of the total bit rate is assigned to channel coding for error correction. Hence, in order to keep the Bit Error Rate (BER) at acceptable levels, the transmission power must be increased. In our research, we assumed that each node has the power required for video transmission over the VSN. Inevitably, the energy consumed for data transmission leads to shortening of the battery life and, due to the nature of DS-CDMA, to increased interference imposed to the other nodes of the network.

The CCU at the network layer plays the role of the coordinator of the overall process of resource allocation. Specifically, it communicates directly with each node, performing source and channel decoding so as to receive the transmitted video sequences. Depending on the amount of motion detected in each video sequence, the central server can request from the nodes to properly adjust their transmission parameters, namely the source coding rate, channel coding rate, and power levels. For instance, if the CCU considers that a node is imaging scenes of great interest, it tries to maximize the picture quality of the specific video by appropriately adjusting its transmission parameters.

We employed the H.264/AVC video coding standard to compress the video sequences imaged by the nodes, using the High profile for 4:2:0 color format video. This standard is targeted at many applications such as video telephony, storage, broadcast, and streaming [36]. The coded video data is organized in Network Abstraction Layer (NAL) units, which are packets containing an integer number of bytes. These units are grouped into Video Coding Layer (VCL) NAL units and non-VCL NAL units. The VCL NAL units contain the data that represents the values of the pixels in the video pictures, while non-VCL NAL units contain parameter sets and supplemental enhancement information [37]. Concerning the H.264/AVC High profile for the aforementioned color format, it has proved to be extremely efficient in coding, taking into consideration the available coding tools for the encoder [36].

2) Channel Coding

Channel coding is used to increase the communication channel reliability by increasing resistance to channel errors. Specifically, it adds redundancy in the video bitstream, unlike source coding, which intends to represent data with the smallest possible number of bits. In our paper, an adaptive Forward Error Correction (FEC) scheme using Rate Compatible Punctured Convolutional (RCPC) codes is utilized for channel coding [14]. These are families of codes with different rates, which can be decoded by the same Viterbi decoder. However, other channel coding schemes can also be used.

The use of RCPC codes allows the use of Viterbi's upper bounds on the bit error probability. Thus, for the bit error probability P_b, it holds that [14],

$$P_\mathrm{b} \leqslant \frac{1}{P} \sum_{d=d_\mathrm{free}}^{\infty} c_d P_d, \tag{1}$$

where P is the period of the code; d_free is the free distance of the code; c_d is the information error weight; and P_d is the probability that the wrong path at distance d is selected.

Let us assume that information is sent over a channel subjected to Additive White Gaussian Noise (AWGN). Also, let Binary Phase Shift Keying (BPSK) be the employed modulation scheme. Then, the probability P_d becomes [14],

$$P_d = \frac{1}{2} \operatorname{erfc}\left(\sqrt{\frac{dR_\mathrm{c}E_k}{N_0}}\right), \tag{2}$$

where,

$$\operatorname{erfc}(x) = \frac{2}{\sqrt{\pi}} \int_x^{\infty} \exp\left(-t^2\right) dt, \tag{3}$$

is the *complementary error function*; R_c is the channel coding rate; and E_k/N_0 is the energy per bit to Multiple Access Interference (MAI) ratio. The index k denotes the corresponding node of the network.

3) Direct-Sequence Code Division Multiple Access

DS-CDMA is the wireless VSN access method that we adopted in our current study. This method allows all nodes to transmit over the same channel, sharing the same bandwidth. Furthermore, since all nodes transmit over the same channel, transmissions are affected by generated interference from the other nodes, mainly due to non-orthogonal spreading codes, possible asynchronous transmissions, and multi-path fading. The target is to limit the interference as much as possible, in order to ameliorate the video quality, retain low power consumption, and achieve the effective exploitation of the system's capacity, without affecting the integrity of the data transmission procedure.

After source and channel coding, each data signal is assigned a spreading code, usually orthogonal or pseudo-random to the codes assigned to the other signals, such that the interference between two signals is minimized. In order to transmit a single bit, a node actually transmits L

chips, where L is the spreading code length. Usually, the *chip rate* (number of transmitted chips per second) is identical for all nodes. We assume that the spreading code length is identical for all nodes. Thus, a constraint on the chip rate corresponds to a constraint on the bit rate. DS-CDMA systems are usually interference-limited systems and therefore, it is common for the thermal noise and background noise to be neglected. The power level for each node $k = 1, 2, \ldots, K$, is given by,

$$S_k = E_k\, R_k, \tag{4}$$

and it is measured in Watts (W), where E_k is the energy per bit, and R_k is the total bit rate used for both source and channel coding.

In fact, S_k refers to the power received by the CCU from node k. Therefore, for given power levels, the required transmission powers for the nodes can be determined through a propagation model. Assuming the Two Ray Ground Reflection (TRGR) model [38] as the propagation model, the transmission power for node k is given by [38],

$$S_{k_{\text{trans}}} = \frac{S_k\, {d_{\text{tr}}}^4}{G_{\text{t}}\, G_{\text{r}}\, h_{\text{t}}^2\, h_{\text{r}}^2}, \tag{5}$$

where d_{tr} is the distance between the transmitter (node) and the receiver (CCU); G_{t} is the transmitter antenna gain; G_{r} is the receiver antenna gain; h_{t} is the height of the transmitter; and h_{r} is the height of the receiver.

Concerning the total bit rate R_k, it is defined as,

$$R_k = \frac{R_{\text{s},k}}{R_{\text{c},k}}, \tag{6}$$

and it is measured in bits per second (bps). The quantity $R_{\text{s},k}$ represents the source coding rate, also measured in bps,while $R_{\text{c},k}$ is the channel coding rate of k-th node. Obviously, since $R_{\text{c},k}$ is the ratio of the number of information bits over the total number of bits, it is a scalar within the range $(0, 1)$ [39].

In our investigation, we followed the assumption that the interference can be approximated by AWGN [28, 40]. Thus, the energy per bit to MAI ratio is given by,

$$\frac{E_k}{I_0} = \frac{\frac{S_k}{R_k}}{\sum\limits_{j \neq k}^{K} \frac{S_j}{W_t}}, \qquad k = 1, 2, \ldots, K, \tag{7}$$

where $I_0/2$ is the two-sided noise power spectral density due to MAI, measured in Watts/Hertz (W/Hz), and W_t is the total available bandwidth, measured in Hertz (Hz). Again, k refers to the corresponding node, while j refers to each interfering node.

In Eq. (7), the following fundamental assumptions were made:

(a) The thermal and background noise were ignored.

(b) The spreading codes used were random and did not have any special properties.

(c) Interference suppression filters were not used.

Assumptions (b) and (c) suggest that no means is used to suppress or limit the co-channel interference, implying that each node admits the power of the other nodes totally as interference. If we drop assumption (a), i.e., assuming that thermal and background noise are rather significant, then, instead of E_k/I_0, we must use the following energy per bit to MAI and noise ratio,

$$\frac{E_k}{I_0 + N_0} = \frac{\frac{S_k}{R_k}}{\sum_{j \neq k}^{K} \frac{S_j}{W_t} + N_0}, \qquad k = 1, 2, \ldots, K, \tag{8}$$

where $N_0/2$ is the power spectral density of the AWGN.

4) Universal Rate-Distortion Characteristics

Image quality is highly related with the number of occurred errors during data transmission. Therefore, the BER determines the expected video distortion, which has an immediate impact on the video quality. In this paper, in order to compute the expected video distortion, Universal Rate-Distortion Characteristics (URDC) are used [39]. URDC express the expected distortion as a function of the bit error probability after channel decoding. Specifically, having compressed the video sequences with the H.264/AVC video codec at specific source coding rates, and for given BERs at each time, we can estimate the expected distortion value [24].

Similarly to relevant studies [24, 41, 25, 42, 43], the model we considered for the expected video distortion per node k is given by,

$$E[D_{\mathrm{s+c},k}] = \alpha \left[\log_{10}\left(\frac{1}{P_{\mathrm{b}}}\right)\right]^{-\beta}, \tag{9}$$

where P_{b} corresponds to the bit error probability or, in other words, to the BER. The parameters α and β are positive, and they are determined through a mean squared error optimization procedure using a limited number of pairs $(E[D_{\mathrm{s+c},k}], P_{\mathrm{b}})$, which are experimentally obtained for specific BERs. The values of these parameters depend on the source coding rate and the video sequence characteristics. Specifically, the parameter α usually takes lower values for video sequences with low amount of motion and higher values for video sequences with high amount of motion [44].

Due to the fact that channel errors and packet drops occur randomly, the video distortion attributed to the lossy compression and channel errors is a random variable. To this end, the video distortion is averaged over a number of independent experiments. Another assumption made in our study was that all nodes transmit data using the same total bit rate. In fact, this constraint results from a fixed overall transmission chip rate and the same processing gain (spreading code length) for all nodes, since it holds that,

$$R_k = \frac{R_{\mathrm{chip}}}{L}, \tag{10}$$

where R_{chip} is the chip rate, measured in chips per second, and L is the spreading code length, measured in chips.

We further assumed that the channel coding rates, $R_{\text{c},k}$, $k = 1, 2, \ldots, K$, can take only discrete values [14] from a set $\mathbf{R}_{\text{c}}$. Assuming that R_k is fixed, from Eq. (6) it follows that the source coding rates $R_{\text{s},k}$, $k = 1, 2, \ldots, K$, must also take discrete values from a set $\mathbf{R}_{\text{s}}$. Namely,

$$R_{\text{c},k} \in \mathbf{R}_{\text{c}}, \qquad R_{\text{s},k} \in \mathbf{R}_{\text{s}}, \qquad k = 1, 2, \ldots, K.$$

Let the index $cb = 1, 2, \ldots, CB$, denote the admissible source coding rate-channel coding rate combinations. Then, the combination $(R_{\text{s},k}, R_{\text{c},k})$ assumes discrete values from a set,

$$\mathbf{R}_{\text{s+c}} = \Big\{(R_{\text{s},k,1}, R_{\text{c},k,1}), \ldots, (R_{\text{s},k,cb}, R_{\text{c},k,cb}), \ldots, (R_{\text{s},k,CB}, R_{\text{c},k,CB})\Big\}.$$

The cardinality of $\mathbf{R}_{\text{s+c}}$ is CB. Evidently, the cardinalities of the sets $\mathbf{R}_{\text{s}}$, $\mathbf{R}_{\text{c}}$, and $\mathbf{R}_{\text{s+c}}$ shall be equal. Increasing the cardinality of these sets, results in significant augmentation of the search space with a consequent impact on the corresponding problem's complexity.

Regarding the power levels of the nodes, unlike previous work [24], in this study we assumed that they can take real values within a predetermined continuous range,

$$S_k \in \mathbf{S} = [s_{\min}, s_{\max}] \subset \mathbb{R}, \qquad k = 1, 2, \ldots, K.$$

Moreover, the parameters α and β of Eq. (9) are functions of the source coding rate and video content characteristics, as previously discussed. Concerning the parameters d_{free} and c_d of Eq. (1), they are functions of the channel coding rate. Thus, α, β, d_{free}, and c_d are functions of the source coding rate-channel coding rate combinations. Substituting Eq. (2) (with I_0 instead of N_0) into Eq. (1) (considering equality in order to use the BER's upper limit), and Eq. (1) into Eq. (9), the expected video distortion becomes,

$$E[D_{\text{s+c},k}](R_{\text{s},k}, R_{\text{c},k}, S) = \alpha(cb)\left[\log_{10}\left(\frac{1}{P_{\text{b}}}\right)\right]^{-\beta(cb)}, \tag{11}$$

where,

$$P_{\text{b}} = \frac{1}{P}\sum_{d=d_{\text{free}}(cb)}^{\infty}\left(c_d(cb)\,\frac{1}{2}\,\text{erfc}\left(\sqrt{dR_{\text{c},k}\left(\frac{\frac{S_k}{R_k}}{\sum_{j\neq k}^{K}\frac{S_j}{W_t} + N_0}\right)}\right)\right),$$

and $k = 1, 2, \ldots, K$. Obviously, the expected video distortion for node k is a function of the source coding rate, $R_{\text{s},k}$, channel coding rate, $R_{\text{c},k}$, as well as of the power levels, $S = (S_1, S_2, \ldots, S_K)^\top$, of all nodes of the network. Therefore, we eventually needed to determine the source-channel coding rate combinations, and the power levels of all nodes, in order to compute the expected video distortion.

4.1.2 Optimization Criteria

We assumed that the sensor nodes participating in the network image scenes that include various motion levels. This is a commonfeature for the majority of real-time VSN applications. The two optimization criteria that we considered in [1] to tackle the problem of optimal resource allocation among the nodes of the wireless VSN are both based on the concept of minimizing video distortion and they are analyzed in the following paragraphs.

1) Minimized Average Distortion

According to the MAD criterion, we needed to determine the optimal vectors of source coding rates, $R_{\mathrm{s}} = (R_{\mathrm{s},1}, R_{\mathrm{s},2}, \ldots, R_{\mathrm{s},K})^\top$, channel coding rates, $R_{\mathrm{c}} = (R_{\mathrm{c},1}, R_{\mathrm{c},2}, \ldots, R_{\mathrm{c},K})^\top$, and power levels, S, such that the overall *average distortion* $D_{\mathrm{ave}}(R_{\mathrm{s}}, R_{\mathrm{c}}, S)$ of the network is minimized, subject to the constraint of equal target bit rate R_{target} for all nodes. This problem can be formally given as follows,

$$\min_{R_{\mathrm{s}}, R_{\mathrm{c}}, S} D_{\mathrm{ave}}(R_{\mathrm{s}}, R_{\mathrm{c}}, S), \tag{12}$$

$$\text{subject to} \quad R_1 = R_2 = \cdots = R_K = R_{\mathrm{target}}, \tag{13}$$

where $D_{\mathrm{ave}}(R_{\mathrm{s}}, R_{\mathrm{c}}, S)$ is defined as follows:

$$D_{\mathrm{ave}}(R_{\mathrm{s}}, R_{\mathrm{c}}, S) = \frac{1}{K} \sum_{k=1}^{K} E[D_{\mathrm{s+c},k}](R_{\mathrm{s},k}, R_{\mathrm{c},k}, S), \tag{14}$$

where k is the node's index and K is the total number of nodes in the VSN. Obviously, this criterion does not assert fairness among the nodes. Hence, distortion is allowed to vary significantly from node to node as far as the average distortion is kept to minimal levels.

2) Minimized Maximum Distortion

The MMD criterion required the determination of the optimal vectors of source coding rates, $R_{\mathrm{s}} = (R_{\mathrm{s},1}, R_{\mathrm{s},2}, \ldots, R_{\mathrm{s},K})^\top$, channel coding rates, $R_{\mathrm{c}} = (R_{\mathrm{c},1}, R_{\mathrm{c},2}, \ldots, R_{\mathrm{c},K})^\top$, and power levels, S, such that the *maximum distortion* $D_{\max}(R_{\mathrm{s}}, R_{\mathrm{c}}, S)$ among all nodes is minimized subject to the constraint of equal target bit rate R_{target} for all nodes, i.e.,

$$\min_{R_{\mathrm{s}}, R_{\mathrm{c}}, S} D_{\max}(R_{\mathrm{s}}, R_{\mathrm{c}}, S), \tag{15}$$

$$\text{subject to} \quad R_1 = R_2 = \cdots = R_K = R_{\mathrm{target}}, \tag{16}$$

where $D_{\max}(R_{\mathrm{s}}, R_{\mathrm{c}}, S)$ is defined as follows,

$$D_{\max}(R_{\mathrm{s}}, R_{\mathrm{c}}, S) = \max_{k \in \{1,2,\ldots,K\}} E[D_{\mathrm{s+c},k}](R_{\mathrm{s},k}, R_{\mathrm{c},k}, S), \tag{17}$$

where k denotes the corresponding node. The MMD criterion may also exhibit deviations of the distortion from node to node, but, in contrast to the MAD criterion, it guarantees that all distortions are kept within acceptable ranges.

3) Further Assumptions

An additional assumption in our study was that the K nodes of the network were clustered into C motion classes, based on the amount of motion in the detected scenes. Without loss of generality, let us consider the case of $C = 2$. In this case, there are two motion classes: a high-motion class, which includes the nodes that detect high levels of motion, and a low-motion class consisting of the nodes that image relatively stationary fields. Each class has its own set of parameters α and β (see Eq. (11)), since they are affected by the amount of motion of each considered video sequence.

A reasonable question that follows the aforementioned assumption, is what happens in case of a possible change in the motion level of a scene. For example, what happens if the relatively stationary scenes of a forest-monitoring application are disturbed by an unexpected passage of an animal or, in a motorway-surveillance application, the scenes that capture intense traffic succeed scenes with infrequent vehicle passing? In such cases, a new classification of the scenes into high- and low-motion classes is required, corresponding to a new optimal resource allocation that is adjusted to the current state of the observed system.

Regarding the node clustering into two classes, the quantities that needed to be determined for each class under a total transmission bit rate constraint, were the following,

$$R_{\text{s+c,high}} = (R_{\text{s,high}}, R_{\text{c,high}})^\top,\ R_{\text{s+c,low}} = (R_{\text{s,low}}, R_{\text{c,low}})^\top,\ S = (S_{\text{high}}, S_{\text{low}})^\top,$$

where $(R_{\text{s,high}}, R_{\text{c,high}})$ and S_{high}, are the source-channel coding rate combination, and the power level, respectively, for the high-motion class of nodes, while $(R_{\text{s,low}}, R_{\text{c,low}})$ and S_{low} are the corresponding quantities for the low-motion class of nodes.

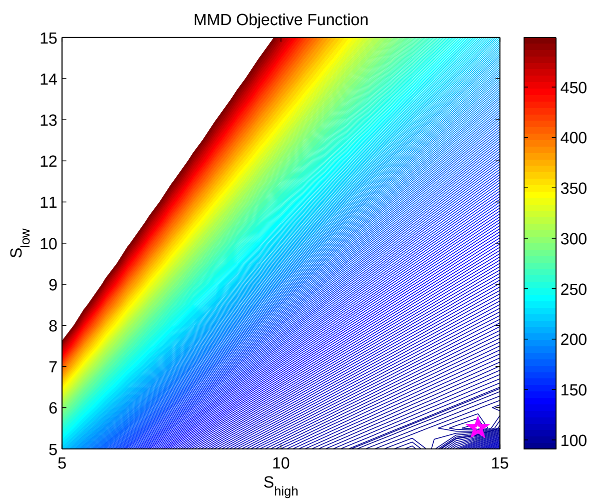

Figure 3: Contour plot of the objective function for the MMD criterion with respect to the power level values of the two motion classes (fixed source-channel coding rate combination).

Since the source-channel coding rate combinations assumed discrete values, while the power levels were continuous, the resulting optimization problems for both the above criteria were of mixed-integer type. Figure 3 illustrates the contour plot of the corresponding landscape for a fixed source-channel coding rate combination (the one that corresponds to the best solution). The two axes stand for the real-valued power levels of the two motion classes. Darker lines denote lower objective values. As we can see, the function has extremely steep regions (upper left part of the figure) as well as almost flat regions (middle to lower part). The star mark denotes the globally optimal power level vector (for the specific source-channel coding rate combination), which lies in a small region near the right lower bound of the search space. The figure refers to the MMD criterion. Similar landscapes were produced for all bit rate-bandwidth combinations, and for both the MAD and MMD criteria. Note that the optimization algorithm optimized the source-channel coding rate combinations as well as the power levels, concurrently. It is easily conceived that the interplay of the discrete variables along with the remarkable changes in slope for the real-valued variables, as well as the discontinuities that may be produced by criteria as the MMD can impose serious difficulties for any optimization algorithm.

4.1.3 Employed Optimization Algorithms

In the following paragraphs we present the employed optimization algorithms, namely PSO, AS, and the hybrid HPSOAS.

1) Particle Swarm Optimization

PSO was introduced in 1995 by Eberhart and Kennedy [15]. It is based on models that simulate flocking behavior and it has close ties with the concurrent concepts of *emergent* and *collective behavior* [45]. PSO is categorized as *swarm intelligence* algorithm within the wider field of intelligent optimization [46, 47]. Its ongoing increasing popularity can be attributed to its efficiency in tackling a plethora of scientific and technological applications, as well as to its easy implementation, which renders it accessible to researchers from various disciplines [46].

PSO uses a population, called *swarm*, of search points, called *particles*, to probe the search space. The particles are randomly initialized (usually uniformly) in the search space. Each particle has three essential features: its *current position* in the search space, a *memory*, where it retains the best position it has ever visited, and an adaptable *velocity* (position shift) that iteratively defines its new position. Also, it assumes a *neighborhood* consisting of other particles,i.e., a subset of the swarm, with which it interacts by means of information exchange. The information originating from the particle's own experience as well as the collective experience, are the main sources of influence for its move in the search space.

Let the general minimization problem,

$$\min_{x \in \mathbf{X} \subset \mathbb{R}^n} f(x),$$

with $f(x)$ being the objective function. Let the set $I = \{1, 2, \ldots, N\}$ denote the indices of the N particles of the swarm. Then, the swarm can be represented as a set of search points,

$$\mathcal{S} = \{x_1, x_2, \ldots, x_N\}.$$

Each particle is an n-dimensional vector,

$$x_i = (x_{i1}, x_{i2}, \ldots, x_{in})^\top \in \mathbf{X}, \qquad i \in I,$$

and its velocity is defined as,

$$v_i = (v_{i1}, v_{i2}, \ldots, v_{in})^\top, \qquad i \in I.$$

Its best position is also an n-dimensional vector,

$$p_i = (p_{i1}, p_{i2}, \ldots, p_{in})^\top \in \mathbf{X}, \qquad i \in I,$$

stored in the memory and iteratively updated as long as the particle moves in $\mathbf{X}$.

The neighborhood, $\mathcal{N}_i$, of the i-th particle can be defined in various ways. A straightforward approach considers as neighbors the closest particles in the search space. However, this approach was shown to produce clusters of particles that rapidly collapse on local minimizers, thereby reducing the (collective) exploration ability of the swarm. An alternative idea is the determination of neighborhoods in abstract spaces instead of the actual search space. An instance that has proved to be very efficient assumes that the particles are ordered on a *ring* based on their indices. In this case, the neighborhoods consist of particles with neighboring indices, having the form,

$$\mathcal{N}_i = \{i-r, \ldots, i-1, i, i+1, \ldots, i+r\} \subseteq I,$$

where $r \in \left\{1, 2, \ldots, \frac{N}{2}\right\}$ is called the neighborhood's *radius*. The indices are assumed to recycle at the ends, i.e., index 1 follows immediately after index N. Evidently, increasing r results in neighborhoods that approximate the whole swarm. Different neighborhood topologies have been proposed in the literature [48, 49]. The neighborhoods control the information flow among the particles as well as the available information that influences the particles' position shifts at each iteration. Therefore, they can have a tremendous impact on PSO's performance.

Let g_i denote the index of the best in the neighborhood of the i-th particle, i.e.,

$$g_i = \arg \min_{j \in \mathcal{N}_i} f(p_j), \qquad i \in I, \tag{18}$$

and let t denote the iteration number. Then, the swarm is updated at each iteration as follows [50]:

$$v_{ij}^{(t+1)} = \chi \left[v_{ij}^{(t)} + c_1 \mathcal{R}_1 \left(p_{ij}^{(t)} - x_{ij}^{(t)} \right) + c_2 \mathcal{R}_2 \left(p_{g_i j}^{(t)} - x_{ij}^{(t)} \right) \right], \tag{19}$$

$$x_{ij}^{(t+1)} = x_{ij}^{(t)} + v_{ij}^{(t+1)}, \tag{20}$$

where $i \in I$; $j = 1, 2, \ldots, n$; and χ is a parameter called the *constriction coefficient*, which can deter the *swarm explosion* effect, i.e., the rapid divergence of the particles due to excessively large velocities [50, 51, 52]. Regarding c_1 and c_2, they are two positive acceleration parameters called the *cognitive* and *social* parameter, respectively. These parameters control the influence of the personal and collective experience (memory) on the particle's move, with equal values promoting a fair tradeoff between them. Finally, $\mathcal{R}_1$ and $\mathcal{R}_2$ are random variables uniformly distributed in the range $[0, 1]$. They introduce stochasticity in PSO and assume a different value for each i and j. Evidently, PSO's update is inherently parallel, since it is performed componentwise.

After updating and evaluating the swarm, memory update takes place in two stages. In the first stage, the personal best position of each particle is updated as follows,

$$p_i^{(t+1)} = \begin{cases} x_i^{(t+1)}, & \text{if } f\left(x_i^{(t+1)}\right) < f\left(p_i^{(t)}\right), \\ p_i^{(t)}, & \text{otherwise,} \end{cases} \qquad i \in I.$$

The determination of new best positions is followed, in the second stage, by the update of all indices g_i, $i \in I$, according to Eq. (18). This completes a PSO iteration. The procedure is repeated until a stopping criterion is satisfied, such as exceeding a prespecified number of function evaluations or reaching a target function value.

Clerc and Kennedy [50] have extensively studied the stability of PSO. Their analysis offered significant mathematical evidence on its proper parameter settings. Based on their analysis, the parameter values,

$$\chi = 0.729, \quad c_1 = 2.05, \quad c_2 = 2.05,$$

have been shown to be a satisfactory starting choice, considered as the default parameter set of the constriction coefficient variant of PSO. Further information and alternative settings can be found in [50, 52].

PSO belongs among the most studied metaheuristics. In addition to [50, 52], further theoretical analyses can be found in [53, 54, 55]. Its theoretical background, well-understood dynamic, as well as its frequently verified efficiency renders PSO a very appealing optimizer. Recently, it has been used with remarkable success in VNS [41, 44, 2, 56, 57, 58, 7, 8, 59].

1.1) Tackling Discrete Variables

Although PSO was primarily designed to handle continuous variables, it has been successfully applied also on integer optimization problems [60, 61, 62, 63, 64]. This can be achieved by introducing integer-arithmetic based operators in PSO. However, in most cases, the resulting PSO variants barely resemble the original PSO dynamics. Alternatively, discrete values can be tackled by solving an extended version of the problem in the continuous space and rounding the candidate solutions to the nearest integers prior to their evaluation with the objective function. The latter procedure has minor effect on the algorithm. Also, it has been shown to work efficiently in various problems, offering motivation for selecting the latter approach in our study.

In the mixed integer optimization problems of the present study, each particle should normally consist of integer and continuous components, corresponding to the discrete and continuous variables as described earlier. Instead, we considered also the integer parameters to be continuous (retaining their bounds) and applied the presented PSO scheme. However, whenever a particle was evaluated with the objective function, its corresponding components were rounded to the nearest integers as follows:

$$x_{ij} = \lfloor x_{ij} + 0.5 \rfloor,$$

where $\lfloor . \rfloor$ is the floor function. This scheme was successfully tested in previous works [41, 44, 2, 56, 57, 58, 7, 8, 59].

1.2) Estimation of Maximum Velocity

A feature usually neglected in PSO implementations is that of *maximum velocity*. Specifically, whenever the velocities are computed by Eq. (19), they undergo a magnitude-restriction test as follows,

$$v_{ij}^{(t+1)} = \begin{cases} v_j^{\max}, & \text{if} \quad v_{ij}^{(t+1)} > v_j^{\max}, \\ -v_j^{\max}, & \text{if} \quad v_{ij}^{(t+1)} < -v_j^{\max}, \\ v_{ij}^{(t+1)}, & \text{otherwise}, \end{cases} \qquad \forall\, i, j, t,$$

where $v_j^{\max}$ is a predefined positive value, possibly different for each $j = 1, 2 \ldots, n$. Obviously, this procedure restricts the velocity components within the corresponding ranges $[-v_j^{\max}, v_j^{\max}]$, preventing the particles from taking large steps that could lead to wide-range oscillations around the best positions or frequently escaping out of the search space. Naturally,this can have considerable impact on PSO's convergence speed. We can easily infer that large values of $v_j^{\max}$ are more appropriate for search spaces with wide flat or low-curvature regions, while significantly smaller values may be required in steep functions with large number of minimizers, especially when they are closely concentrated.

Typically, maximum velocity is determined as the maximum absolute distance allowed to be traveled by the particle in a single step at each component direction. For this purpose, it is usually defined as a fraction of the corresponding search space's range in the specific component direction. For example, if the search space is defined as $\mathbf{X} = [x_1^{\min}, x_1^{\max}] \times \cdots \times [x_n^{\min}, x_n^{\max}]$, then the following restriction is commonly used,

$$v_j^{\max} = \gamma_j \left(x_j^{\max} - x_j^{\min} \right), \qquad \gamma_j \in (0, 1], \quad j = 1, 2 \ldots, n. \tag{21}$$

Available information on the form of the objective function may dictate larger or smaller values of the parameters γ_j. For example, the Lipschitz property can provide useful insight regarding the degree of variation of the objective function in the whole search space. However, in most cases such information is either unavailable or very laborious to be computed.

In such cases, we can approximately estimate the Lipschitz constant by considering its *modulus of continuity* (MoC) $\delta > 0$, which is locally defined in a subset $\mathbf{B} \subset \mathbf{X}$ of the search space as follows,

$$|f(x) - f(y)| \leqslant \delta \,\|x - y\|\,, \qquad \forall\, x, y \in \mathbf{B}.$$

Estimating the MoC around solutions obtained in preliminary experiments as well as on randomly selected points in the search space can partially reveal the local behavior of the objective function. This, in turn, can lead to more appropriate selection of the maximum velocity thresholds described above. The estimation can be easily conducted through Monte Carlo sampling within the corresponding region $\mathbf{B}$.

In our preliminary experiments, we observed that PSO performance in terms of convergence speed exhibited large deviations per optimization criterion for some cases. Thorough examination of the corresponding landscapes revealed the importance of proper velocity setting. Thus, we employed the procedure described above to obtain estimations of the maximum velocities for each optimization criterion based on Monte Carlo approximations of the MoC.

2) Active-Set Optimization Method

Constrained optimization problems are usually tackled by splitting the initial problem into simpler subproblems than can be solved and used as the basis of an iterative process. The AS is an iterative method that is used for solving a sequence of quadratic subproblems, guaranteeing the feasibility of the final solution [17, 18]. The main mechanism is based on the solution of the Karush-Kuhn-Tucker (KKT) equations, which guarantee the optimality for a constrained optimization problem.

Let us assume again the minimization problem as declared in the description of PSO,

$$\min_{x \in \mathbf{X} \subset \mathbb{R}^n} f(x),$$

subject to m constraints (these constraints may be implicitly given as defining relations of the search space $\mathbf{X}$),

$$G_i(x) = 0, \qquad i = 1, \ldots, m_e, \tag{22}$$

$$G_i(x) \leq 0, \qquad i = m_e + 1, \ldots, m. \tag{23}$$

The vector function $G(x) = (G_1(x), \ldots, G_m(x))^\top$ returns a vector of length m that includes the equality and inequality constraint values at x. The corresponding KKT equations are given by,

$$\nabla f(x) + \sum_{i=1}^{m} \lambda_i \, \nabla G_i(x) = 0 \tag{24}$$

$$\lambda_i \, G_i(x) = 0, \qquad i = 1, \ldots, m_e, \tag{25}$$

$$\lambda_i \geq 0, \qquad i = m_e + 1, \ldots, m. \tag{26}$$

Equation (24) depicts the canceling process of the gradients between the objective function $f(x)$ and the active constraints $G_i(x)$ at x, through the use of the Lagrange multipliers λ_i, $i = 1, \ldots, m$. Lagrange multipliers are used in order to balance the deviations in magnitude of the objective function and constraint gradients. Due to the fact that only active constraints are included in the gradients canceling, non-active constraints are assigned $\lambda_i = 0$, as it is stated implicitly by Eqs. (25)-(26).

Thus, the AS method is based on the solution of the KKT equations and attempts to compute the Lagrange multipliers directly. It searches solutions in the feasible sets and if a minimizer is found during each iteration, followed by a decrease in the value of the objective function, the algorithm terminates after a user-defined stopping criterion. Such a criterion can be the maximum iteration number, the maximum number of function evaluations, the function tolerance, the tolerance of the optimal point x etc.

In our problem, we used the robust implementation of the original Matlab® Optimization Toolbox. Further details on this implementation can be found in [65].

3) Hybrid PSO-AS Optimization Method

Motivated by the benefits of both PSO and AS optimization algorithms, we combined their features introducing a hybrid PSO-AS approach, which is denoted HPSOAS. This hybrid approach can be categorized as a *memetic algorithm* [19] and employs AS as local optimizer for further improving the findings of PSO.

Algorithm 1 HPSOAS

Require: Initialize PSO algorithm.

```
loop
  if (not stopping) then
    Update swarm and best positions.
    if (new overall best position is found) then
      Apply AS on the new best position.
      Make AS's solution the new overall best position.
    end if
  end if
end loop
```

Specifically, when the overall best position of PSO changes, a local search procedure with AS is initiated from this point, in order to further improve it. The procedure is sketched in Alg. 1. Although PSO and in many cases also AS were capable of successfully approximating the optimal solution in our experiments, the HPSOAS scheme was significantly more time-efficient, yet retaining the solutions' quality. Its success lies on the fact that AS was rapidly improving the PSO's best findings, thereby providing better attractors (best positions) for the particles, while at the same time it surmounted the sensitivity of AS on the initial conditions (starting point).

4.2 Game-Theoretic Solutions through Intelligent Optimization for Efficient Resource Management in Wireless Visual Sensor Networks

In this work, we assumed the network infrastructure as it was described in Section 4.1.1 and we dealt with the resource allocation problem, under a game-theoretic perspective.

4.2.1 Background Information

The utility function, U_{cl}, constitutes a measure of relative satisfaction for each motion class cl. In our problem, it is defined equivalently to the PSNR [56]:

$$U_{cl} = 10 \log_{10} \frac{255^2}{E[D_{\mathrm{s+c},cl}]}, \qquad cl = 1, 2, \ldots, C, \tag{27}$$

and thus, it is measured in deciBel (dB). The quantity $E[D_{\mathrm{s+c},cl}]$ represents the expected video distortion for motion class cl, given by Eq. (11). Clearly, higher values of the utility function correspond to higher received video qualities.

The vector $U = (U_1, U_2, \ldots, U_C)^\top$ contains the utilities for all C motion classes. The feasible set, $\mathbf{U}$, encompasses all possible vectors U that result from all possible combinations of the source and channel coding rates as well as the power levels of all motion classes, when pure strategies are allowed. (A pure strategy defines a deterministic action of a player). Also, it shall satisfy the following conditions [10]:

(1) $\mathbf{U} \subset \mathbb{R}^C$ is comprehensive, closed and bounded-above.

(2) Free disposal is allowed.

The first condition stipulates that a set $\mathbf{U} \subset \mathbb{R}^C$ shall be comprehensive. This means that if X is in $\mathbf{U}$ and $Y \leqslant X$, then Y is in $\mathbf{U}$ as well [66]. Additionally, the same set shall also include all its boundary points (i.e., be closed) and be bounded from above. A set $\mathbf{U}$ is bounded-above, if there exists X such that $Y \leqslant X$ for all $Y \in \mathbf{U}$.

Regarding the second condition, free disposal means that each player is permitted to dispose of utility, if required. The physical meaning in the case of video is that a class of nodes is allowed to purposely add noise to its video to degrade the video quality. Obviously, this is an irrational decision and will never be chosen. However, in our formulation we should not restrict the possible choices of the players regarding the handling of their resources, unless they lead to cases that are impossible to be implemented. Specifically, if $Y \leqslant X$, and X is a feasible point for all classes of nodes, it follows that Y can be achieved by the players also by mutually agreeing to dispose of utility, unilaterally or multilaterally. In this paper [2], we assumed that free disposal is allowed for the feasible set and therefore, this statement clearly implies that the feasible set $\mathbf{U}$ is also comprehensive [10, 66].

Each player expects by participating in a game that it will receive at least as high a utility as it would get without joining the game (without collaborating). This fact constitutes an incentive for the players to negotiate. The disagreement point is the vector of minimum utilities that each player expects by joining the game without cooperating with the other players, and it is what each player will get even in cases of negotiation failure. It is defined as $dp = (dp_1, dp_2, ..., dp_C)^\top$, for all C players (classes of nodes), and it also belongs to the feasible set.

The outcome of a game is said to be Pareto-optimal if there is no other outcome that concurrently favors all players. In this work [2], we refered to Pareto-optimality in the strong sense, which implies that there is no other outcome where at least one player strictly increases its utility and no player decreases its utility. The Pareto-optimal points, which are members of the feasible set and give each node a utility that is greater than or equal to the dp, form the bargaining set.

4.2.2 Nash Bargaining Solution

In our problem, the Nash bargaining solution offered a distribution rule in order to achieve a mutually agreeable, fair and efficient allocation of the node classes' transmission parameters. Specifically, the NBS, denoted as $F(\mathbf{U}, dp)$ for the feasible set $\mathbf{U}$ and the dp, shall adhere to the following axioms [66]:

(1) *Individual Rationality*: $F(\mathbf{U}, dp) \geqslant dp$.

(2) *Pareto-Optimality*: $X > F(\mathbf{U}, dp) \Rightarrow X \notin \mathbf{U}$.

(3) *Invariance to Affine Transformations*: Given any strictly increasing affine transformation $\tau()$, it holds that $F(\tau(\mathbf{U}), \tau(dp)) = \tau(F(\mathbf{U}, dp))$.

(4) *Independence of Irrelevant Alternatives*: If $dp \in \mathbf{Y} \subseteq \mathbf{U}$, then $F(\mathbf{U}, dp) \in \mathbf{Y} \Rightarrow F(\mathbf{Y}, dp) = F(\mathbf{U}, dp)$.

The first two axioms imply that the NBS belongs to the bargaining set and the third axiom stipulates that the NBS is unaffected by affine transformation scalings of the utility function. The last axiom states that, if the bargaining solution, $F(\mathbf{U}, dp)$, for the feasible set $\mathbf{U}$ also belongs to a subset $\mathbf{Y}$ of the feasible set, then $F(\mathbf{Y}, dp)$ shall be the same as $F(\mathbf{U}, dp)$, since none of the extra elements of $\mathbf{U}$ were chosen as a solution when they were available. Thus, their unavailability in $\mathbf{Y}$ should be irrelevant.

Provided that the aforementioned conditions are satisfied, the NBS maximizes the Nash product [10, 56, 66]:

$$F(\mathbf{U}, dp) = \arg \max_{U \geqslant dp} \prod_{cl=1}^{C} (U_{cl}(R_{\mathrm{s},cl}, R_{\mathrm{c},cl}, S) - dp_{cl})^{a_{cl}}, \tag{28}$$

subject to the following constraints:

(a) $R_k = R_{\text{target}}$ (fixed bit rate).

(b) $S_{cl} \in \mathbf{P} = [s_{\min}, s_{\max}] \subset \mathbb{R}_+^*$ (bounded power).

(c) $\sum_{cl=1}^{C} a_{cl} = 1,\ a_{cl} \geqslant 0,\ cl = 1, 2, \ldots, C$.

The parameter a_{cl} assigned to each factor of the Nash product is called bargaining power and declares the advantage of each player in the considered game. Higher bargaining powers imply more advantaged players, and vice versa.

Since the determination of the bargaining powers is crucial for the performance and efficiency of the NBS, in this paper [2] we proposed two versions of the NBS, the NNBS and the CNBS. For the NNBS, we assumed that each node has the same advantage in the resource allocation game. Practically, given the constraint that the sum of all bargaining powers is equal to 1, and considering an equally fair game for all nodes, it follows that each class of nodes cl is assigned a bargaining power equal to $a_{cl} = 1/K_{cl}$, with K_{cl} representing the cardinality of class cl. For the CNBS, we assumed that each class of nodes is put in a similar position by the rules of the considered game. Therefore, assuming C motion classes, and considering the constraint for the total sum of the bargaining powers, it is implied that $a_{cl} = 1/C$, for the cl class of nodes.

Apart from the bargaining powers, another component that directly affects the Nash product is the dp, as derived from Eq. (28). For this reason, we shall pay attention to the appropriate determination of this vector. In [25], we assumed that the disagreement point corresponds to the vector of utilities that the motion classes get if they behave selfishly, without collaborating with each other. Following this reasoning, a class of nodes that desires to achieve the best possible received video quality regardless of the intentions of the other classes, will have to transmit using the maximum power. However, if all motion classes adopt this strategy, they will all select to transmit at maximum power, thereby reaching a Nash equilibrium. This occurs since each motion class adopts the strategy that is the best response to the strategies followed by the other classes.

However, such a selection for the *dp* heavily favors the classes of nodes that capture videos with low motion, which get high utility and have no incentive to collaborate [25]. For this reason, in the present study we assumed that the *dp* is imposed by the system designer and expresses the minimum acceptable video quality for each class of nodes, for the particular application.

In order to solve the mixed-integer optimization problems of this work, resulting from the discrete source-channel coding rate combinations and the continuous power levels, we employed the PSO algorithm, for both considered NBS-based approaches. PSO's performance was compared with the performance of three deterministic optimization methods, which were used as benchmarks, such as AS, which was described in more detail in Section 4.1.3, Interior-Point (IP) and Trust-Region-Reflective (TRR).

4.3 Geometric Bargaining Approach for Optimizing Resource Allocation in Wireless Visual Sensor Networks

In this paper [3], we considered the network infrastructure as it was described in Section 4.1.1 and we dealt with the resource allocation problem, using the Kalai-Smorodinsky bargaining solution.

4.3.1 Game-Theory Basics

A resource allocation outcome is *strongly Pareto-optimal* if there can not be another feasible outcome, which is strictly preferred by at least one node, and weakly preferred by the other nodes. In other words, this means that all nodes maintain the payoff they hold and at least one node increases its utility. Instead, a *weakly Pareto-optimal* allocation of resources is strictly preferred by all the nodes of the network, meaning that all of them increase their utilities [66]. All the points that are characterized as Pareto-optimal, strongly and/or weakly, are points of the feasible set and consist the bargaining set, which is thus a subset of the feasible set.

The vector that consists of the maximum achievable utilities that each node can get by participating in the resource allocation game is called *utopian point*, and is defined as:

$$U_{MAX}(\mathbf{U}, dp) = (\max U_1, \max U_2, \ldots, \max U_K)^\top \geq dp. \tag{29}$$

The maximum possible utility, $\max U_k$, for node k, has to be greater or at least equal to the utility that node k can get at its disagreement point, dp_k. Since the available resources are usually limited, it is impossible for all nodes to benefit at the same time. Therefore, the utopian point does not belong to the feasible set.

4.3.2 Kalai-Smorodinsky Bargaining Solution

The Kalai-Smorodinsky bargaining solution $F(\mathbf{U}, dp)$, for the feasible set $\mathbf{U}$, and the dp, is the solution that satisfies the following axioms [66, 67, 68]:

i) $F(\mathbf{U}, dp) \geq dp$.

ii) $Y \gg F(\mathbf{U}, dp) \Rightarrow Y \notin \mathbf{U}$.

iii) Given any strictly increasing affine transformation $\tau()$, it holds that $F(\tau(\mathbf{U}), \tau(dp)) = \tau(F(\mathbf{U}, dp))$.

iv) Suppose that $dp \in \mathbf{U}' \subseteq \mathbf{U}$ and U_{MAX} is identical for both $(\mathbf{U}, dp)$ and $(\mathbf{U}', dp)$. Then, if $F(\mathbf{U}', dp)$ is a Pareto-optimal point of $\mathbf{U}$, it holds that $F(\mathbf{U}, dp) = F(\mathbf{U}', dp)$.

The first two axioms state that the bargaining solution lies in the bargaining set. Particularly, the second one specifies that the solution $F(\mathbf{U}, dp)$ is weakly Pareto-optimal, i.e., if there is a point Y that is strictly preferred by all nodes, then Y does not belong to the feasible set. The third condition stipulates that if the utility function or the disagreement point are scaled by an affine transformation, the bargaining solution remains unaffected. The axiom of *strong individual monotonicity*, described by the fourth axiom, presents the circumstances under which two sets have the same solution.

According to [69], the KSBS is found by taking the maximal element of the feasible set (lying on the bargaining set), on the line connecting the disagreement point and the utopian point (Fig. 4). It should be stressed that the KSBS can be applied either to convex or to non-convex feasible sets, satisfying the aforementioned conditions. The only difference lies in the weak/strong Pareto-optimality axiom, which holds for non-convex/convex feasible sets, respectively. As it was mentioned before, weak Pareto-optimality declares that all nodes prefer the payoff they get with Y more than the payoff they get with $F(\mathbf{U}, dp)$. Strong Pareto-optimality means that all nodes like Y at least as much as $F(\mathbf{U}, dp)$ and that at least one node likes Y strictly more than $F(\mathbf{U}, dp)$. In this work, experimentation proved that the examined feasible sets were all slightly non-convex sets, and due to this, the KSBS had to satisfy the condition of weak Pareto-optimality [10, 67, 68].

4.3.3 Geometric Approach

Let us now describe the procedure that we followed in order to solve the problem under investigation. We seek the rule that allocates fairly and efficiently the discrete source and channel coding rates, and the continuous power levels among all the nodes of the network. This rule is defined by the KSBS, which is calculated at the CCU. For simplicity reasons, we grouped the nodes into $C = 2$ motion classes, based on the amount of motion in the scenes they detect. However, other values of C could also be used. Hence, two motion classes were formed. A high-motion class consisting of the nodes that detect high levels of motion and a low-motion class consisting of the nodes that detect low levels of motion. Since the KSBS is found by taking the element of the bargaining set that also lies on the line that connects the disagreement point and the utopian point, we approached the problem of the current paper under a geometric perspective. The bargaining solutions were derived geometrically, directly from the graphical representation of each considered feasible set.

Figure 4 gives a useful intuition about the feasible set and the KSBS. Specifically, it depicts the feasible set $\mathbf{U}$, when there are two classes of nodes in the network. U_1 declares the utility for the first class of nodes and U_2 for the second class of nodes. In our work, these quantities represented the corresponding PSNR values for each class of nodes. The utopian point U_{MAX} lies outside the feasible set, as it was anticipated. In the same figure, the diamond represents the KSBS, $F(\mathbf{U}, dp)$, for the feasible set $\mathbf{U}$ and the dp.

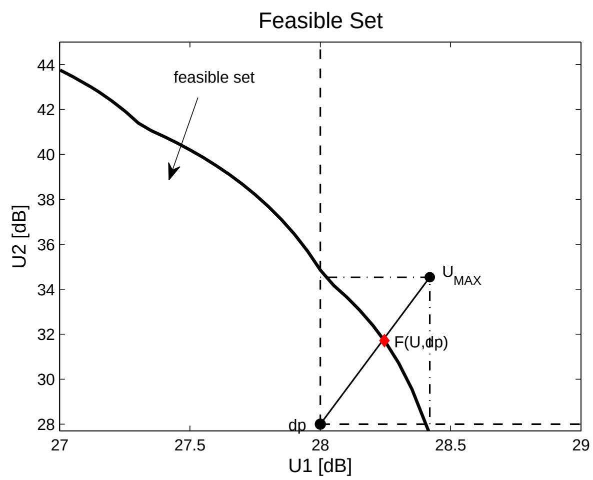

Figure 4: A feasible set and the KSBS.

Each utility allocation, represents a feasible point, which comes from a different combination of the nodes' transmission parameters, resulting in a different utility assignment for each node. Thus, considering all possible combinations of the transmission parameters, we had the feasible set. In the following, in order to determine the bargaining set, namely the Pareto-optimal points of the feasible set, we partitioned the x-axis of the feasible set in small, equal segments. For each segment of the x-axis, we kept the point with the highest value in the y-axis. The set that was formed including the points with the highest values in the y-axis, for each segment of the x-axis, formed the bargaining set. In order to find the equation that describes the bargaining set, a polynomial of second degree was used, since it was a good approximation for this set. Specifically, we had the equation:

$$U_2 = \alpha_1 U_1^2 + \alpha_2 U_1 + \alpha_3, \tag{30}$$

where the coefficients $\alpha_1, \alpha_2, \alpha_3$ were estimated in a least square sense for a few (U_1, U_2) pairs.

In the following, we set the dp at a specific value and we computed the vector of the utopian point, $U_{MAX}(\mathbf{U}, dp)$, which corresponded to the maximum achievable utilities for each class of nodes. We connected the disagreement point with the utopian point with a straight line and found the equation of this line. Specifically, we had the equation:

$$U_2 = \frac{\max U_2 - dp_2}{\max U_1 - dp_1}(U_1 - dp_1) + dp_2. \tag{31}$$

Therefore, having a set of equations, Eqs. (30) and (31), we solved the system. The point that resulted from solving the system was the intersection point of the curve and the straight line and corresponded to the Kalai-Smorodinsky bargaining solution that we sought to find. This point belongs to the bargaining set and is unique, as we can see for example in Fig. 4. Therefore, it is a Pareto-optimal point. Concisely, the steps for the calculation of the KSBS are described in Algorithm 2.

As it was previously mentioned, each feasible point comes from a combination of the nodes' transmission parameters. Specifically, in our problem, it corresponded to a power level value and a combination of source and channel coding rate values, assuming a maximum power constraint and a fixed bit rate constraint. Allowing continuous values for the power levels, we had an infinite number of points in the feasible set. Thus, in order to graphically determine the KSBS, discretization of the power levels was necessary. Therefore, we constrained the power levels to take values within a set of predetermined range, with a step size equal to 10^{-1}.

Algorithm 2 KSBS Calculation

1. Determine all feasible points (U_1, U_2).
2. Determine the feasible points (U_1, U_2) that form the bargaining set.
3. Determine the coefficients $\alpha_1, \alpha_2, \alpha_3$ of $U_2 = \alpha_1 U_1^2 + \alpha_2 U_1 + \alpha_3$, in a least square sense for a few (U_1, U_2) feasible points.
4. Determine $dp = (dp_1, dp_2)^\top$.
5. Determine $U_{MAX}(\mathbf{U}, dp) = (\max U_1, \max U_2)^\top$.
6. Connect dp and $U_{MAX}(\mathbf{U}, dp)$ with a straight line.
7. Find $U_2 = \frac{\max U_2 - dp_2}{\max U_1 - dp_1}(U_1 - dp_1) + dp_2$.
8. Solve the system of $U_2 = \alpha_1 U_1^2 + \alpha_2 U_1 + \alpha_3$ and $U_2 = \frac{\max U_2 - dp_2}{\max U_1 - dp_1}(U_1 - dp_1) + dp_2$.
9. $F(\mathbf{U}, dp)$ is the intersection point of the system.

Clearly, the smaller the step size, the higher the computational complexity of the problem and vice versa. Due to this fact, in this work we chose the value of 10^{-1} for the step size of the power levels. This assumption had minor and trivial effects on the achieved performance for the nodes, incurring solutions for the PSNR values with differences to the third or fourth decimal digit compared to the PSNR values obtained after assuming a smaller step size i.e., 10^{-3} or 10^{-4}. In our opinion, these utility differences were negligible compared to the great gain of the problem's complexity reduction and clearly, this quality difference can not be perceived by the human eye.

4.3.4 Performance Evaluation

In this work, the results of the KSBS were compared with the corresponding results of the NBS, MTU and w.MTU. The NBS is able to provide a Pareto-optimal solution, adhering to a set of four axioms [56, 66]. For the two motion classes, it can be found by maximizing the Nash product:

$$F(\mathbf{U}, dp) = \arg \max_{U \geqslant dp} [(U_1(R_{\mathrm{s},1}, R_{\mathrm{c},1}, S) - dp_1)^{a_1} (U_2(R_{\mathrm{s},2}, R_{\mathrm{c},2}, S) - dp_2)^{a_2}], \tag{32}$$

such that $a_1 + a_2 = 1$. The subscript 1 denotes the high-motion class of nodes, while 2 the low-motion class of nodes. The parameters a_1 and a_2 represent the bargaining powers assigned to the high- and low-motion class of nodes, respectively. The bargaining powers declare the relative advantage that each class of nodes has in the negotiation. We assume that the bargaining powers are proportional to the number of nodes in each class [56]. Thus, $a_1 = N_1/K$ and $a_2 = N_2/K$, where N_1 represents the number of nodes in the high-motion class and N_2 the number of nodes in the low-motion class.

The MTU and w.MTU both aim at the maximization of the total system utility. Specifically, the MTU maximizes:

$$\max [U_1(R_{\mathrm{s},1}, R_{\mathrm{c},1}, S) + U_2(R_{\mathrm{s},2}, R_{\mathrm{c},2}, S)]. \tag{33}$$

The w.MTU assumes weights for each class of nodes that are proportional to the cardinality N_{cl}, of each class cl. Therefore, the resulting equation under maximization is:

$$\max [a_1 U_1(R_{\mathrm{s},1}, R_{\mathrm{c},1}, S) + a_2 U_2(R_{\mathrm{s},2}, R_{\mathrm{c},2}, S)], \tag{34}$$

where the weight a_1 equals $a_1 = N_1/K$ and the weight a_2 equals $a_2 = N_2/K$.

In the present work, we were also interested in studying the behavior of the KSBS under the assumption that unfairness is measured in terms of the total utility loss incurred to both motion classes. For this purpose, we applied a metric that captures both relative performance and relative fairness issues [12, 4]. A prerequisite in order to use this metric was the existence of a scheme that gathers the highest total amount of utility cumulatively for both motion classes, compared to the other examined schemes. In this study, this scheme was the MTU. Also, we considered that none of the examined schemes was simultaneously preferred by both motion classes compared to the other schemes.

Assuming that the criterion that maximizes the unweighted version of the total system utility, namely the MTU, was used as the reference criterion, we defined the performance to fairness (PF) metric [12, 4] as:

$$PF(MTU, Cons) = \frac{\sum_{cl=1}^{C} (U_{cl}^{MTU} - U_{cl}^{Cons})}{\sum_{cl=1}^{C} \max(0, U_{cl}^{Cons} - U_{cl}^{MTU})}, \tag{35}$$

where $Cons$ refers to each considered scheme and cl declares each considered class of nodes of the C motion classes. The numerator of the above equation quantifies the total performance gain of using the MTU over $Cons$ and the denominator quantifies the unfairness of using the MTU over $Cons$.

In order to make a more reliable estimation about the fairness and performance of the KSBS, we also evaluated each tested scheme in the resource domain (power consumption). Specifically, a desirable scheme could combine high total utility, fairness, and low levels of power consumption

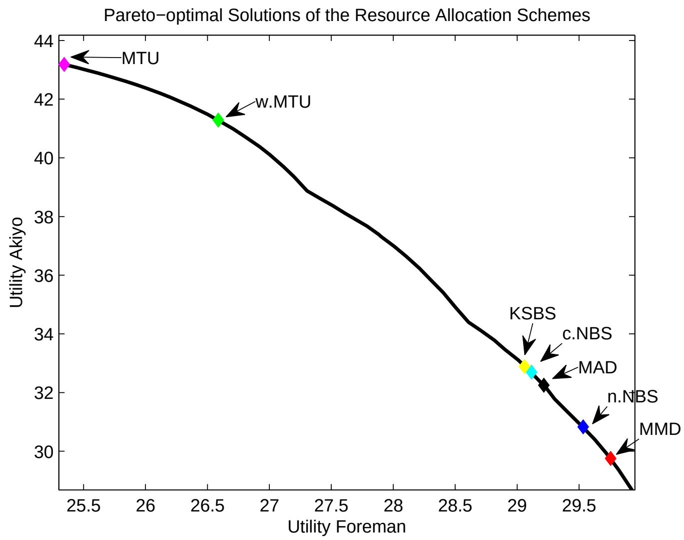

Figure 5: Pareto-optimality of the solutions.

for all nodes. Inspired by this fact, for each of the KSBS, NBS, MTU and w.MTU, we estimated the total power consumption, cumulatively for all nodes, grouped into C motion classes, i.e.,

$$\sum_{cl=1}^{C} S_{cl}, \tag{36}$$

where S_{cl} represents the power level of class cl. Therefore, we studied the total power consumption in combination with the total utility, for each examined scheme.

4.4 Fairness Issues in Resource Allocation Schemes for Wireless Visual Sensor Networks

All of the schemes presented in our previous works, i.e., the MAD, MMD, NNBS, CNBS, KSBS, MTU and w.MTU, were able to provide Pareto-optimal solutions. Therefore, there was no single scheme that would be selected by all nodes to be the best. Figure 5 graphically depicts the Pareto-optimal solutions achieved by each of the considered schemes assuming a node clustering into two motion classes. Specifically, in this case, 70 nodes imaged scenes with high levels of motion and 30 nodes imaged scenes with low levels of motion.

Since an ideal scheme offers high amounts of total utility cumulatively for all nodes, behaves equally fairly to all of them by assigning similar utilities and also consumes low amounts of power for all nodes, for the results evaluation obtained from all presented schemes, in this work [4] we investigated four different fairness notions (considering that the nodes of the network were clustered into two classes, based on the amount of motion in the captured scenes), each of which investigated fairness under a different point of view, considering different fairness and performance aspects at each time.

1) *Performance to Fairness Metric* (PF)

   This metric captures both relative performance and relative fairness issues. It assumes that the total utility achieved by both motion classes using a specific scheme is higher under one scheme compared to the utility achieved by all other competing schemes. Also, we considered that none of the examined schemes was simultaneously preferred by both motion classes compared to the other schemes. Assuming that the criterion that maximizes the unweighted version of the total system utility, namely the MTU, was used as the reference criterion for this metric, we defined the PF metric [12] as in Eq.(35).

2) *Jain's Index* (JI)

   This index measures how close to equal is a resource allocation for the two motion classes. Specifically, it is defined as [13]:

$$JI_{Cons}(U) = \frac{\left| \sum_{cl=1}^{C} U_{cl}^{Cons}(R_{\mathrm{s},cl}, R_{\mathrm{c},cl}, S)\right|^2}{C \cdot \sum_{cl=1}^{C} (U_{cl}^{Cons}(R_{\mathrm{s},cl}, R_{\mathrm{c},cl}, S))^2}, \tag{37}$$

   where $Cons$ refers to each considered scheme and U corresponds to the vector of utilities of all C motion classes. It takes values between 0 and 1 and this boundedness helps us to understand intuitively the fairness index. The closer the JI value is to unity, the more "equal" the resource allocation is for the two motion classes. Therefore, this metric provides a quantitative value to the fairness of the allocation.

3) *Total Utility Metric*

   This metric examines the total utility that a scheme will bring cumulatively from both motion classes. According to this metric, the most efficient scheme is the scheme that gathers the highest overall system utility, without examining how close are the utilities achieved by each class of nodes, but only the sum of all utilities as a whole. Specifically, this metric computes:

$$\sum_{cl=1}^{C} U_{cl}, \tag{38}$$

   for the C motion classes.

4) *Total Power Metric*

   This metric investigates the major issue of power consumption by each scheme. Each node of the VSN spends an amount of power in order to assure a reliable video transmission and to maintain the quality of the video reception. On the other hand, it is necessary to keep low amounts of power consumption, since the sensor nodes are battery-operated systems and the prolongation of the battery lifetime is an important issue. Furthermore, in a DS-CDMA system, increased transmission power for a node implies increased interference to the other nodes. Thus, low transmission power is required in order to avoid degradation of the video qualities of the other nodes. Therefore, the Total Power metric calculates the total amount of consumed power required cumulatively for all C motion classes, given by Eq.(36)

4.5 Distortion-Aware Joint Scheduling and Resource Allocation for Wireless Video Transmission

In our proposed system of [5], we took advantage of the interference reduction characteristics of both DS-CDMA and TDMA. Particularly, the time scheduling property of TDMA was used to coordinate transmissions of DS-CDMA based nodes. Thus, we utilized a hybrid DS-CDMA over TDMA system, henceforth denoted as HTCDMA. According to this HTCDMA technique, time is divided in time frames of duration t_f and each time frame is divided in N time slots of duration ts. Hence, $t_f = N\,ts$. During each time slot, more than one nodes are allowed to transmit simultaneously on a common frequency channel, as depicted in the example of Fig. 6. Each node is assigned a unique spreading code, which can be reused in consecutive time slots.

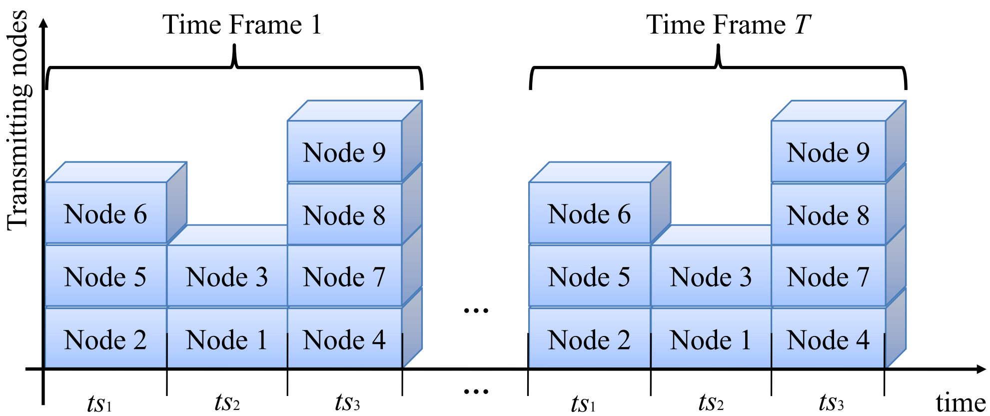

Figure 6: Example of scheduling in the proposed HTCDMA system, where the time frame is divided in three time slots.

A single-cell single hop system with K wireless nodes and one Base Station (BS) was considered. The nodes communicated the rate-distortion characteristics, (see Eq. (9)), to the BS. The BS exploited this information to optimally determine the subset of the transmitting nodes per time slot and the optimal resources (power level, source and channel coding rate) per transmitting node, over a whole time frame. This process was repeated periodically every T time frames. The parameter T was set by the base station. Moreover, it was assumed that each node was allowed to transmit only once within a time frame. Under the assumption of a constant spreading code length, L, and the constraint of identical chip rate, $R_{\text{chip},k}$, for each node k, the transmission bit rate for each node R_k was correspondingly constant during a time slot, since $R_k = R_{\text{chip},k}/L$. Furthermore, the constant bit rate R_k secured that the fraction $R_{\text{s},k}/R_{\text{c},k}$ was identical for each node.

Under these assumptions, this paper [5] coped with the problem of selecting a subset M_i of nodes for transmission per time slot i and the joint allocation of the source coding rate, $R_{\text{s},k}$, the channel coding rate, $R_{\text{c},k}$, as well as the power level S_k of each node k for all the time slots of a time frame, such that a function $\mathcal{F}(.)$ of the overall end-to-end expected video distortion is minimized. According to this, it needed to employ a distortion-related function $\mathcal{F}(.)$ that will guide the optimization process. For this purpose, in the present paper we utilized the NBS and the MAD optimization schemes.

In order to find the NBS, $\mathcal{G}(\mathbf{U}, dp)$ with $dp \in \mathbf{U}$, we had to maximize the Nash product. Particularly, we determined the subset of transmitting nodes per time slot i and the utilities vector U such that the Nash product is maximized over a time frame:

$$\max_{\substack{M_1, M_2, \ldots, M_N, \\ R_\mathrm{s}, R_\mathrm{c}, S}} \prod_{i=1}^{N} \prod_{k \in M_i} (U_k - dp_k)^{bp_k} , \tag{39}$$

subject to

$$U_k \geq dp_k, \tag{40}$$

$$S_{\min} \leqslant S_k \leqslant S_{\max}, \tag{41}$$

$$(R_{\mathrm{s},k}, R_{\mathrm{c},k}) \in \{(R_\mathrm{s}^1, R_\mathrm{c}^1), \ldots, (R_\mathrm{s}^Z, R_\mathrm{c}^Z)\}, \ Z \in \mathbb{N}^*, \tag{42}$$

$$\frac{R_\mathrm{s}^1}{R_\mathrm{c}^1} = \frac{R_\mathrm{s}^2}{R_\mathrm{c}^2} = \ldots = \frac{R_\mathrm{s}^Z}{R_{\mathrm{c},}^Z} = R_k, \tag{43}$$

where Z is the number of the available source and channel coding rates, and M_i is the set of the indices of the selected nodes for transmission per time slot i, which satisfies the following properties:

(i) $M_i \neq \varnothing, \forall\, i \in \{1, 2, \ldots, N\}$;

(ii) $M_1 \bigcap M_2 \bigcap \ldots \bigcap M_N = \varnothing$;

(iii) $M_1 \bigcup M_2 \bigcup \ldots \bigcup M_N = \{1, 2, \ldots, K\}$.

The bargaining powers $bp = (bp_1, bp_2, \ldots, bp_K)^\top$, that express which node is more favored by the bargaining rules [66], were all considered equal to $1/K$. Besides this, we assumed that dp is the lowest acceptable PSNR value and is determined by the application requirements.

Regarding he MAD criterion, it minimized the average end-to-end video distortion over a time frame, by optimally determining the subset of transmitting nodes per time slot i, as well as the source coding rate, $R^*_{\mathrm{s},k}$, channel coding rate, $R^*_{\mathrm{c},k}$, and power level, S^*_k for each node k, i.e.,

$$\min_{\substack{M_1, M_2, \ldots, M_N, \\ R_\mathrm{s}, R_\mathrm{c}, S}} \frac{1}{N} \sum_{i=1}^{N} \left(\frac{1}{|M_i|} \sum_{k \in M_i} E[D_{\mathrm{s+c},k}] \right) \tag{44}$$

subject to the constraints of Eqs. (41)-(43) and where $|.|$ denotes the cardinality of a set.

4.6 Resource Allocation in Visual Sensor Networks Using a Reinforcement Learning Framework

The quality of a video sequence is highly related with the lossy compression techniques applied at the encoder as well as with the number of occurred errors during wireless data transmissions.

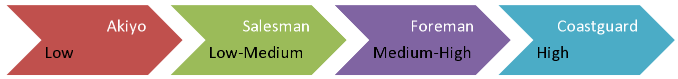

Figure 7: Motion level represented by each video sequence.

Consequently, in order to achieve the maximization of the network QoS, in this paper [6], we focused on both these problem aspects.

The H.264/AVC codec has the flexibility to determine the frequency of IDR-frames on the encoding side. Since IDR-frames are independently coded frames, the errors that occur within a GoP propagate to the following frames until the next IDR-frame is found. Generally, the more IDR-frames are included in a video stream, the more editable it is and the greater its size is. Since predictive coding techniques are applied during encoding, the effect of channel errors on the video can have a tremendous impact after video transmission over error-prone environments. Thus, it is important to apply techniques that ensure a tolerable level of QoS.

It is widely accepted that scene changes or large variations can happen at any location in a video stream. This means that it is important to consider the video content in order to wisely arrange each of the IDR-, P- and B-frames in a GoP. Clearly, in the beginning of a new scene or after an abrupt scene change, an IDR-frame insertion is required in order to prohibit poor prediction for the next frames, since this type of intra frames does not allow the following frames to use frames appearing before it as references. Alternatively, when low levels of motion are included in a video stream, it is more efficient to use more P- or B-frames, instead of IDR-frames, to enhance video coding performance.

In this work [6], we experimented on the GoP length, i.e., the distance between two consecutive IDR-frames, during the encoding process of the video sequences. We assumed that the nodes of the considered VSN record four different levels of motion: low, low-medium, medium-high and high. Thus, they were clustered in four motion classes, based on the motion level included in the scenes they recorded. Figure 7 presents the different motion levels represented by each considered video sequence.

Each of the video sequences was compressed using four different GoP lengths, at three different source coding rates. We simulated video transmission through the channel by dropping packets from the video streams, at three different BERs. Our previous experience with URDCs [24, 25], had shown that it is an efficient tool that can be used to express the expected distortion $E[D_{\mathrm{s+c},k}]$ of node k, as a function of the bit error probability (bit error rate), P_{b}, after channel decoding. Similarly, in this paper, we made use of the URDCs given by Eq. (9). Due to the fact that channel errors and packet drops occur randomly, the video distortion attributed to lossy compression and channel errors is a random variable. In light of this, the video distortion was averaged over a number of independent experiments. The parameters α and β of Eq. (9) were then determined through a mean squared error optimization procedure, using a small number of $(E[D_{\mathrm{s+c},k}], P_{\mathrm{b}})$ pairs.

Hence, each motion class had its own set of α and β parameters, which also depend on the source-channel coding rate and GoP length. Having compressed each video bitstream using four different GoP lengths, we tested all possible GoP length combinations of all video bitstreams. Each different combination resulted in different values for the α and β parameters. For each (α,β) pairwise values, we run the optimization procedure using various schemes. Those (α,β) values that satisfied the objective of each scheme were chosen as optimal. The GoP length for each motion class that produced the optimal (α,β) values was proven to be the most efficient one, since it led to the ultimate video quality enhancement.

Given that the K nodes of the VSN were grouped into M motion classes, it followed that the expected distortion $E[D_{\mathrm{s+c},cl}]$ for the motion class cl was a function of the source coding rate, for class cl, channel coding rate, for class cl, and power levels of all motion classes. The utility function was defined equivalently to the PSNR [25], measured in dB. The larger the value of the utility function, the better the video quality for motion class cl, and vice versa. The optimization criteria used in order to determine the nodes' transmission parameters were the MAD, NBS, and MTU.

Afterwards, we introduced the formulation of the resource allocation problem as an MDP [32] and we also presented the RL scheme, which was incorporated in the controller, i.e., the CCU. The resource allocation problem considered in this study [6] was treated as a discrete optimization problem (discrete nodes' transmission parameters). Although in the past this problem had been encountered using the heuristic optimization methodology of ES [24, 25], this was not feasible in the specific work. In our case, the controller had to select among a considerably larger set of possible variable combinations compared with the previous works. Additionally, the major handicap of the ES algorithm is its computational complexity, which renders its use prohibitive in the online mode.

According to our proposed methodology, the learning optimization problem was formulated in a sequential decision framework and was modeled as an MDP [32]. Roughly speaking, an MDP involves a decision agent (controller) that repeatedly observes the current state of the controlled system, takes a decision among the ones allowed in that state, and then observes a new state as well as a reward that will drive its future decisions. The MDP is typically denoted as a tuple $\{\mathcal{X},\mathcal{U},\mathcal{R},\mathcal{P},\gamma\}$, where $\mathcal{X}$ and $\mathcal{U}$ are the state and action spaces, respectively; $\mathcal{R}$ is the reward function that specifies the importance of each transition; $\mathcal{P}$ is the state transition distribution; and $\gamma \in [0,1]$ is the discount factor that determines the importance of the future rewards.

In the learning problem of resource allocation studied in this paper [6], we considered the state space as the Cartesian product of eight sets;

$$\mathcal{X} \triangleq C_1 \times C_2 \times C_3 \times C_4 \times S_1 \times S_2 \times S_3 \times S_4.$$

In this way, a state was represented as an eight-dimensional vector. Each of the first four variables denoted the source-channel coding rate combination for the motion class cl ($C_{cl} \in \{1,2,3\}$) and each of the remaining variables denoted the power level for the motion class cl, ($S_{cl} \in \{5,7,9,11,13,15\}$), $cl = \{1,\ldots,4\}$. Moreover, the action space consisted of 17 actions, two for each dimension. At each time step, the controller was able to increase or decrease one of the state variables. Additionally, we gave the ability to the controller to leave the state variables unchanged, by remaining at the same state. Regarding the reward function, it specified the gain obtained during a transition from the current state $\boldsymbol{x}$ to the next state $\boldsymbol{x'}$, as given by the difference between the values of the objective functions corresponding to the specific states.

A stationary policy $\pi : \mathcal{X} \rightarrow \mathcal{U}$ is a mapping from states to actions and denotes a mechanism for choosing actions appropriately. The notion of value function is of central interest in RL tasks. Given a policy π, the value $V^{\pi}(\boldsymbol{x})$ of a state $\boldsymbol{x}$ was defined as the expected discounted sum of rewards, obtained, starting from this state and following the policy:

$$V^{\pi}(\boldsymbol{x}) = E_{\pi}\left[\mathcal{R}(\boldsymbol{x}_t) + \gamma V^{\pi}(\boldsymbol{x}_{t+1}) | \boldsymbol{x}_t = \boldsymbol{x}\right]. \tag{45}$$

This was actually a Bellman equation, which expressed a relationship between the value of a state and the values of its successor states. Similarly, the state-action value function $Q(\boldsymbol{x}, u)$ denoted the expected cumulative reward as received by taking action u in state $\boldsymbol{x}$, and following policy π:

$$Q^{\pi}(\boldsymbol{x}, u) = E_{\pi}\left[\mathcal{R}(\boldsymbol{x}_t) + \gamma V^{\pi}(\boldsymbol{x}_{t+1}) | \boldsymbol{x}_t = \boldsymbol{x}, u_t = u\right]. \tag{46}$$

The objective of an RL task is to estimate an optimal policy π^* by choosing actions that yield the optimal state-action value function: $\pi^*(\boldsymbol{x}) = \arg\max_u Q^*(\boldsymbol{x}, u)$.

The TD family of algorithms [31] provides an elegant framework for solving prediction problems. The main advantage of this class of algorithms is its ability to learn directly from raw experience, without any further information. One of the most popular TD algorithms is the SARSA algorithm [70], which is a bootstrapping technique. More specifically, this is an on-policy control method, which is based on the state-action value function estimation. The predicted Q value of the new visited state-action pair and the received reward were used to calculate an improved estimate for the Q value of the previous visited state-action pair:

$$\delta_t = r_t + \gamma Q(\boldsymbol{x}_{t+1}, u_{t+1}) - Q(\boldsymbol{x}_t, u_t). \tag{47}$$

The above quantity is known as the one-step TD error and was used for adjusting the weights of the policy, by performing a stochastic gradient descent scheme:

$$Q(\boldsymbol{x}_t, u_t) \leftarrow Q(\boldsymbol{x}_t, u_t) + \eta\delta_t, \tag{48}$$

where the parameter η is the learning rate that controls the update rule. Moreover, we combined the SARSA algorithm with the eligibility traces, SARSA(λ) [70], allowing the update rule to propagate the TD error backward over the current trajectory of states. It has been proven that TD algorithms are able to find the optimal policy with probability 1 [71]. This fact gave us the opportunity to find the optimal variable combination with certainty, starting from each initial state and following the learned policy.

4.7 Priority-Based Cross-Layer Optimization for Multihop DS-CDMA Visual Sensor Networks

In this work [7], we considered a multihop wireless VSN with K source nodes and M relay nodes. All nodes communicate with each other using DS-CDMA at the physical layer. Each node uses

L chips for a single bit transmission, thus a node n is associated with a spreading sequence of length L. The interference from other nodes to the node of interest is modeled as AWGN. For a wireless VSN with $N = K + M$ nodes, a node's received power at a specific distance from node n is $S_n^{\mathrm{rec}} = E_n R_n$ in Watts. E_n is the energy per bit and $R_n = R_{\mathrm{s},n}/R_{\mathrm{c},n}$, $n = 1, 2, \ldots, N$, is the total transmission bit rate for source and channel coding, where $R_{\mathrm{s},n}$ is the source coding rate and $R_{\mathrm{c},n}$ the channel coding rate. We assumed that interference exists on each link across the path to the CCU from nodes that are in the effective transmission range. Letting $\mathbf{J}$ be the set of interfering nodes for each hop h, it is assumed that $|\mathbf{J}| \leq N$, where $|.|$ denotes the cardinality of a set. The energy per bit to MAI and noise ratio is different in each link, depending on the nodes causing interference to the considered node n and can be expressed for the h-th hop of a path as follows:

$$\frac{E_n}{I_0 + N_0} = \frac{\frac{S_n^{\mathrm{rec}}}{R_n}}{\sum_{j=1, j \neq n}^{|\mathbf{J}|} \frac{S_j^{\mathrm{rec}}}{W_{\mathrm{t}}} + N_0} \tag{49}$$

where $I_0/2$ is the two sided noise power spectral density due to MAI, $N_0/2$ is the two sided noise power spectral density of background noise in W/Hz, W_{t} is the total bandwidth in Hz and $S_{\mathrm{j}}^{\mathrm{rec}}$ is the received power of node $j \in \mathbf{J}$ that causes interference to node n. Given that the transmission bit rate is equal to R_{chip}/L, where the chip rate R_{chip} is the same for all nodes of the network, we were able to obtain different values for the transmission bit rates of each hop using a different spreading code length L. A smaller L increases the transmission bit rate but it also decreases the energy per bit. Thus, the BER is also increased.

As signal energy decreases across the link from a source node to a receiver node, the effective transmission range of a node n and the received signal power S_n^{rec} at a distance d from node n had to be estimated. For this purpose, we took into account two well-known radio propagation models; the Free Space model and the TRGR model [38]. Regarding these models, let h_r and h_t be the heights of receiver and transmitter antennas respectively, $l \geq 1$ the system loss factor, λ the wavelength of the carrier signal, G_t and G_r the transmit and receive antenna gains, respectively, and S_n^{trans} the transmission power of node n. For a node n at distance d from the receiver, the *cross-over distance* $d_0 = (4\pi h_r h_t \sqrt{l})/\lambda$ determines which model is used as follows:

(i) If $d < d_0$, the received power is given by the Friis formula of Free Space model:

$$S_n^{\mathrm{rec}}(d) = S_n^{\mathrm{trans}} \frac{G_t G_r \lambda^2}{((4\pi)^2 d^2 l)} \qquad \text{(FS Model)}. \tag{50}$$

(ii) If $d > d_0$, the received power is given by:

$$S_n^{\mathrm{rec}}(d) = S_n^{\mathrm{trans}} \frac{G_t G_r h_t^2 h_r^2}{(d^4 l)} \qquad \text{(TRGR Model)}. \tag{51}$$

For a certain transmission power of a node, the received power at a distance d can be derived from the aforementioned models.

The video sequences were compressed using the H.264/AVC standard. Also, regarding channel coding, we used RCPC codes [14], so as to estimate the bit error probability using Viterbi's upper bounds. The nodes of the considered wireless VSN could transmit video sequences with different motion levels. The CCU managed the received power, source coding, and channel coding rate aiming at the optimal performance for all nodes.

We proposed an efficient method for solving the resource allocation problem for a multi-hop DS-CDMA wireless VSN, formulated as follows: Under the constraint that imposes the same transmission bit rate R_j, $j \in \mathbf{J}$, for the interfering nodes of hop h, determine for each source node k the source coding rate $R_{\mathrm{s},k}$, the channel coding rate $R_{\mathrm{c},k}$ and the received power $S^{\mathrm{rec}}_{\mathrm{S},k} \in \left[S^{min}_{\mathrm{S}}, S^{max}_{\mathrm{S}}\right]$, and for each relay node m the channel coding rate $R_{\mathrm{c},m}$ and the received power $S^{\mathrm{rec}}_{\mathrm{R},m} \in \left[S^{min}_{\mathrm{R}}, S^{max}_{\mathrm{R}}\right]$, so that a function of the overall end-to-end expected video distortion $E[D_{\mathrm{s+c},k}]$ for each source node k is minimized, i.e.

$$(R^*_{\mathrm{s}}, R^*_{\mathrm{c}}, S^{\mathrm{rec}*}) = \arg \min_{R_{\mathrm{s}}, R_{\mathrm{c}}, S^{\mathrm{rec}}} f(E[D_{\mathrm{s+c},1]}, \ldots, E[D_{\mathrm{s+c}],K}]),$$

where $S^{\mathrm{rec}} = (S^{\mathrm{rec}}_{\mathrm{S},1}, \ldots, S^{\mathrm{rec}}_{\mathrm{S},K}, S^{\mathrm{rec}}_{\mathrm{R},1}, ..., S^{\mathrm{rec}}_{\mathrm{R},M})^\top$;
$R_{\mathrm{s}} = (R_{\mathrm{s},1}, \ldots, R_{\mathrm{s},K})^\top$;
$R_{\mathrm{c}} = (R_{\mathrm{c,S},1}, \ldots, R_{\mathrm{c,S},K}, R_{\mathrm{c,R},1}, \ldots, R_{\mathrm{c,R},M})^\top$
are the vectors of received power, source coding rate and channel coding rate of source nodes $k = 1, 2, \ldots, K$ and relay nodes $m = 1, 2, \ldots, M$, respectively. The type of the function $f(.)$ is different for each one of the deployed optimization criteria.

Assuming that $Pb_{h,k}$ is the bit error probability for hop h and the source node k, then the end-to-end bit error probability across an H-hop path for k is:

$$Pb_k = 1 - \prod_{h=1}^{H} (1 - Pb_{h,k}). \tag{52}$$

In conjunction with Eq. (52), the expected distortion due to lossy compression and channel errors was given by the model used in [24]:

$$E[D_{\mathrm{s+c},k}] = \alpha_k \left[\log_{10} \left(\frac{1}{1 - \prod\limits_{h=1}^{H} (1 - Pb_{h,k})} \right) \right]^{-\beta_k} \tag{53}$$

where parameters $\alpha_k > 0$ and $\beta_k > 0$ depend on the motion level of the transmitted video sequence and the source coding rate and may vary in time. Values of α_k for high motion video sequences are generally greater than those for low motion video sequences [57]. These parameters were determined using mean squared error optimization for a few ($E[D_{\mathrm{s+c},k}]$, Pb_k) pairs and the $E[D_{\mathrm{s+c},k}]$ values were estimated at the encoder using the Recursive Optimal Per-pixel Estimate (ROPE) model [72]. As an estimate of the bit error probabilities for the transmitting node n at the h-th hop (after channel decoding), we used the Viterbi upper bound for RCPC codes, which is

$$Pb_{h,n} = \frac{1}{2P} \sum_{d=d_{\mathrm{free}}}^{\infty} c_d \,\mathrm{erfc} \left(\sqrt{d R_{\mathrm{c},n} \left[\frac{E_n}{I_0 + N_0} \right]} \right) \tag{54}$$

NBS Variant	Bargaining Power per Source Node
e.NBS	$bp_k = 1/K$
w.NBS	$bp_k = \alpha_k / \sum_{j=1}^{K} \alpha_j ; j = 1, 2, \ldots, K$

Table 1: Bargaining powers for the e.NBS and w.NBS criteria.

where P is the period of the used code, d_{free} is the free distance of the code, c_d is the information error weight, and erfc(.) is the complementary error function given by $\text{erfc}(z) = \left(2 \int_z^{\infty} \exp(-t^2)dt\right)/\sqrt{\pi}$.

For the minimization of the distortion, three priority-based optimization criteria were used. The first two criteria were based on the Nash bargaining solution from game theory, which allocates resources as a result of the bargaining game among the nodes. The consideration for the bargaining powers for each NBS variant employed in this paper is depicted in Table 1. The last criterion minimized a weighted aggregation of the distortions of the videos of all nodes. These criteria resulted in global optimization problems that were resolved by the PSO algorithm, an effective and efficient algorithm with linear complexity to both the number of the iterations and utilized particles [46].

4.8 Power-Aware QoS Enhancement in Multihop DS-CDMA Visual Sensor Networks

In this work [8], we considered a multihop DS-CDMA wireless VSN. We assumed that interference exists on each link across the path to the base station from nodes that are in the effective transmission range. A constraint imposed in the considered multihop wireless VSN was that each relay node m needs to use a sufficient bit rate for the simultaneous forwarding of the video data, which is related to source coding rate of the related source nodes. Hence, the transmission bit rate of a relay m is

$$R_m \geq \frac{\sum_{z \in \mathbf{Z}} R_{\text{s},z}}{R_{\text{c,R},m}}, \tag{55}$$

where $\mathbf{Z}$ is the set that includes the source nodes that use relay node m for their data forwarding and $R_{\text{c,R},m}$ is the channel coding rate for the relay node m.

We assumed clear line of sight for our model and in order to calculate the received power at a node, we employed a mixed scenario that consists of two propagation models; the FS and TRGR models [38] as described in Section 4.7. In the present paper [8], we proposed a method that offers enhancement of the end-to-end video quality and manages the transmitted power of the wireless VSN nodes. Our method aimed at optimally allocating the source and channel coding rates and the transmitted powers among the source nodes of a wireless VSN and simultaneously the necessary channel coding rates and transmitted powers to the relay nodes. For the assignment of the available resources, a compromise between the power consumption and the distortion of the delivered video sequences had to be established. Therefore, we define a bi-objective problem that actually minimizes a function of both the expected distortions of the received videos and the received powers.

We first defined the vectors for the source and channel coding rates, and the received powers of source nodes $k = 1, 2, \ldots, K$ and relay nodes $m = 1, 2, \ldots, M$, respectively, as presented in Section 4.7. For each source node k, the source coding rate $R_{\mathrm{s},k}$, the channel coding rate $R_{\mathrm{c,S},k}$ and the received power $S_{\mathrm{S},k}^{\mathrm{rec}} \in \left[S_{\mathrm{S}}^{min}, S_{\mathrm{S}}^{max}\right]$ and for each relay node m the channel coding rate $R_{\mathrm{c,R},m}$ and the received power $S_{\mathrm{R},m}^{\mathrm{rec}} \in \left[S_{\mathrm{R}}^{min}, S_{\mathrm{R}}^{max}\right]$ were determined, so that the weighted aggregation of the expected video distortion $E[D_{\mathrm{s+c},k}]$ of all source nodes and the aggregation of the received powers from both the source and the relay nodes is minimized, i.e.

$$\min_{R_{\mathrm{s}}, R_{\mathrm{c}}, S^{\mathrm{rec}}} \left(\gamma \sum_{k=1}^{K} w_k E\{D_{\mathrm{s+c},k}\} + \delta \sum_{n=1}^{K+M} S_n^{\mathrm{rec}} \right), \tag{56}$$

where K is the total number of nodes constituting the network, and M is the total number of the relay nodes. The amount w_k is a weighting factor for the aggregated distortion, and γ, δ are weighting factors with $\gamma + \delta = 1$. The weighting factors (γ, δ) indicate the tradeoff among the two formulated objectives, i.e. the enhancement of video quality versus the minimization of the transmission power consumption. The problem was solved under the consideration of the constraints that all interfering nodes transmit using the same bit rate and that each relay node m uses a sufficient bit rate for the simultaneous forwarding of the received video data (Eq. (55)).

Using different weights w_k for the aggregation of the end-to-end video distortion of all source nodes (see Eq. (56)), we can favor different source nodes. Thus, the resources were allocated so that nodes with higher weights can deliver videos with enhanced end-to-end video quality. We considered the following different cases:

1. Using Equal Weights for the Aggregation of Distortion (EWAD): We assumed that all source nodes had equal weights, i.e. $w_k = 1$, which means that their video quality enhancement was of equal importance.

2. Using Motion-related Weights for the Aggregation of Distortion (MWAD): The weights were motion-related, since they were tuned according to parameters α_k, which reflect the motion level of each recorded video. The weight for each source node k was:

$$w_k = \frac{\alpha_k}{\sum_{i=1}^{K} \alpha_i}, \tag{57}$$

   given that $\sum_{k=1}^{K} w_k = 1$. In particular, high motion nodes had a higher priority in the minimization of their distortion, and thus, in the enhancement of the delivered video quality.

In the proposed scheme, the received and transmitted powers were assumed to take continuous values within a specified range, whereas the source and channel coding rates could only have discrete values. As the formulated multi-variable optimization problems were mixed-integer problems, the PSO algorithm was selected [46]. PSO is an efficient and adjustable population-based optimization algorithm that was inspired by social behavior of a colony, e.g. a flock of birds. This technique actually mimics the behavior of a population, the swarm, that consists of a number of individuals, the particles. The swarm has a fixed size of particles that search for the function minimum in a multidimensional space.

4.9 A No-Reference Bitstream-Based Perceptual Model for Video Quality Estimation of Videos Affected by Coding Artifacts and Packet Losses

NR models have a limited source of input information compared to FR or RR models. Due to this, we extracted a large set of bitstream-based features that are expected to affect perceptual video quality in order to enhance prediction accuracy. These features, based on how they relate to the different types of distortion, can be characterized as content features, signal features, error features, features related to the distance from the reference frame used for concealment, and motion features. Table 2 summarizes the used features and the attributes through which they are related towards video quality.

Table 2: Description of the employed features.

Feature	Description	Attribute
1.Intra[%]	The percentage of I coded MBs in a slice.	Content Structure
2.I4 $\times$ 4inIslice[%]	The percentage of MBs of size 4×4 in an I slice.	Content Structure
3.I16 $\times$ 16inIslice[%]	The percentage of MBs of size 16×16 in an I slice.	Content Structure
4.IinPslice[%]	The percentage of I coded MBs in a P slice.	Content Structure
5.P[%]	The percentage of P coded MBs in a slice.	Content Structure
6.PSkip[%]	The percentage of P MBs coded as PSkip in a slice.	Content Structure
7.P16 $\times$ 16[%]	The percentage of P MBs coded with no sub-partition of MBs in a slice.	Content Structure
8.P8 $\times$ 16[%]	The percentage of P MBs coded with 8×16 and 16×8 partition of MBs in a slice.	Content Structure
9.P8 $\times$ 8[%]	The percentage of P MBs coded with 8×8 partition of MBs in a slice.	Content Structure
10.P8 $\times$ 8Sub[%]	The percentage of P MBs coded with 8×8 in a sub-partition of MBs in a slice.	Content Structure
11.P4 $\times$ 8[%]	The percentage of P MBs coded with 4×8 and 8×4 sub-partition of MBs in a slice.	Content Structure
12.P4 $\times$ 4[%]	The percentage of P MBs coded with 4×4 sub-partition of MBs in a slice.	Content Structure
13-20.B modes	B modes that correspond to the same features as given in features 5 to 12, but for B MBs.	Content Structure
21-22.$\Delta \mathrm{MV_x}$, $\Delta \mathrm{MV_y}$	The average measures of motion vector difference values for x and y direction in a slice.	Content Motion
23-24.$\mathrm{avg(MV_x), avg(MV_y)}$	The average measures of motion vector values for x and y directions in a slice.	Content Motion
25.$\mathrm{MV_0}$[%]	The percentage of motion vector values equal to zero for x and y direction in a slice.	Content Motion
26.$\Delta \mathrm{MV_0}$[%]	The percentage of motion vector difference values equal to zero in a slice.	Content Motion
27.Motion Intensity 1	$\sum_{i=1}^{N} \sqrt{{MV_{x_i}}^2 + {MV_{y_i}}^2}$ $MV_a, a \in [x, y]$ represents the average value of motion vectors in an MB in a-direction N is the total number of MBs in a slice.	Content Motion
28.Motion Intensity 2	$\sqrt{avg(MV_x)^2 + avg(MV_y)2}$	Content Motion
29-30. $\mathrm{\lvert avg(MV_x)\rvert}$, $\mathrm{\lvert avg(MV_y)\rvert}$	The average measures of absolute motion vector values for x and y direction in a slice.	Content Motion
31.Motion Intensity 3	$\sum_{i=1}^{N} \sqrt{\lvert(MV_x)\rvert_i^2 + \lvert(MV_y)\rvert_i^2}$ $\lvert(MV_a)\rvert$ represents the absolute value of motion vectors in an MB in a-direction	Content Motion
32.Motion Intensity 4	$\sqrt{\lvert avg(MV_x)\rvert^2 + \lvert avg(MV_y)\rvert^2}$.	Content Motion
33.NotStill	Boolean. True, if the magnitude of a slice is over $1/10^{\text{th}}$ of the highest magnitude value of all sequences.	Content Motion
34.HighMot	Boolean. True, if the magnitude of a slice is over $8/10^{\text{th}}$ of the highest magnitude value of all sequences.	Content Motion
35-36.MaxResEngy, MeanResEngy	The maximum and mean residual energy over all the MBs of a slice.	Signal
37.LR	Boolean. True, if a slice is lost.	Error
38.LostSinFrm	Number of lost slices in a frame.	Error
39.Height	Vertical location of the lost slice within the frame.	Error
40.TMDR	Number of frames affected by a lost slice.	Error
41.SpatialExtend	Number of consecutive lost slices in a frame.	Error
42.SpatialExtend2	Boolean. True, if SpatialExtend=2.	Error
43.SpatialExtendFrm	Boolean. True, if all slices of a frame are lost.	Error
44.Error1Frm	Boolean. True, if TMDR=1.	Error
45.DistToRef	Distance in frames between the current frame and the reference frame used for concealment.	Concealment
46.FarConceal	Boolean. True if $\lvert$DistToRef$\rvert \geq 3$.	Concealment

All of these features were computed for each slice of the considered sequences, while they were averaged to take an estimation for each sequence as a whole. Afterwards, we employed the

LASSO regression method [73]. It is a linear model that can be used for both feature selection and video quality estimation [74]. It is useful in some contexts due to its tendency to prefer solutions with fewer parameter values, effectively reducing the number of variables upon which the given solution is dependent. This method minimizes the residual sum of squares, subject to the sum of the absolute value of the coefficients being less than a constant. Mathematically, for a given nonnegative λ value, it solves the following penalized least squares problem:

$$\min_{w}\left(\frac{1}{2}\sum_{i=1}^{n}\Big(y_i - w^{\top}\phi(x_i)\Big)^2 + \frac{\lambda}{2}\sum_{j=1}^{m}|w_i|\right). \tag{58}$$

From Eq. (58) we observe that the fitted coefficients minimize the mean squared difference between the n-by-1 vector y of measured perceptual quality values and the vector $\phi(x_i)$ of m-by-1 values at observation x_i, which includes the values for all examined features for a particular slice, and w is the m-by-1 vector of regression coefficients, including the intercept w_0. The minimization problem involves the penalization of the sum of the absolute values of the regression coefficients. The parameter λ controls the amount of the regularization. The larger the λ values are, the more coefficients w_i are driven to zero, leading in this way to a sparse model representation. For our experiments, we selected the λ value that corresponds to the lowest Root Mean Squared Error (RMSE) value of the first term of Eq. (58).

According to Video Quality Experts Group (VQEG) phase II report on the validation of objective methods of VQA [75], the performance of an objective quality prediction model can be evaluated by the Pearson Correlation Coefficient (PCC), which describes the prediction accuracy, the Spearman Rank Order Correlation Coefficient (SROCC), which describes the monotonicity, and the consistency in terms of the Outlier Ratio (OR). In light of this, in this work [9], we presented statistics considering all these metrics as well as we assessed the prediction error of our models (for the MOS, SSIM and VQM) using the Normalized Mean Squared Error (NRMSE) and Mean Absolute Error (MAE) metrics. Furthermore, we studied the number of features selected by LASSO in order build our models.

5 Results and Discussion

5.1 A Study on Visual Sensor Network Cross-Layer Resource Allocation Using Quality-Based Criteria and Metaheuristic Optimization Algorithms

Based on the observation that high values of the parameter α (see Eq. (11)) imply high video sequence motion and vice versa, we assumed that the K nodes of the network were clustered into $C = 2$ motion classes, namely a *high-motion* and a *low-motion* class. The “Foreman” video sequence was used to represent the class of nodes that detect high motion levels, while the “Akiyo” video sequence was used to represent the class of nodes that capture more stationary fields. The resolution of both video sequences was the Quarter Common Intermediate Format (QCIF). Thus, one set of URDC curves was needed per video sequence.

The procedure for the computation of the expected video distortion can be concisely described as follows: for given BER, we determine the rate of the packet loss according to the Real-Time Transport Protocol (RTP). Then, packets are dropped from the video bit stream under investigation. We continue decoding the corrupted video sequence with the H.264/AVC video codec and, finally, the expected video distortion is obtained. Due to the existence of random channel errors in VSNs, the same procedure is repeated for 300 times and the expected video distortion is averaged over all these experiments to offer a more reliable estimation.

After the computation of the expected video distortion, the parameters α and β of Eq. (11) were determined using least squares optimization from data obtained using a few BERs. Specifically, we considered the BER values 10^{-7}, 10^{-6}, and 10^{-5}, while each of the "Foreman" and "Akiyo" video sequences was compressed at 32 kbps, 48 kbps, 64 kbps, 72 kbps, and 96 kbps. Furthermore, the characteristics for both video sequences were obtained at a rate of 15 frames per second.

The employed modulation scheme was the BPSK, while RCPC codes with mother code of rate 1/4 were used for channel coding [14]. Also, the considered target bit rate constraints were equal to 96 kbps and 144 kbps. Thus, the corresponding source-channel coding rate combinations for each motion class, resulting from the above bit rate constraints were,

(a) $R_{\text{target}} = 96$ kbps that results in,

$$(R_{\text{s,high}}, R_{\text{c,high}}), (R_{\text{s,low}}, R_{\text{c,low}}) \in \{(32, 1/3), (48, 1/2), (64, 2/3)\}.$$

(b) $R_{\text{target}} = 144$ kbps that results in,

$$(R_{\text{s,high}}, R_{\text{c,high}}), (R_{\text{s,low}}, R_{\text{c,low}}) \in \{(48, 1/3), (72, 1/2), (96, 2/3)\}.$$

For the power levels S, we assumed continuous values within the range $\mathbf{S} = [5.0, 15.0]$ (Watts), while for the bandwidth W_t two different values were examined, namely 20 MHz and 15 MHz. The total number of nodes that composed our network was $K = 100$.

1) Algorithms Parameters

PSO was considered with its default parameter set defined in Section 4.1.3. Also, a swarm of $N = 40$ particles was employed, under the ring topology of radius $r = 1$. In our problem, each particle x_i was 4-dimensional, defined as,

$$x_i = \left(S_{\text{high}},\, S_{\text{low}},\, R_{\text{s+c,high}},\, R_{\text{s+c,low}}\right)^{\top}, \qquad i = 1, 2, \ldots, 40,$$

containing the power level and the source-channel coding rate combination for each motion class (denoted as "high" and "low", respectively). Furthermore, the discrete parameters, i.e., source and channel coding rate combinations, were represented in the particle with continuous values within the range $\mathbf{R} = [0.6, 3.4]$. However, they were rounded to the nearest integer for the particle's evaluation. Specifically, we assumed the following correspondences,

$$R_{\text{target}} = 96 \text{ kbps} \begin{cases} 1 \longrightarrow (32, 1/3) \\ 2 \longrightarrow (48, 1/2) \\ 3 \longrightarrow (64, 2/3) \end{cases},$$

and

$$R_{\text{target}} = 144 \text{ kbps} \begin{cases} 1 \longrightarrow (48, 1/3) \\ 2 \longrightarrow (72, 1/2) \\ 3 \longrightarrow (96, 2/3) \end{cases} .$$

Besides that, the maximum velocities were set based on the MoC estimation procedure described in Section 4.1.3. The corresponding values of γ in Eq. (21) for the 4 component directions in our problem were determined as follows,

$$\gamma^{\text{MAD}} = (0.1, 0.1, 0.03, 0.03)^\top, \qquad \gamma^{\text{MMD}} = (1, 1, 1, 1)^\top.$$

For each problem instance, PSO was executed 30 times for a maximum number of 1000 iterations and the best solution was recorded.

Regarding the AS method, it was also applied on each problem instance 30 times from different initial conditions. However, AS was capable of providing only the power levels, since it works only on continuous search spaces. For the discrete source-channel coding rate combinations, we used exhaustive search among all possible pair values, i.e., 3 admissible values for each of the two motion classes, resulting in $3 \times 3 = 9$ cases. Thus, a single application of AS required 9 optimization runs, one for each discrete combination, and the final solution was selected as the best one among the obtained 9 solutions.

Finally, identical experiments were conducted using the proposed hybrid algorithm HPSOAS. The parameter setting of HPSOAS was the same with that of PSO. HPSOAS exhibited similar performance with PSO in terms of solution quality for each problem instance. Note that all algorithms (PSO, AS, HPSOAS) were equipped with exactly the same total computational budget in terms of function evaluations, namely 40000 function evaluations, in order to achieve fair comparisons among them.

2) Presentation and Analysis of Results

All experiments were conducted on an Intel® Core™ 2 Quad CPU @ 2.50 GHz with 4.00 GB RAM, using the Matlab environment. For each problem instance, PSO and HPSOAS converged on the same solutions in all 30 experiments. Specifically, the obtained values of the objective functions (for the two optimization criteria) were identical up to 15-20 decimal digits, and therefore, they were considered to be essentially identical. However, this was not the case for AS, which produced inferior solutions in some cases due to its dependency on the initial conditions and the peculiarities of the objective function landscape. Nevertheless, in the rest problem instances it achieved the same solutions as the other two algorithms.

Our first group of experiments was conducted under the assumption that thermal and background noise were neglected, namely $N_0 = 0$ W/Hz. The experiments were repeated in a second round, assuming that the aforementioned noise was significant. In this case, noise of magnitude $N_0 = 10^{-7}$ W/Hz was added in our computations.

In the case where thermal and background noise were neglected and the AWGN was introduced entirely from the interference among the nodes, PSO detected a multitude of solutions for the power levels of both motion classes, all of which had the same ratio $S_{\text{high}}/S_{\text{low}}$, up to $4-5$ decimal digits.

All these solutions achieved the best objective values for both the MAD and MMD optimization criteria. This is a consequence of the fact that the ratio E_k/I_0 in Eq. (7) is invariant under the multiplication of all power levels with the same constant. Therefore, estimation of the optimal ratio $S_{\text{high}}/S_{\text{low}}$ becomes the main goal rather than the determination of specific values for the power levels. In contrast to the power levels, the corresponding optimal source and channel coding rate combinations were unique in all solutions provided by PSO. Moreover, when thermal and background noise were added, PSO reported unique solutions for all transmission parameters. It is worth mentioning that the video quality for each motion class $cl \in \{1, 2\}$, was estimated by using the PSNR, as described in Eq. (27), measured in dB.

Tables 40-36 report the obtained direction components of the solution vectors (transmission parameters) that correspond to the best objective values of both MAD and MMD, by all algorithms (the inferior solutions produced by AS in some cases are omitted), for the case where thermal and background noise were considered to be negligible, namely $N_0 = 0$ W/Hz. More specifically, the tables report the obtained source coding rates, channel coding rates, power levels and PSNR values, for both motion classes, optimization criteria and different node distributions and settings of the bit rate and bandwidth values. Since in this case we were interested in the optimal power level ratios, rather than the determination of the specific values of S_{high} and S_{low}, we cited indicative S_{high} and S_{low} values that correspond to the best objective value.

Tables 37-10 report the corresponding results under the assumption that thermal and background noise power spectral density are equal to $N_0 = 10^{-7}$ W/Hz. The corresponding tables per combination of bit rate and bandwidth are summarized below,

(a) Bit rate 96 kbps and bandwidth 20 MHz: Tables 40 and 38.

(b) Bit rate 96 kbps and bandwidth 15 MHz: Tables 31 and 8.

(c) Bit rate 144 kbps and bandwidth 20 MHz: Tables 33 and 9.

(d) Bit rate 144 kbps and bandwidth 15 MHz: Tables 35 and 10.

The $K = 100$ nodes of the network were assigned to the two motion classes in different proportions, called *node distributions*. Each line in the tables corresponds to a different node distribution, denoted as "$N_{\text{high}} - N_{\text{low}}$", where

$$N_{\text{high}}, N_{\text{low}} \in \{10, 30, 50, 70, 90\}, \quad N_{\text{high}} + N_{\text{low}} = K = 100,$$

meaning that the corresponding classes consist of a number of N_{high} nodes capturing high-motion scenes and N_{low} nodes capturing low-motion scenes, respectively. Moreover, the combination of source-channel coding rates, the power level and the PSNR of the high-motion class are represented as $(R_{\text{s,high}}, R_{\text{c,high}})$, S_{high}, $PSNR_{\text{high}}$, respectively, while $(R_{\text{s,low}}, R_{\text{c,low}})$, S_{low}, and $PSNR_{\text{low}}$, are the corresponding parameters for the low-motion class.

A close inspection of the results, demonstrates that the MAD criterion works favorably for the low-motion class of nodes, equipping it with better image quality than the high-motion class. Concerning the MMD criterion, it is rather unbiased, offering identical PSNR values to both motion

Table 3: $R_{\text{target}} = 96\,\text{kbps},\ W_t = 20\,\text{MHz},\ N_0 = 0$ W/Hz.

MAD						
$N_{\text{high}} - N_{\text{low}}$	$(R_{\text{s,high}}, R_{\text{c,high}})$	S_{high}	$(R_{\text{s,low}}, R_{\text{c,low}})$	S_{low}	$PSNR_{\text{high}}$	$PSNR_{\text{low}}$
$10 - 90$	$(64, 2/3)$	10.7080	$(64, 2/3)$	5.9845	32.9787	36.7642
$30 - 70$	$(64, 2/3)$	8.6240	$(64, 2/3)$	5.0000	31.3844	35.1131
$50 - 50$	$(64, 2/3)$	15.0000	$(32, 1/3)$	7.0428	30.9419	32.8537
$70 - 30$	$(48, 1/2)$	15.0000	$(32, 1/3)$	7.6070	29.2296	32.2582
$90 - 10$	$(48, 1/2)$	9.8451	$(32, 1/3)$	5.0000	28.2705	31.2943
MMD						
$N_{\text{high}} - N_{\text{low}}$	$(R_{\text{s,high}}, R_{\text{c,high}})$	S_{high}	$(R_{\text{s,low}}, R_{\text{c,low}})$	S_{low}	$PSNR_{\text{high}}$	$PSNR_{\text{low}}$
$10 - 90$	$(64, 2/3)$	13.3488	$(64, 2/3)$	5.0000	35.7218	35.7218
$30 - 70$	$(64, 2/3)$	12.6814	$(32, 1/3)$	5.0000	33.4049	33.4049
$50 - 50$	$(64, 2/3)$	13.0847	$(32, 1/3)$	5.0000	31.6114	31.6114
$70 - 30$	$(64, 2/3)$	13.4344	$(32, 1/3)$	5.0000	29.7737	29.7737
$90 - 10$	$(48, 1/2)$	15.0000	$(32, 1/3)$	5.7234	28.3919	28.3919

Table 4: $R_{\text{target}} = 96\,\text{kbps},\ W_t = 15\,\text{MHz},\ N_0 = 0$ W/Hz.

MAD						
$N_{\text{high}} - N_{\text{low}}$	$(R_{\text{s,high}}, R_{\text{c,high}})$	S_{high}	$(R_{\text{s,low}}, R_{\text{c,low}})$	S_{low}	$PSNR_{\text{high}}$	$PSNR_{\text{low}}$
$10 - 90$	$(64, 2/3)$	10.5000	$(32, 1/3)$	5.0000	31.4521	33.3203
$30 - 70$	$(48, 1/2)$	9.8486	$(32, 1/3)$	5.0000	29.0488	32.0672
$50 - 50$	$(48, 1/2)$	9.8262	$(32, 1/3)$	5.0000	27.7763	30.7930
$70 - 30$	$(32, 1/3)$	11.2833	$(32, 1/3)$	7.4632	26.7596	31.6151
$90 - 10$	$(32, 1/3)$	15.0000	$(32, 1/3)$	10.1943	26.4203	31.1774
MMD						
$N_{\text{high}} - N_{\text{low}}$	$(R_{\text{s,high}}, R_{\text{c,high}})$	S_{high}	$(R_{\text{s,low}}, R_{\text{c,low}})$	S_{low}	$PSNR_{\text{high}}$	$PSNR_{\text{low}}$
$10 - 90$	$(64, 2/3)$	12.7296	$(32, 1/3)$	5.0000	33.0047	33.0047
$30 - 70$	$(64, 2/3)$	13.2312	$(32, 1/3)$	5.0000	30.7191	30.7191
$50 - 50$	$(48, 1/2)$	13.1569	$(32, 1/3)$	5.0000	28.5991	28.5991
$70 - 30$	$(32, 1/3)$	12.3831	$(32, 1/3)$	5.0213	27.1521	27.1521
$90 - 10$	$(32, 1/3)$	15.0000	$(32, 1/3)$	6.7090	26.5321	26.5321

Table 5: $R_{\text{target}} = 144\,\text{kbps},\ W_t = 20\,\text{MHz},\ N_0 = 0$ W/Hz.

MAD						
$N_{\text{high}} - N_{\text{low}}$	$(R_{\text{s,high}}, R_{\text{c,high}})$	S_{high}	$(R_{\text{s,low}}, R_{\text{c,low}})$	S_{low}	$PSNR_{\text{high}}$	$PSNR_{\text{low}}$
$10 - 90$	$(72, 1/2)$	15.0000	$(48, 1/3)$	7.7859	30.3384	32.7780
$30 - 70$	$(48, 1/3)$	15.0000	$(48, 1/3)$	9.3816	28.0307	31.8708
$50 - 50$	$(48, 1/3)$	7.7427	$(48, 1/3)$	5.0000	27.1339	30.9034
$70 - 30$	$(48, 1/3)$	15.0000	$(48, 1/3)$	9.9501	26.3745	30.0843
$90 - 10$	$(48, 1/3)$	15.0000	$(48, 1/3)$	10.1822	25.7146	29.3731
MMD						
$N_{\text{high}} - N_{\text{low}}$	$(R_{\text{s,high}}, R_{\text{c,high}})$	S_{high}	$(R_{\text{s,low}}, R_{\text{c,low}})$	S_{low}	$PSNR_{\text{high}}$	$PSNR_{\text{low}}$
$10 - 90$	$(72, 1/2)$	15.0000	$(48, 1/3)$	6.3505	32.3213	32.3213
$30 - 70$	$(48, 1/3)$	11.6678	$(48, 1/3)$	5.0000	29.6328	29.6328
$50 - 50$	$(48, 1/3)$	10.5707	$(48, 1/3)$	5.0000	28.0449	28.0449
$70 - 30$	$(48, 1/3)$	9.8198	$(48, 1/3)$	5.0000	26.8317	26.8317
$90 - 10$	$(48, 1/3)$	9.2654	$(48, 1/3)$	5.0000	25.8461	25.8461

Table 6: $R_{\text{target}} = 144\,\text{kbps},\ W_t = 15\,\text{MHz},\ N_0 = 0$ W/Hz.

MAD						
$N_{\text{high}} - N_{\text{low}}$	$(R_{\text{s,high}}, R_{\text{c,high}})$	S_{high}	$(R_{\text{s,low}}, R_{\text{c,low}})$	S_{low}	$PSNR_{\text{high}}$	$PSNR_{\text{low}}$
$10-90$	$(48, 1/3)$	15.0000	$(48, 1/3)$	10.0856	26.0091	29.6842
$30-70$	$(48, 1/3)$	15.0000	$(48, 1/3)$	10.4477	24.9842	28.5810
$50-50$	$(48, 1/3)$	15.0000	$(48, 1/3)$	10.7484	24.1375	27.6704
$70-30$	$(48, 1/3)$	15.0000	$(48, 1/3)$	11.0045	23.4146	26.8932
$90-10$	$(48, 1/3)$	15.0000	$(48, 1/3)$	11.2265	22.7829	26.2145
MMD						
$N_{\text{high}} - N_{\text{low}}$	$(R_{\text{s,high}}, R_{\text{c,high}})$	S_{high}	$(R_{\text{s,low}}, R_{\text{c,low}})$	S_{low}	$PSNR_{\text{high}}$	$PSNR_{\text{low}}$
$10-90$	$(48, 1/3)$	12.3251	$(48, 1/3)$	5.6041	28.7266	28.7266
$30-70$	$(48, 1/3)$	9.6409	$(48, 1/3)$	5.0000	26.5538	26.5538
$50-50$	$(48, 1/3)$	15.0000	$(48, 1/3)$	8.4876	25.0406	25.0406
$70-30$	$(48, 1/3)$	15.0000	$(48, 1/3)$	9.0465	23.8711	23.8711
$90-10$	$(48, 1/3)$	11.0000	$(48, 1/3)$	6.9700	22.9148	22.9148

Table 7: $R_{\text{target}} = 96\,\text{kbps},\ W_t = 20\,\text{MHz},\ N_0 = 10^{-7}$ W/Hz.

MAD						
$N_{\text{high}} - N_{\text{low}}$	$(R_{\text{s,high}}, R_{\text{c,high}})$	S_{high}	$(R_{\text{s,low}}, R_{\text{c,low}})$	S_{low}	$PSNR_{\text{high}}$	$PSNR_{\text{low}}$
$10-90$	$(64, 2/3)$	15.0000	$(64, 2/3)$	8.4148	32.9280	36.7442
$30-70$	$(64, 2/3)$	15.0000	$(64, 2/3)$	8.7092	31.3549	35.0942
$50-50$	$(64, 2/3)$	15.0000	$(32, 1/3)$	7.0445	30.9207	32.8401
$70-30$	$(48, 1/2)$	15.0000	$(32, 1/3)$	7.6110	29.2156	32.2485
$90-10$	$(48, 1/2)$	15.0000	$(32, 1/3)$	7.6210	28.2575	31.2847
MMD						
$N_{\text{high}} - N_{\text{low}}$	$(R_{\text{s,high}}, R_{\text{c,high}})$	S_{high}	$(R_{\text{s,low}}, R_{\text{c,low}})$	S_{low}	$PSNR_{\text{high}}$	$PSNR_{\text{low}}$
$10-90$	$(64, 2/3)$	15.0000	$(64, 2/3)$	5.6298	35.6857	35.6857
$30-70$	$(64, 2/3)$	15.0000	$(32, 1/3)$	5.9121	33.3853	33.3853
$50-50$	$(64, 2/3)$	15.0000	$(32, 1/3)$	5.7300	31.5918	31.5918
$70-30$	$(64, 2/3)$	15.0000	$(32, 1/3)$	5.5814	29.7539	29.7539
$90-10$	$(48, 1/2)$	15.0000	$(32, 1/3)$	5.7257	28.3789	28.3789

Table 8: $R_{\text{target}} = 96\,\text{kbps},\ W_t = 15\,\text{MHz},\ N_0 = 10^{-7}$ W/Hz.

MAD						
$N_{\text{high}} - N_{\text{low}}$	$(R_{\text{s,high}}, R_{\text{c,high}})$	S_{high}	$(R_{\text{s,low}}, R_{\text{c,low}})$	S_{low}	$PSNR_{\text{high}}$	$PSNR_{\text{low}}$
$10-90$	$(64, 2/3)$	15.0000	$(32, 1/3)$	7.1567	31.4147	33.3082
$30-70$	$(48, 1/2)$	15.0000	$(32, 1/3)$	7.6223	29.0315	32.0576
$50-50$	$(48, 1/2)$	15.0000	$(32, 1/3)$	7.6366	27.7619	30.7834
$70-30$	$(32, 1/3)$	15.0000	$(32, 1/3)$	9.9299	26.7537	31.6109
$90-10$	$(32, 1/3)$	15.0000	$(32, 1/3)$	10.2012	26.4153	31.1736
MMD						
$N_{\text{high}} - N_{\text{low}}$	$(R_{\text{s,high}}, R_{\text{c,high}})$	S_{high}	$(R_{\text{s,low}}, R_{\text{c,low}})$	S_{low}	$PSNR_{\text{high}}$	$PSNR_{\text{low}}$
$10-90$	$(64, 2/3)$	15.0000	$(32, 1/3)$	5.8898	32.9863	32.9863
$30-70$	$(64, 2/3)$	15.0000	$(32, 1/3)$	5.6668	30.7003	30.7003
$50-50$	$(48, 1/2)$	15.0000	$(32, 1/3)$	5.7028	28.5851	28.5851
$70-30$	$(32, 1/3)$	15.0000	$(32, 1/3)$	6.0882	27.1463	27.1463
$90-10$	$(32, 1/3)$	15.0000	$(32, 1/3)$	6.7141	26.5271	26.5271

Table 9: $R_{\text{target}} = 144\,\text{kbps},\ W_t = 20\,\text{MHz},\ N_0 = 10^{-7}$ W/Hz.

MAD						
$N_{\text{high}} - N_{\text{low}}$	$(R_{\text{s,high}}, R_{\text{c,high}})$	S_{high}	$(R_{\text{s,low}}, R_{\text{c,low}})$	S_{low}	$PSNR_{\text{high}}$	$PSNR_{\text{low}}$
$10 - 90$	$(48, 1/3)$	15.0000	$(48, 1/3)$	9.0621	29.0841	33.0421
$30 - 70$	$(48, 1/3)$	15.0000	$(48, 1/3)$	9.3985	28.0076	31.8577
$50 - 50$	$(48, 1/3)$	15.0000	$(48, 1/3)$	9.6979	27.1164	30.8916
$70 - 30$	$(48, 1/3)$	15.0000	$(48, 1/3)$	9.9590	26.3597	30.0736
$90 - 10$	$(48, 1/3)$	15.0000	$(48, 1/3)$	10.1896	25.7016	29.3630
MMD						
$N_{\text{high}} - N_{\text{low}}$	$(R_{\text{s,high}}, R_{\text{c,high}})$	S_{high}	$(R_{\text{s,low}}, R_{\text{c,low}})$	S_{low}	$PSNR_{\text{high}}$	$PSNR_{\text{low}}$
$10 - 90$	$(72, 1/2)$	15.0000	$(48, 1/3)$	6.3510	32.2887	32.2887
$30 - 70$	$(48, 1/3)$	15.0000	$(48, 1/3)$	6.4367	29.6111	29.6111
$50 - 50$	$(48, 1/3)$	15.0000	$(48, 1/3)$	7.1026	28.0276	28.0276
$70 - 30$	$(48, 1/3)$	15.0000	$(48, 1/3)$	7.6444	26.8170	26.8170
$90 - 10$	$(48, 1/3)$	15.0000	$(48, 1/3)$	8.1007	25.8331	25.8331

Table 10: $R_{\text{target}} = 144\,\text{kbps},\ W_t = 15\,\text{MHz},\ N_0 = 10^{-7}$ W/Hz.

MAD						
$N_{\text{high}} - N_{\text{low}}$	$(R_{\text{s,high}}, R_{\text{c,high}})$	S_{high}	$(R_{\text{s,low}}, R_{\text{c,low}})$	S_{low}	$PSNR_{\text{high}}$	$PSNR_{\text{low}}$
$10 - 90$	$(48, 1/3)$	15.0000	$(48, 1/3)$	10.1179	25.9716	29.6706
$30 - 70$	$(48, 1/3)$	15.0000	$(48, 1/3)$	10.4608	24.9646	28.5689
$50 - 50$	$(48, 1/3)$	15.0000	$(48, 1/3)$	10.7574	24.1222	27.6593
$70 - 30$	$(48, 1/3)$	15.0000	$(48, 1/3)$	11.0116	23.4013	26.8828
$90 - 10$	$(48, 1/3)$	15.0000	$(48, 1/3)$	11.2325	22.7709	26.2046
MMD						
$N_{\text{high}} - N_{\text{low}}$	$(R_{\text{s,high}}, R_{\text{c,high}})$	S_{high}	$(R_{\text{s,low}}, R_{\text{c,low}})$	S_{low}	$PSNR_{\text{high}}$	$PSNR_{\text{low}}$
$10 - 90$	$(48, 1/3)$	15.0000	$(48, 1/3)$	6.8309	28.7016	28.7016
$30 - 70$	$(48, 1/3)$	15.0000	$(48, 1/3)$	7.7878	26.5355	26.5355
$50 - 50$	$(48, 1/3)$	15.0000	$(48, 1/3)$	8.4948	25.0255	25.0255
$70 - 30$	$(48, 1/3)$	15.0000	$(48, 1/3)$	9.0528	23.8579	23.8579
$90 - 10$	$(48, 1/3)$	15.0000	$(48, 1/3)$	9.5102	22.9029	22.9029

classes. These remarks are derived from all combinations of bit rate-bandwidth considered in our experiments.

Moreover, the MMD criterion assigns higher PSNR values to high-motion class of nodes than the MAD criterion, in the corresponding cases. Indeed, the PSNR differences between the two criteria is inversely proportional to the cardinality of the high-motion class of nodes. Thus, the MMD criterion can be considered as the most appropriate choice in cases where we are interested in the amelioration of the high-motion scenes rather than improving the quality of the low-motion scenes. Surveillance applications are typical examples of such cases. On the contrary, the MAD criterion appears to be more suitable in cases where high video quality of low-motion scenes is desirable.

Considering the noisy case, in general, no significant changes in PSNR values are observed after the addition of noise, except for a marginal reduction of no more than 0.01 dB, which has imperceptible impact to the video quality. Similarly to the noiseless case,the high-motion class of nodes requires more power than the low-motion class. More specifically, the power levels of the high-motion class of nodes are not only higher than that of the low-motion class, but also they actually take their maximum possible value.

Special attention shall be paid to the case of distributing 10 nodes in the high-motion class and 90 nodes in the low-motion class, which is reported in Table 9, for the MAD criterion. Despite the addition of noise, an increase of PSNR is observed for the low-motion class compared to the corresponding case in Table 33, for the same criterion. This is attributed to the fact that, under the influence of noise, the power level of the low-motion class is increased. Thus, the ratio E_k/I_0 also increases as follows from Eq. (7).

Additional information regarding the performance of the proposed schemes is graphically illustrated in figures. Specifically, Fig. 8(a) depicts the differences of the received PSNR between the MAD and MMD criteria for both the high- and low-motion class of nodes, for all node distributions and refers to the case of $R_{\text{target}} = 96$ kbps, $W_t = 20$ MHz, and $N_0 = 0$ W/Hz.The last column of the same figure shows the accumulated PSNR difference between MAD and MMD, also for all node distributions. This figure manifests that, cumulatively for all node distributions, the decrease in PSNR achieved by the MMD criterion for the low-motion class of nodes is considerably higher than the corresponding gain for the high-motion class of nodes. For the case of a bit rate of 96 kbps and a bandwidth of 20 MHz, the MMD increases the total PSNR for all members of the high-motion class by 6.0986 dB, while the total PSNR for all members of the low-motion class decreases by 9.3798 dB. Therefore, despite the fact that the MMD offers equal PSNR values to both motion classes, it is proved to be less fair than it was initially perceived, since it disfavors the low-motion class of nodes.

An additional piece of information is provided by Fig. 8(b) that depicts the optimal ratios $S_{\text{high}}/S_{\text{low}}$ for the two optimization criteria when the number of nodes imaging high levels of motion increases, while that of the nodes imaging low levels of motion decreases. The specific figure refers to the case of $R_{\text{target}} = 96$ kbps, $W_t = 20$ MHz, and $N_0 = 0$ W/Hz and offers strong evidence that the MAD criterion requires much less power than the MMD. Spending less power for data transmission means that a stronger channel coding is used, capable of correcting a higher number of channel errors. From Eq. (6), it follows that the channel coding rate is inversely proportional to the data compression rate, highlighting the importance of considering the special characteristics of the video sequence (high- against low-motion), when determining the optimal power levels.

Moreover, the power received by the CCU from the low-motion class of nodes is always less than that of the high-motion class for both optimization criteria, as it is confirmed in the tables for all the examined bit rate-bandwidth combinations. Hence, since the nodes that image high levels of motion need higher power levels than those in the low-motion class, it is reasonable that the ratio E_k/I_0 of Eq. (7) exhibits further decrease when the cardinality of the high-motion class is larger than that of the low-motion class. Naturally, this incurs a reduction to the PSNR values for both motion classes.

Actually, this fact explains the downward trend of the PSNR values illustrated in Figs. 9 and 10, for both motion classes, for all examined bit rate and bandwidth combinations. Specifically, Fig. 9(a) includes the PSNR variations for the high-motion class of nodes, while Fig. 9(b) illustrates

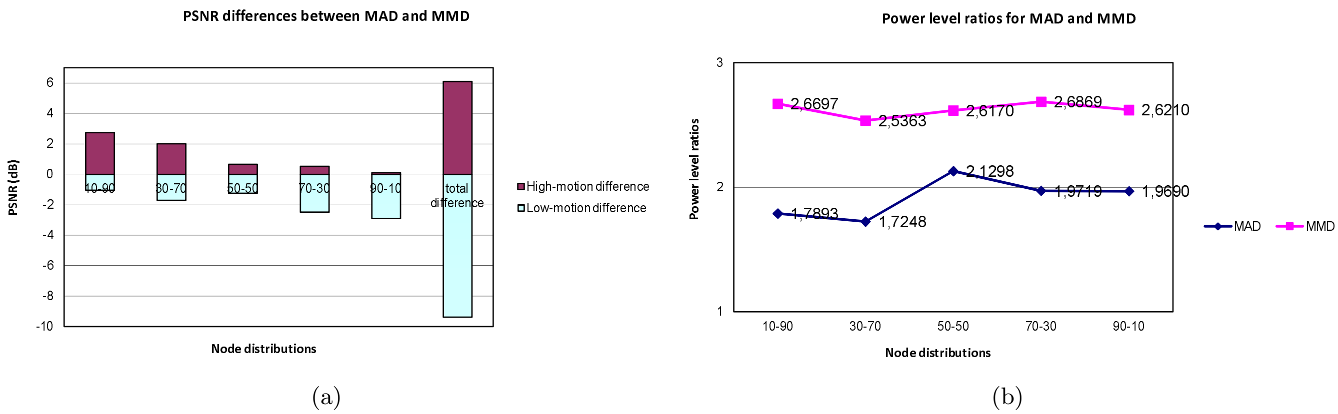

Figure 8: PSNR differences (a) and power level ratios (b) for the MAD and MMD criteria, for various node distributions, with $R_{\text{target}} = 96$ kbps, $W_t = 20$ MHz, and $N_0 = 0$ W/Hz.

the same results for the low-motion class of nodes for the MAD criterion. Figure 10 offers the corresponding information for the MMD criterion. Note that for the MMD case, the PSNR values for both motion classes were identical.

Another issue that gained our interest was the efficiency of PSO against that of AS in terms of the number of iterations required for obtaining solutions of same quality with AS. Figure 11 offers this information. In particular, it illustrates the number of iterations required by PSO, averaged over the 30 independent experiments, to detect the same solution with AS for different levels of precision, namely 3, 4, 5, and 6 decimal digits. In each subfigure, both criteria are compared for all examined bit rate and bandwidth combinations. Figures 11(a) and 11(b) present the aforementioned results for the node distribution "30-70", while Figs. 11(c) and 11(d) for the node distribution "70-30". Moreover, Figs. 11(a) and 11(c) refer to the noiseless case ($N_0 = 0$ W/Hz), and Figs. 11(b) and 11(d) to the noisy case ($N_0 = 10^{-7}$ W/Hz).

From the figures, we corroborate that PSO requires fewer iterations to achieve same quality solutions with the AS algorithm for lower precisions. As expected, increasing precision is accompanied by a higher number of iterations. Furthermore, it is obvious that the MMD criterion needs more function evaluations than MAD to achieve the optimal solution, while the addition of noise incurs an increase to the number of iterations for both optimization criteria. The aforementioned confirmations derive from all considered bit rate-bandwidth combinations and node distributions.

Figure 12 presents the success ratio of AS in achieving the optimal solution, for both MAD and MMD criteria. Particularly, each of the cases as referred to this figure corresponds to the results of each corresponding table. For example, Case 3 corresponds to the results of Table 34, when $R_{\text{target}} = 144$ kbps, $W_t = 20$ MHz, and $N_0 = 0$ W/Hz. For this case, we observe that for the MAD it has a success ratio of 100%, and 99.33% for MMD. For the MAD criterion, this means that each of the node distributions manages to achieve the same best solution in all 30 experiments. In contrast, the success ratio for MMD implies that one experiment out of 30, for a specific node

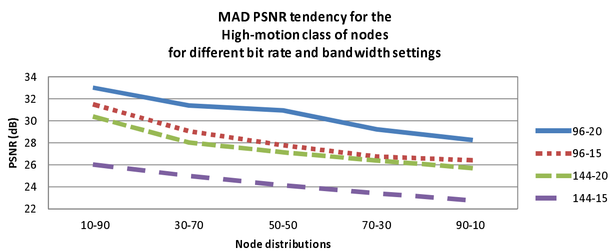

(a)

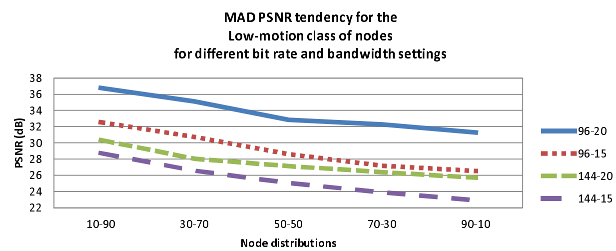

(b)

Figure 9: PSNR tendency for the MAD criterion (a) for the high-motion, and (b) low-motion class of nodes, for various node distributions, with $R_{\text{target}} = 96$ kbps, $W_t = 20$ MHz, and $N_0 = 0$ W/Hz.

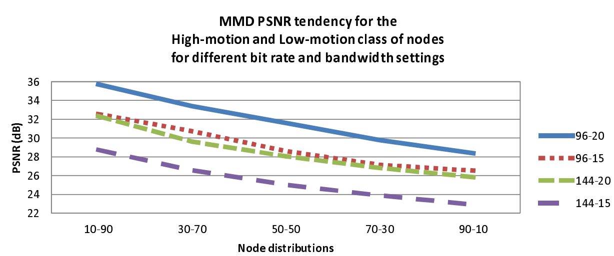

Figure 10: PSNR tendency for the MMD criterion, for both motion classes, for various node distributions, with $R_{\text{target}} = 96$ kbps, $W_t = 20$ MHz, and $N_0 = 0$ W/Hz.

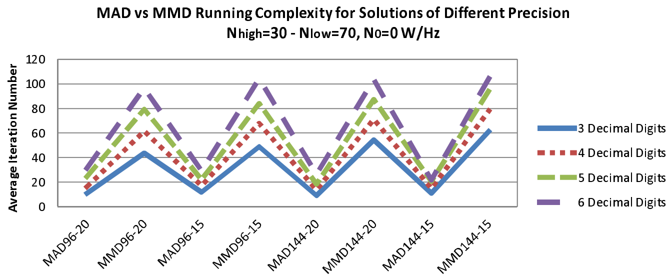

(a)

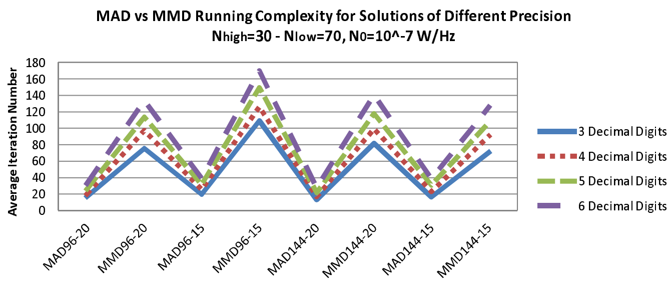

(b)

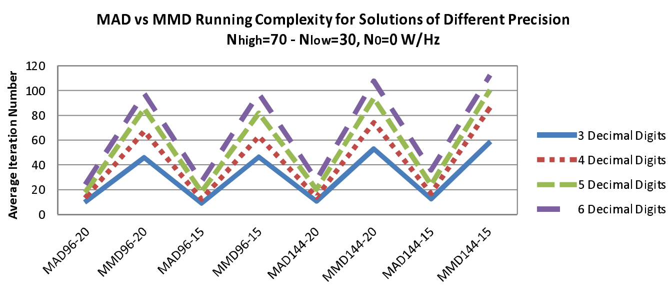

(c)

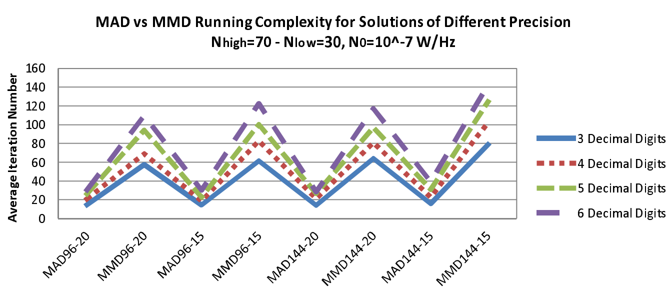

(d)

Figure 11: Average number of iterations required by PSO to obtain the solution given by AS, for both criteria, and precision of 3, 4, 5 and 6 decimal digits, for all examined bit rate-bandwidth combinations, for two different node distributions. Figures 11(a) and 11(c) correspond to the noiseless case, while Figs. 11(b) and 11(d) refer to the noisy case.

distribution, failed to reach the best solution.

Interpreting the AS efficiency for MAD and MMD, we infer that for the MAD criterion it is capable of detecting the best solution in most of the cases and exhibits better performance than for MMD. The superiority for MAD is clearer in noisy cases (Cases $5-8$) where for MMD it presents success ratios of nearly 70%. Although it may seems high, we indicatively refer that for the case of $N_{\text{high}} = 90 - N_{\text{low}} = 10$ of Table 10, only 7/30 experiments reach the optimal solution. Therefore, this figure sheds light on the weakness of AS in detecting always the best solution, while it also demonstrates that its efficiency depends both on the initially supplied starting point as well as on the objective function to be optimized.

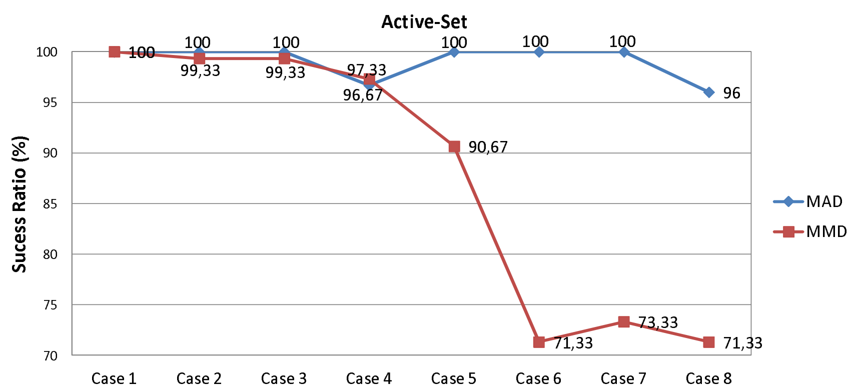

Figure 12: Success ratio of AS in finding the optimal solution.

Lastly, Table 11 offers an intuition regarding the execution time required by each optimization algorithm averaged over 30 experiments per problem instance. Also, the total running times needed for the execution of all cases of node distributions for each specific bit rate and bandwidth combination, are presented. The same table includes results for both criteria and all cases of considered bit rate and bandwidth for both the noiseless and noisy cases. We shall note that AS was set to execute 40000 function evaluations (as PSO and HPSOAS), with the function tolerance set to 10^{-15} and the tolerance of the candidate optimal solution to 10^{-15}. We set the function and optimal point tolerances to such levels since we confirmed that the PSNR results provided by the AS were different from those of PSO even to the first decimal digit for some cases. At this point, we should recall that the AS method was run sequentially 9 times for each tested case in order to evaluate all possible combinations of bit rate and bandwidth. The execution times of this method are averaged over the number of successful experiments per case.

An overall inspection of the results denotes that despite PSO is able to reach the optimal solutions efficiently in all 30 experiments of each considered case, as opposed to AS, it still needs more time to be executed compared to both AS and HPSOAS. Particularly, more time is needed as more nodes are assigned to the low-motion class of nodes. Moreover, it follows that MAD takes less time to reach the optimal point compared to MMD, while in the noisy case the MMD needs the double time to achieve the optimal solution compared to the noiseless case, using the PSO.

Commenting on the AS execution times, it is clear from Table 11 that it requires less time compared to PSO, with two exceptions for the noiseless case of MMD criterion when the bit rate is set to 144 kbps. This probably means that the randomly supplied starting points are far away from the optimal solution and that the shape of the objective function complicates further the finding of the solution. Additionally, we may think that the AS method follows the brute force approach testing all possible cases of source and channel pair values, increasing the overall problem's complexity. Therefore, this method is impractical to applications where problems with higher dimensions exist. For example, if we had made the assumption for a node clustering into 10 motion classes, the AS should be executed 3^{10} times in order to determine the optimal source and channel coding rate combinations for each motion class, instead of the 3^2 times of our problem.

Therefore, in order to surmount all weaknesses of both PSO and AS keeping their benefits at the same time, we resorted to the development of the HPSOAS optimization method, as described in Section4.1.3. Table 11 demonstrates that the optimization of MMD criterion using the HPSOAS method requires significantly less time compared to both PSO and AS. Similarly, the MAD optimized under the use of the HPSOAS saves much execution time compared to PSO and the same holds also in the half cases compared to AS.

Interesting enough are also the conclusions drawn by Fig 13. The goal of the specific illustration is to give us an insight regarding the overall execution times for each of the MAD and MMD criteria, when we aggregate the total times for each considered bit rate and bandwidth combination, for both the noiseless and noisy cases. Evidently, it follows that the MMD takes longer to converge compared to the MAD, for all considered optimization methods. Moreover, for the MMD it is clear that HPSOAS needs about $1/6^{th}$ and $1/4^{th}$ of the corresponding time of PSO and AS, respectively, in order to converge to the optimal point. Further is the gain in time by adopting the HPSOAS to the MAD criterion instead of PSO. In this case, HPSOAS reaches the optimal solution in about $1/12^{th}$ of PSO's time. Comparable execution times are required accumulatively by both AS and HPSOAS for the MAD criterion.

Summarizing, HPSOAS keeps the following strong points that renders its use very appealing: i) it is not sensitive to initial conditions, ii) there is no need to execute an exhaustive search in order to determine the discrete parameters of this work, iii) it can be applied to problems of higher dimensions without a tremendous effect on problem's complexity, and iv) it takes much less time for its execution compared to other stochastic methods.

5.2 Game-Theoretic Solutions through Intelligent Optimization for Efficient Resource Management in Wireless Visual Sensor Networks

The VSN considered in this paper consisted of $K = 102$ nodes, which capture videos of various amounts of motion. In order to simulate the various amounts of motion included in the videos, we used a number of video sequences, which were downloaded from [76]. The video sequences used as well as the amount of motion in each one is depicted in Fig. 14.

All video sequences were at QCIF resolution and were encoded at 15 frames per second. From the "Salesman" video sequence we kept only the first 300 frames in order to have the same length

Table 11: Average execution times (in seconds).

	$R_{\text{target}} = 96\,\text{kbps}$, $W_t = 20\,\text{MHz}$, $N_0 = 0$ W/Hz						$R_{\text{target}} = 96\,\text{kbps}$, $W_t = 20\,\text{MHz}$, $N_0 = 10^{-7}$ W/Hz					
	MAD			MMD			MAD			MMD		
$N_{\text{high}} - N_{\text{low}}$	PSO	AS	HPSOAS	PSO	AS	HPSOAS	PSO	AS	HPSOAS	PSO	AS	HPSOAS
$10 - 90$	148.78	4.67	5.43	154.34	7.36	9.71	154.83	4.93	10.70	319.55	7.08	13.24
$30 - 70$	117.27	4.91	3.74	125.29	97.94	16.41	124.11	5.20	11.90	245.21	51.37	41.91
$50 - 50$	81.74	6.43	3.59	94.55	53.01	32.22	87.08	5.61	0.85	185.45	47.82	48.75
$70 - 30$	51.77	6.27	0.79	53.56	43.78	8.78	56.75	5.95	1.23	122.51	53.13	23.14
$90 - 10$	25.44	6.47	0.61	29.01	125.44	13.29	28.15	8.88	4.04	58.87	70.79	50.42
Total time	425.00	28.75	14.16	456.75	327.53	80.41	450.92	30.57	28.72	931.59	230.19	177.46

	$R_{\text{target}} = 96\,\text{kbps}$, $W_t = 15\,\text{MHz}$, $N_0 = 0$ W/Hz						$R_{\text{target}} = 96\,\text{kbps}$, $W_t = 15\,\text{MHz}$, $N_0 = 10^{-7}$ W/Hz					
	MAD			MMD			MAD			MMD		
$N_{\text{high}} - N_{\text{low}}$	PSO	AS	HPSOAS	PSO	AS	HPSOAS	PSO	AS	HPSOAS	PSO	AS	HPSOAS
$10 - 90$	182.11	3.32	15.89	183.22	12.38	37.24	169.20	4.64	2.85	352.83	28.09	27.30
$30 - 70$	151.86	6.32	6.32	129.84	20.86	21.51	141.15	5.76	13.33	295.61	51.79	13.05
$50 - 50$	121.44	6.17	18.32	99.39	131.27	28.98	103.18	5.58	10.96	243.32	92.02	27.58
$70 - 30$	68.89	6.63	5.52	63.67	165.39	40.93	61.64	6.00	0.61	133.04	86.56	17.84
$90 - 10$	29.69	9.53	1.18	26.83	114.67	17.44	29.10	8.97	2.65	52.54	90.14	31.35
Total time	553.99	25.45	47.23	502.95	444.57	146.10	504.27	30.95	30.40	1077.34	348.60	117.12

	$R_{\text{target}} = 144\,\text{kbps}$, $W_t = 20\,\text{MHz}$, $N_0 = 0$ W/Hz						$R_{\text{target}} = 144\,\text{kbps}$, $W_t = 20\,\text{MHz}$, $N_0 = 10^{-7}$ W/Hz					
	MAD			MMD			MAD			MMD		
$N_{\text{high}} - N_{\text{low}}$	PSO	AS	HPSOAS	PSO	AS	HPSOAS	PSO	AS	HPSOAS	PSO	AS	HPSOAS
$10 - 90$	183.50	4.51	19.78	176.71	26.23	13.75	148.45	5.50	7.07	359.43	48.07	85.15
$30 - 70$	137.70	5.60	4.72	147.39	106.24	12.33	120.21	5.16	10.33	284.55	89.94	47.53
$50 - 50$	107.84	6.17	12.90	119.47	116.33	22.95	88.51	4.46	1.24	217.15	95.29	26.18
$70 - 30$	69.08	6.38	22.96	86.76	198.52	59.87	60.34	5.18	21.44	166.85	109.61	24.80
$90 - 10$	26.34	7.57	4.26	29.97	201.45	24.68	25.05	6.65	2.35	90.57	105.50	51.44
Total time	524.46	30.23	64.62	560.30	648.77	133.58	442.56	26.95	42.43	1118.55	448.41	235.10

	$R_{\text{target}} = 144\,\text{kbps}$, $W_t = 15\,\text{MHz}$, $N_0 = 0$ W/Hz						$R_{\text{target}} = 144\,\text{kbps}$, $W_t = 15\,\text{MHz}$, $N_0 = 10^{-7}$ W/Hz					
	MAD			MMD			MAD			MMD		
$N_{\text{high}} - N_{\text{low}}$	PSO	AS	HPSOAS	PSO	AS	HPSOAS	PSO	AS	HPSOAS	PSO	AS	HPSOAS
$10 - 90$	152.84	3.65	2.44	155.06	176.00	13.98	166.51	4.60	1.67	343.07	77.41	25.07
$30 - 70$	122.65	6.08	0.54	127.42	101.08	8.32	142.24	4.92	16.71	299.31	75.09	17.36
$50 - 50$	93.27	7.39	10.83	100.01	178.71	50.09	106.31	5.22	22.97	243.20	98.60	23.78
$70 - 30$	57.95	6.85	0.95	59.56	333.43	17.66	61.56	5.54	12.71	172.14	102.95	53.07
$90 - 10$	32.31	9.38	4.95	31.83	313.93	27.19	28.04	6.77	3.44	75.48	106.72	30.97
Total time	459.02	33.35	19.71	473.88	1103.15	117.24	504.66	27.05	57.5	1133.20	460.77	150.25

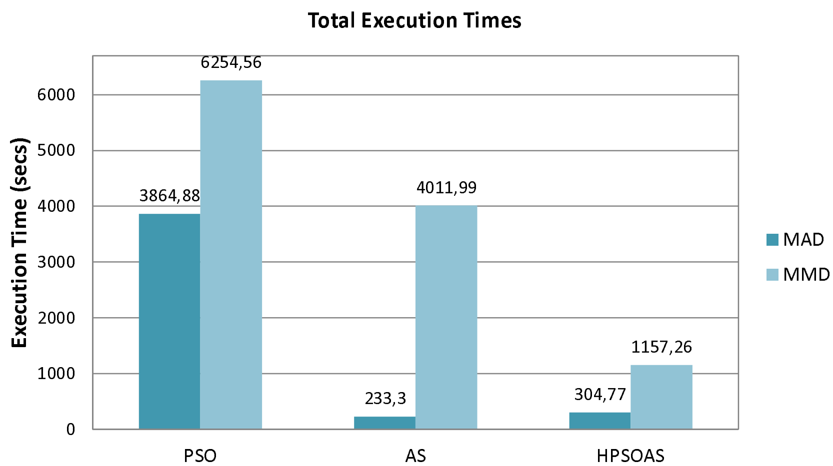

Figure 13: Total execution times of all node distributions and bit rate-bandwidth combinations of both noiseless and noisy cases, for MAD and MMD, using all optimization methods.

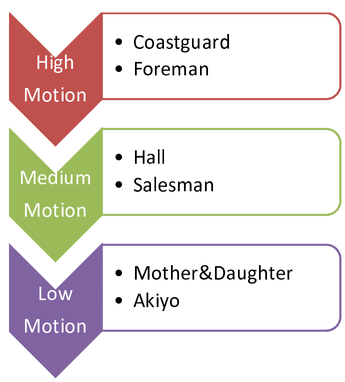

Figure 14: The used video sequences and the amount of motion described by each of them.

for all video sequences. Additionally, we assumed that the K nodes of the VSN are clustered into $C = 6$ motion classes, with each sequence being a representative of a motion class. For the node distributions into the six motion classes we considered the following cases:

- **Case 1:** $K_{\mathbf{a}} = K_{\mathbf{md}} = K_{\mathbf{s}} = K_{\mathbf{h}} = K_{\mathbf{f}} = K_{\mathbf{c}} = 17$.
- **Case 2:** $K_{\mathbf{a}} = K_{\mathbf{md}} = 25, K_{\mathbf{s}} = K_{\mathbf{h}} = K_{\mathbf{f}} = K_{\mathbf{c}} = 13$.
- **Case 3:** $K_{\mathbf{a}} = K_{\mathbf{md}} = K_{\mathbf{f}} = K_{\mathbf{c}} = 13, K_{\mathbf{s}} = K_{\mathbf{h}} = 25$.
- **Case 4:** $K_{\mathbf{a}} = K_{\mathbf{md}} = K_{\mathbf{s}} = K_{\mathbf{h}} = 13, K_{\mathbf{f}} = K_{\mathbf{c}} = 25$.

K_{a} denotes the cardinality of the class that is represented by the "Akiyo" video sequence, while $K_{\mathrm{md}}, K_{\mathrm{s}}, K_{\mathrm{h}}, K_{\mathrm{f}}$ and K_{c} denote the cardinality of the class that is represented by the "Mother&Daughter", "Salesman", "Hall", "Foreman" and "Coastguard" video sequences, respectively. In all four node distributions described above, the total number of nodes was equal to $K = 102$ nodes. In Case 1, all classes included exactly the same number of nodes; in Case 2 more nodes described low amounts of motion; in Case 3 more nodes described medium amounts of motion and in Case 4 more nodes described high amounts of motion. For the assessment of the perceptual visual quality of the video sequences, the PSNR video quality metric was used, which is equal to the utility function of Eq. (27), and is measured in dB.

The RCPC codes used for channel coding had a mother code of rate 1/4 [14]. Also, two different cases were considered for the bit rate R_k: i) 96 kbps and ii) 144 kbps. Taking into account these bit rate constraints, it follows that the source-channel coding rate combinations can take the following discrete values:

i) $R_k = 96$ kbps

$$\mathbf{R}_{\mathrm{s+c}} = \Big\{(32, 1/3), (38.4, 4/10), (48, 1/2), (64, 2/3), (76.8, 4/5)\Big\}$$

$$\begin{aligned}
cb_{cl} &= 1 \longrightarrow (32, 1/3)\\
cb_{cl} &= 2 \longrightarrow (38.4, 4/10)\\
cb_{cl} &= 3 \longrightarrow (48, 1/2)\\
cb_{cl} &= 4 \longrightarrow (64, 2/3)\\
cb_{cl} &= 5 \longrightarrow (76.8, 4/5)
\end{aligned}$$

ii) $R_k = 144$ kbps

$$\mathbf{R}_{\mathrm{s+c}} = \Big\{(48, 1/3), (57.6, 4/10), (72, 1/2), (96, 2/3), (115.2, 4/5)\Big\}$$

$$\begin{aligned}
cb_{cl} &= 1 \longrightarrow (48, 1/3)\\
cb_{cl} &= 2 \longrightarrow (57.6, 4/10)\\
cb_{cl} &= 3 \longrightarrow (72, 1/2)\\
cb_{cl} &= 4 \longrightarrow (96, 2/3)\\
cb_{cl} &= 5 \longrightarrow (115.2, 4/5).
\end{aligned}$$

The index $cl \in \{\mathrm{a}, \mathrm{md}, \mathrm{s}, \mathrm{h}, \mathrm{f}, \mathrm{c}\}$ denotes the class of nodes that is represented by the "Akiyo", "Mother&Daugter", "Salesman", "Hall", "Foreman" and "Coastguard" video sequence, respectively. Concerning the power levels, they can take continuous values from the set $\mathbf{P} = [5.0, 15.0]$, measured in Watts (W). For the bandwidth, W_t, we examined the following values per bit rate constraint, R_k:

i) $R_k = 96$ kbps   2) $R_k = 144$ kbps

a) $W_t = 20$ MHz

b) $W_t = 15$ MHz

a) $W_t = 30$ MHz

b) $W_t = 22.5$ MHz

Since $R_k = 144$ kbps is 1.5 times the $R_k = 96$ kbps, the same reasoning was followed for the bandwidth values. Specifically, $W_t = 30$ MHz is 1.5 times the $W_t = 20$ MHz and $W_t = 22.5$ MHz is 1.5 times the $W_t = 15$ MHz. This corresponds to keeping the spreading code length the same for both cases.

In order to maximize the Nash product, PSO was used to minimize its negative. Specifically:

$$\begin{aligned} f(x) = -\Big(&(U_{\mathrm{a}}(cb_{\mathrm{a}}, S_{\mathrm{a}}) - dp_{\mathrm{a}})^{a_{\mathrm{a}}} \cdot (U_{\mathrm{md}}(cb_{\mathrm{md}}, S_{\mathrm{md}}) - dp_{\mathrm{md}})^{a_{\mathrm{md}}} \\ &\cdot (U_{\mathrm{s}}(cb_{\mathrm{s}}, S_{\mathrm{s}}) - dp_{\mathrm{s}})^{a_{\mathrm{s}}} \cdot (U_{\mathrm{h}}(cb_{\mathrm{h}}, S_{\mathrm{h}}) - dp_{\mathrm{h}})^{a_{\mathrm{h}}} \\ &\cdot (U_{\mathrm{f}}(cb_{\mathrm{f}}, S_{\mathrm{f}}) - dp_{\mathrm{f}})^{a_{\mathrm{f}}} \cdot (U_{\mathrm{c}}(cb_{\mathrm{c}}, S_{\mathrm{c}}) - dp_{\mathrm{c}})^{a_{\mathrm{c}}} \Big), \end{aligned} \tag{59}$$

where the particle $x = \big(S_{\mathrm{a}},\, S_{\mathrm{md}},\, S_{\mathrm{s}},\, S_{\mathrm{h}},\, S_{\mathrm{f}},\, S_{\mathrm{c}},\, cb_a,\, cb_{md},\, cb_s,\, cb_h,\, cb_f,\, cb_c\big)^\top$ consists of the power levels, as well as the combinations of source and channel coding rates, for all motion classes. The discrete components of the particle, i.e., the source and channel coding rate combinations, cb_{a}, cb_{md}, cb_{s}, cb_{h}, cb_{f}, cb_{c}, were let to assume continuous values within the range $\mathbf{R} = [0.6, 5.4]$. However, they were rounded to the nearest integer whenever the particle was evaluated.

Regarding PSO, identical parameter settings were used for both NNBS and CNBS criteria. Specifically, the default parameter set defined in Section 4.1.3 was selected and a swarm of $N = 100$ particles following the ring topology with radius $r = 1$ was used. Moreover, since PSO is a stochastic algorithm, its performance was evaluated over 30 independent experiments. At each experiment, the algorithm was executed for $Iter = 700$ iterations (which correspond to 70000 function evaluations for the 100 particles) and the best solution was recorded. Hence, taking into account that the number of particles (N) and the number of iterations ($Iter$) both depend on the number of motion classes (C), the complexity of PSO is $O(C \cdot N \cdot Iter)$.

Presentation and Discussion of Results

We first explored the effect of the value of the disagreement point vector in the results of the NBS-based criteria. Tables 12-15 show the achieved PSNR values for the NNBS and CNBS criteria, using the PSO as the optimization solver. We tested different selections of the dp vector, for the same bit rate and bandwidth combination. The tested values for the vector of the dp were also different for each bit rate and bandwidth combination, since they must be feasible values using the available bit rate and bandwidth, at each time. Additionally, all the elements of a dp vector were equal. Although this is not obligatory, we made this assumption in an effort to be equally fair to all motion classes.

In practice, video that includes high amounts of motion is particularly important in surveillance applications, since this is where the action occurs. From the presented experimental results, we confirmed that increasing the values of the dp vector results in favoring the nodes that image high

Table 12: PSNR values for different dp, using PSO, for $R_k = 96$ kbps and $W_t = 20$ MHz.

		NNBS				CNBS			
	Sequences	**dp = 28**	**dp = 27**	**dp = 26**	**dp = 25**	**dp = 28**	**dp = 27**	**dp = 26**	**dp = 25**
Case 1	"Akiyo"	36.5112	36.6797	36.8173	36.9319	36.5112	36.6797	36.8173	36.9319
	"Mother&Daughter"	34.5452	34.6279	34.6957	34.7521	34.5452	34.6279	34.6957	34.7521
	"Salesman"	33.0986	33.0871	33.0777	33.0697	33.0986	33.0871	33.0777	33.0697
	"Hall"	33.8855	33.9285	33.9637	33.9929	33.8855	33.9285	33.9637	33.9929
	"Foreman"	33.5774	33.6097	33.6378	33.6621	33.5774	33.6097	33.6378	33.6621
	"Coastguard"	**31.7825**	31.6143	31.4685	31.3413	**31.7825**	31.6143	31.4685	31.3413
Case 2	"Akiyo"	36.9809	36.8912	37.1221	37.2022	36.9424	36.9382	36.9356	36.9334
	"Mother&Daughter"	34.9393	34.8361	34.9994	35.0243	33.6715	33.6401	33.6110	33.5875
	"Salesman"	33.3904	33.2421	33.3045	33.2733	33.6637	33.6380	33.6148	33.5940
	"Hall"	34.2718	35.2623	35.4899	35.5408	35.8310	35.9345	36.0190	36.0895
	"Foreman"	35.0184	34.8631	35.1263	35.1739	**35.3444**	35.3347	35.3289	35.3239
	"Coastguard"	**32.8463**	32.6105	31.7981	31.6474	**32.7816**	32.7745	32.7702	32.7665
Case 3	"Akiyo"	36.9558	36.8917	37.0031	37.1001	37.4139	37.5529	37.6663	37.7609
	"Mother&Daughter"	34.8905	34.8361	34.8806	34.9213	35.4221	35.4903	35.5448	35.5896
	"Salesman"	33.3543	33.2422	33.2158	33.1963	32.8240	32.8028	32.7937	32.7862
	"Hall"	34.2239	34.1341	35.3394	35.4096	33.1350	33.0680	33.0095	32.9582
	"Foreman"	34.0659	34.8633	33.9198	33.9284	**35.7753**	35.7898	35.7631	35.7409
	"Coastguard"	**32.8041**	32.6106	31.6680	31.5307	**33.1541**	33.1083	33.0887	33.0725
Case 4	"Akiyo"	35.8036	36.1377	36.3882	36.5839	37.0979	37.5082	37.8145	38.0531
	"Mother&Daughter"	33.8701	34.0992	34.2704	34.4030	35.1134	35.4458	35.6941	35.8869
	"Salesman"	32.5969	32.6923	32.7593	32.8080	33.5191	33.6951	33.8216	33.9162
	"Hall"	33.2280	33.4080	33.5419	33.6446	35.5853	36.0320	36.3737	36.6444
	"Foreman"	32.6798	32.8640	33.0096	33.1267	**30.7193**	30.5880	30.4715	30.3670
	"Coastguard"	**30.1005**	29.8555	29.6511	29.4783	**29.8901**	29.6107	29.3772	29.1796

Table 13: PSNR values for different dp, using PSO, for $R_k = 96$ kbps and $W_t = 15$ MHz.

		NNBS				CNBS			
	Sequences	**dp = 26**	**dp = 25**	**dp = 24**	**dp = 23**	**dp = 26**	**dp = 25**	**dp = 24**	**dp = 23**
Case 1	"Akiyo"	35.6945	35.9260	36.1113	36.2636	35.6945	35.9260	36.1113	36.2636
	"Mother&Daughter"	33.5979	33.7564	33.8830	33.9863	33.5979	33.7564	33.8830	33.9863
	"Salesman"	32.2508	32.3180	32.3695	32.4100	32.2508	32.3180	32.3695	32.4100
	"Hall"	32.8823	33.0063	33.1049	33.1850	32.8823	33.0063	33.1049	33.1850
	"Foreman"	**30.2644**	30.1824	30.1099	30.0453	**30.2644**	30.1824	30.1099	30.0453
	"Coastguard"	**29.2214**	29.0370	28.8818	28.7496	**29.2214**	29.0370	28.8818	28.7496
Case 2	"Akiyo"	36.1434	36.3211	36.4657	36.5859	35.3258	35.3934	35.2294	35.4980
	"Mother&Daughter"	34.0389	34.1504	34.2403	34.3142	32.5165	32.5537	33.0002	32.6025
	"Salesman"	32.5823	32.6143	32.6382	32.6564	32.7412	32.7807	33.1431	32.8332
	"Hall"	33.3179	33.3982	33.4622	33.5142	33.5278	33.6192	34.1380	33.7512
	"Foreman"	**30.6672**	30.5615	30.4680	30.3847	32.5214	32.6343	31.1627	32.8104
	"Coastguard"	**29.5215**	29.3229	29.1539	29.0087	**29.6692**	29.4868	29.6795	29.1970
Case 3	"Akiyo"	36.0155	36.2113	36.3704	36.5026	36.3045	36.4973	36.6539	36.7839
	"Mother&Daughter"	33.9130	34.0407	34.1441	34.2294	34.1980	34.3268	34.4307	34.5161
	"Salesman"	32.4877	32.5319	32.5659	32.5927	31.5356	31.5615	31.5818	31.5980
	"Hall"	33.1933	33.2889	33.3659	33.4290	31.7751	31.7760	31.7738	31.7697
	"Foreman"	**30.5507**	30.4550	30.3709	30.2964	32.8400	32.8961	32.9403	32.9756
	"Coastguard"	**29.4348**	29.2427	29.0802	28.9414	**29.6321**	29.4531	29.3008	29.1699
Case 4	"Akiyo"	34.9081	35.2441	35.5041	35.7124	35.8943	36.2671	36.5527	36.7796
	"Mother&Daughter"	32.8337	33.0818	33.2741	33.4280	33.7938	34.0965	34.3282	34.5117
	"Salesman"	31.6736	31.8085	31.9101	31.9892	32.3982	32.5737	32.7042	32.8046
	"Hall"	32.1320	32.3380	32.4979	32.6256	33.0756	33.3444	33.5502	33.7129
	"Foreman"	**29.5999**	29.5560	29.5162	29.4799	**29.0024**	28.8656	28.7452	28.6382
	"Coastguard"	**28.7254**	28.5630	28.4288	28.3160	**28.2780**	28.0378	27.8366	27.6658

Table 14: PSNR values for different dp, using PSO, for $R_k = 144$ kbps and $W_t = 30$ MHz.

		NNBS				**CNBS**			
	Sequences	**dp = 28**	**dp = 27**	**dp = 26**	**dp = 25**	**dp = 28**	**dp = 27**	**dp = 26**	**dp = 25**
Case 1	"Akiyo"	36.4608	36.7424	36.9780	37.1782	36.4608	36.7424	36.9780	37.1782
	"Mother&Daughter"	34.5607	34.7048	34.8257	34.9284	34.5607	34.7048	34.8257	34.9284
	"Salesman"	33.6832	33.7449	33.7959	33.8382	33.6832	33.7449	33.7959	33.8382
	"Hall"	34.0215	34.1143	34.1915	34.2564	34.0215	34.1143	34.1915	34.2564
	"Foreman"	33.5108	33.5653	33.6114	33.6504	33.5108	33.5653	33.6114	33.6504
	"Coastguard"	**30.9488**	30.6709	30.4247	30.2056	**30.9488**	30.6709	30.4247	30.2056
Case 2	"Akiyo"	36.9372	37.4978	37.6764	37.8302	35.3652	35.4299	35.4863	35.5358
	"Mother&Daughter"	34.9906	35.4015	35.4793	35.5459	33.5877	33.5149	33.4510	33.3944
	"Salesman"	34.0740	34.3847	34.4003	34.4124	34.9117	34.9451	34.9743	34.9999
	"Hall"	34.4212	34.7646	34.8034	34.8357	35.2744	35.3324	35.3829	35.4272
	"Foreman"	33.9734	34.3446	34.3610	34.3739	34.9981	35.0481	35.0932	35.1340
	"Coastguard"	**32.7052**	31.1199	30.8668	30.6401	**33.5649**	33.4763	33.3962	33.3237
Case 3	"Akiyo"	36.9433	37.1866	37.3925	37.5692	37.6623	37.9145	38.1293	38.3148
	"Mother&Daughter"	34.9962	35.1135	35.2129	35.2982	35.6522	35.7891	35.9063	36.0077
	"Salesman"	34.0791	34.1199	34.1538	34.1819	32.6142	32.4898	32.3800	32.2823
	"Hall"	34.4263	34.4957	34.5540	34.6033	32.9227	32.8314	32.7509	32.6794
	"Foreman"	33.9795	34.0190	34.0526	34.0812	34.7077	34.7907	34.8639	34.9287
	"Coastguard"	**31.2108**	30.9324	30.6851	30.4646	**33.3202**	33.2569	33.1990	33.1457
Case 4	"Akiyo"	35.4595	35.9111	36.2769	36.5806	36.6970	37.2631	37.7171	38.0907
	"Mother&Daughter"	33.6705	33.9479	34.1759	34.3666	34.7734	35.1841	35.5176	35.7938
	"Salesman"	32.8784	33.0533	33.1971	33.3171	33.8763	34.1849	34.4358	34.6434
	"Hall"	33.1952	33.4086	33.5836	33.7294	34.2192	34.5617	34.8392	35.0684
	"Foreman"	**31.6048**	31.5892	31.5741	31.5590	**30.8078**	30.6425	30.4941	30.3591
	"Coastguard"	**30.4360**	30.2016	29.9977	29.8190	**29.8923**	29.5397	29.2286	28.9526

Table 15: PSNR values for different dp, using PSO, for $R_k = 144$ kbps and $W_t = 22.5$ MHz.

		NNBS				**CNBS**			
	Sequences	**dp = 26**	**dp = 25**	**dp = 24**	**dp = 23**	**dp = 26**	**dp = 25**	**dp = 24**	**dp = 23**
Case 1	"Akiyo"	34.1645	34.4186	34.5889	34.6786	34.1645	34.4186	34.5889	34.6786
	"Mother&Daughter"	32.0453	32.1855	32.3602	32.5980	32.0453	32.1855	32.3602	32.5980
	"Salesman"	31.1217	31.1968	31.2682	31.3454	31.1217	31.1968	31.2682	31.3454
	"Hall"	31.5210	31.6229	31.8874	31.9786	31.5210	31.6229	31.8874	31.9786
	"Foreman"	**29.2876**	29.2015	29.0012	28.9201	**29.2876**	29.2015	29.0012	28.9201
	"Coastguard"	**28.0057**	27.7981	27.5629	27.3057	**28.0057**	27.7981	27.5629	27.3057
Case 2	"Akiyo"	34.8552	35.0496	35.2546	35.5378	33.1191	33.2324	33.3648	33.5678
	"Mother&Daughter"	32.6833	32.7767	32.9886	33.2501	31.0925	31.0872	31.2674	31.3897
	"Salesman"	31.7107	31.7459	31.8761	32.0452	32.6571	32.7461	32.8964	33.1562
	"Hall"	32.1199	32.1790	32.3564	32.5648	33.0788	33.1889	33.3617	33.4879
	"Foreman"	**29.8588**	29.7500	29.6420	29.5273	**30.8089**	30.7803	30.6348	30.2468
	"Coastguard"	**28.4254**	28.2047	28.1036	28.0010	**29.1200**	28.9639	28.7464	28.5560
Case 3	"Akiyo"	34.5609	34.7806	34.8978	35.1762	35.7362	36.0013	36.2564	36.5963
	"Mother&Daughter"	32.4107	32.5241	32.7896	32.9968	33.5056	33.6763	33.7888	34.2165
	"Salesman"	31.4588	31.5112	31.7862	31.9689	30.0895	30.0402	30.2658	30.5986
	"Hall"	31.8640	31.9414	32.3619	32.6891	30.4669	30.4470	30.6790	30.8970
	"Foreman"	**29.6126**	29.5140	29.3456	29.2165	**30.6207**	30.6106	30.0631	29.7532
	"Coastguard"	**28.2447**	28.0299	27.8962	27.6031	**28.9827**	28.8393	28.6866	28.4650
Case 4	"Akiyo"	33.0309	33.3978	33.5698	33.8938	34.4020	34.8576	35.1395	35.4443
	"Mother&Daughter"	31.0128	31.2392	31.0012	30.8964	32.2639	32.5963	32.3363	32.1161
	"Salesman"	30.1727	30.3207	30.6896	30.8896	31.3233	31.5783	31.8622	32.1116
	"Hall"	30.5520	30.7328	30.9863	31.3489	31.7262	32.0093	32.4658	32.6874
	"Foreman"	**28.4022**	28.3533	28.0130	27.7985	**27.4835**	27.3023	27.1542	26.9868
	"Coastguard"	**27.3516**	27.1656	26.8543	26.6366	**26.6678**	26.3748	26.2010	26.0012

motion levels more than the rest of the nodes, a fact that is expounded by the achieved PSNR values for each motion class. This is what the values in bold denote in Tables 12-15. In addition, the amelioration of the video quality becomes more perceivable in videos with poor quality rather than in videos with good visual quality. Therefore, we assigned to *dp* the highest values among the tested ones for each combination of bit rate and bandwidth. Thus, all our experiments with the NNBS and CNBS have been conducted using:

i) $dp = 28$ dB for the cases:

  a) $R_k = 96$ kbps and $W_t = 20$ MHz
  b) $R_k = 144$ kbps and $W_t = 30$ MHz

ii) $dp = 26$ dB for the cases:

  a) $R_k = 96$ kbps and $W_t = 15$ MHz
  b) $R_k = 144$ kbps and $W_t = 22.5$ MHz.

In Tables 26-19 we report the results for the four different node distributions and all considered criteria, solved by PSO, for all bit rate and bandwidth combinations. The reported quantities at each line of the tables are the power level, S, the combination of source and channel coding rate, (R_s,R_c), and the achieved utility, PSNR, per class. The values in bold refer to the total power levels and achieved PSNR values for all node distributions and criteria.

Studying the performance of NNBS and CNBS, we observed that when all motion classes have the same cardinality (Case 1), both NBS approaches offer exactly the same solution, i.e, the same PSNR values to all motion classes. In Case 2, the NNBS offers higher PSNR values compared to the CNBS, to the nodes that describe low amounts of motion. In Case 3, the same criterion (NNBS) assigns higher PSNR values compared to the CNBS, to the nodes that describe medium amounts of motion and in Case 4, higher PSNR values are assigned to the nodes that describe high amounts of motion, using also the NNBS compared to the CNBS. In all other cases, the CNBS "beats" the NNBS, by assigning higher PSNR values compared to the latter.

Continuing, the performance of the NNBS and CNBS criteria was compared with the performance achieved by the MAD and MMD criteria proposed in [1]. The MAD criterion minimizes the average distortion of the videos received by all nodes. For the Cases 2 and 3, a wise selection between NNBS and CNBS can always give higher PSNR results compared to the MAD, to all motion classes. For the Cases 1 and 4 the same can also be done, but with some exceptions.

The MMD criterion minimizes the maximum (worst) distortion among all the videos captured by the nodes and this solution is achieved when all nodes have the same distortion. In the considered DS-CDMA wireless VSN, reducing the distortion of a node by increasing its transmission power, increases the interference with the other nodes and thus, their distortion is increased. Hence, if we want to minimize the worst distortion among the nodes, we have to increase the transmission power of the "worst" node. Typically, this criterion offers the same utilities to all nodes. From the obtained results we observed that the MMD in all examined cases assigns exactly the same PSNR values to both classes of nodes that describe high amounts of motion. Also, in the large majority of the cases, the same PSNR values are also assigned to the sequence/sequences that describe medium amounts of motion. Last but not least, there are also some cases where all motion classes enjoy exactly the same PSNR values.

However, these results revealed that there are some cases where some nodes receive a lower distortion than that of the other nodes. At the same time, in these cases, these nodes need the lowest possible transmission power. Specifically, they need 5.0000 Watts, which is the low bound of the considered power level range. As a result, these nodes achieve lower distortions than the rest of the nodes, despite the fact that they use the least possible power. Evidently, if we had allowed a smaller low bound for the power level range, the specific nodes would use even less power and thus, all nodes would receive exactly the same distortion (thus, the same PSNR).

Comparing the performance of the MMD criterion with the performance of the NNBS and CNBS criteria, the latters can be wisely used so as to assign higher PSNR values to the low and medium video sequences, with some exceptions for the case of $R_k = 96$ kbps and $W_t = 20$ MHz.

Additionally, the higher the amounts of motion included in a sequence, the higher the power level that is required and also, the lower the PSNR value that is achieved. At this point, we should point out that the PSO algorithm is able to detect a number of optimal solutions for the power levels of all motion classes, all of which can attain the optimum value for the Nash product. Indeed, from Eq. (7), it follows that the multiplication of all power levels with the same constant leaves the ratio E_k/I_0 unaffected. This is because we assumed that thermal and background noise is negligible compared with the interference. In our results, we normalized the power levels so that the lowest allocated power is equal to 5.0000 Watts.

However, the source-channel coding rate combinations were unique in all examined cases. The nodes that describe high motion usually use more bits to compress their data and leave fewer bits that can be used to protect the sequence from transmission errors. In the following, Tables 26-19 confirmed our conviction that decreasing the bandwidth while keeping the bit rate constant, the value of Eq. (7) decreases, incurring a PSNR decrease to all motion classes.

For the total consumed power, there is no specific scheme that requires the highest amounts of power levels in all cases of a specific bit rate and bandwidth combination, except for the case of $R_k = 144$ kbps and $W_t = 22.5$ MHz, where the MMD criterion clearly needs far more power compared to the other schemes. Furthermore, it seems that Case 2 is the most demanding in resources (in terms of power) compared to the other three cases, when $R_k = 96$ kbps and $W_t = 20$ MHz, and $R_k = 144$ kbps and $W_t = 30$ MHz. The same holds also in half cases of $R_k = 96$ kbps and $W_t = 15$ MHz, and $R_k = 144$ kbps and $W_t = 22.5$ MHz. Last but not least, the highest total PSNR values are achieved in Case 2 of all examined bit rate and bandwidth combinations, with only an isolated exception.

All of the optimization criteria examined in this paper, i.e., the Nash bargaining solution (particularly here the two approaches NNBS and CNBS), the MAD and the MMD provide Pareto-optimal solutions. Specifically for the NBS, let us assume that the provided solution (the solutions from the NNBS and CNBS), i.e., the solution that maximizes the Nash product is not Pareto-optimal. This means that there is another solution where at least one node strictly increases its utility and no node decreases its utility. However, such a solution would lead to an even greater

Table 16: Experimental Results using PSO for $R_k = 96$ kbps and $W_t = 20$ MHz.

		NNBS			CNBS			MAD			MMD		
	Sequences	**S**	$(\mathbf{R_s}, \mathbf{R_c})$	**PSNR**	**S**	$(\mathbf{R_s}, \mathbf{R_c})$	**PSNR**	**S**	$(\mathbf{R_s}, \mathbf{R_c})$	**PSNR**	**S**	$(\mathbf{R_s}, \mathbf{R_c})$	**PSNR**
Case 1	"Akiyo"	5.0000	(32,1/3)	36.5112	5.0000	(32,1/3)	36.5112	5.0000	(32,1/3)	36.2808	5.0000	(32,1/3)	37.0690
	"Mother&Daughter"	6.1970	(32,1/3)	34.5452	6.1970	(32,1/3)	34.5452	6.3500	(32,1/3)	34.4621	5.0000	(32,1/3)	33.7349
	"Salesman"	5.8840	(32,1/3)	33.0986	5.8840	(32,1/3)	33.0986	6.2000	(32,1/3)	33.1756	5.2662	(32,1/3)	32.9946
	"Hall"	6.8140	(32,1/3)	33.8855	6.8140	(32,1/3)	33.8855	7.0500	(32,1/3)	33.8988	5.4199	(32,1/3)	32.9946
	"Foreman"	14.0260	(48,1/2)	33.5774	14.0260	(48,1/2)	33.5774	14.6000	(48,1/2)	33.6466	12.2326	(48,1/2)	32.9946
	"Coastguard"	14.4270	(48,1/2)	31.7825	14.4270	(48,1/2)	31.7825	15.0000	(48,1/2)	31.8157	15.0000	(64,2/3)	32.9946
	Total	**52.3480**		**203.4004**	**52.3480**		**203.4004**	**54.2118**		**203.2796**	**47.9187**		**202.7823**
Case 2	"Akiyo"	5.0000	(32,1/3)	36.9809	5.0000	(32,1/3)	36.9424	5.0000	(32,1/3)	36.9572	5.0000	(38.4,4/10)	35.0808
	"Mother&Daughter"	6.1387	(32,1/3)	34.9393	5.0555	(32,1/3)	33.6715	6.1150	(32,1/3)	34.8931	5.0000	(32,1/3)	34.2562
	"Salesman"	5.8296	(32,1/3)	33.3904	6.2451	(32,1/3)	33.6637	6.0468	(32,1/3)	33.5344	5.8396	(32,1/3)	33.8069
	"Hall"	6.7451	(32,1/3)	34.2718	8.3800	(38.4,4/10)	35.8310	6.8460	(32,1/3)	34.3374	5.6838	(32,1/3)	33.8069
	"Foreman"	14.5715	(64,2/3)	35.0184	15.0000	(64,2/3)	35.3444	14.5421	(64,2/3)	34.9341	12.0802	(48,1/2)	33.8069
	"Coastguard"	15.0000	(64,2/3)	32.8463	15.0000	(64,2/3)	32.7816	15.0000	(64,2/3)	32.8065	15.0000	(64,2/3)	33.8069
	Total	**53.2849**		**207.4471**	**54.6806**		**208.2346**	**53.5499**		**207.4627**	**48.6036**		**204.5646**
Case 3	"Akiyo"	5.0000	(32,1/3)	36.9558	5.2132	(32,1/3)	37.4139	5.0000	(32,1/3)	36.9399	5.0000	(32,1/3)	37.4428
	"Mother&Daughter"	6.1139	(32,1/3)	34.8905	6.4668	(32,1/3)	35.4221	6.0062	(32,1/3)	34.7674	5.0000	(32,1/3)	34.1410
	"Salesman"	5.8058	(32,1/3)	33.3543	5.0000	(32,1/3)	32.8240	5.9207	(32,1/3)	33.4298	5.7001	(32,1/3)	33.6265
	"Hall"	6.7184	(32,1/3)	34.2239	5.4524	(32,1/3)	33.1350	6.7194	(32,1/3)	34.2095	5.6214	(32,1/3)	33.6265
	"Foreman"	13.6258	(48,1/2)	34.0659	14.9177	(64,2/3)	35.7753	13.6744	(48,1/2)	34.0777	12.1153	(48,1/2)	33.6265
	"Coastguard"	15.0000	(64,2/3)	32.8041	15.0000	(64,2/3)	33.1541	15.0000	(64,2/3)	32.7774	15.0000	(64,2/3)	33.6265
	Total	**52.2636**		**206.2945**	**52.0501**		**207.7244**	**52.3207**		**206.2017**	**48.4368**		**206.0898**
Case 4	"Akiyo"	5.0000	(32,1/3)	35.8036	5.0000	(32,1/3)	37.0979	5.0000	(32,1/3)	35.6996	5.0000	(32,1/3)	36.0568
	"Mother&Daughter"	6.1890	(32,1/3)	33.8701	6.2010	(32,1/3)	35.1134	6.3910	(32,1/3)	33.9843	5.0000	(32,1/3)	32.6348
	"Salesman"	5.8750	(32,1/3)	32.5969	5.8895	(32,1/3)	33.5191	6.1889	(32,1/3)	32.7776	5.0000	(32,1/3)	31.9587
	"Hall"	6.8130	(32,1/3)	33.2280	7.9245	(38.4,4/10)	35.5853	7.1161	(32,1/3)	33.4128	5.1498	(32,1/3)	31.5385
	"Foreman"	14.4575	(48,1/2)	32.6798	9.4885	(32,1/3)	30.7193	15.0000	(48,1/2)	32.9506	12.6278	(32,1/3)	31.5385
	"Coastguard"	12.6450	(32,1/3)	30.1005	9.9345	(32,1/3)	29.8901	12.2593	(32,1/3)	29.8803	15.0000	(48,1/2)	31.5385
	Total	**50.9795**		**198.2789**	**44.4380**		**201.9251**	**51.9553**		**198.7052**	**47.7776**		**195.2658**

Table 17: Experimental Results using PSO for $R_k = 96$ kbps and $W_t = 15$ MHz.

		NNBS			CNBS			MAD			MMD		
	Sequences	**S**	$(\mathbf{R_s}, \mathbf{R_c})$	**PSNR**	**S**	$(\mathbf{R_s}, \mathbf{R_c})$	**PSNR**	**S**	$(\mathbf{R_s}, \mathbf{R_c})$	**PSNR**	**S**	$(\mathbf{R_s}, \mathbf{R_c})$	**PSNR**
Case 1	"Akiyo"	5.0000	(32,1/3)	35.6945	5.0000	(32,1/3)	35.6945	5.0000	(32,1/3)	35.0168	5.0000	(32,1/3)	35.2312
	"Mother&Daughter"	6.0230	(32,1/3)	33.5979	6.0230	(32,1/3)	33.5979	6.4010	(32,1/3)	33.3981	5.0000	(32,1/3)	31.7377
	"Salesman"	5.5620	(32,1/3)	32.2508	5.5620	(32,1/3)	32.2508	6.1295	(32,1/3)	32.2877	5.0000	(32,1/3)	31.3134
	"Hall"	6.5455	(32,1/3)	32.8823	6.5455	(32,1/3)	32.8823	7.0970	(32,1/3)	32.8212	5.1860	(32,1/3)	30.6941
	"Foreman"	10.8655	(32,1/3)	30.2644	10.8655	(32,1/3)	30.2644	12.2990	(32,1/3)	30.4978	12.3134	(32,1/3)	30.6941
	"Coastguard"	10.6320	(32,1/3)	29.2214	10.6320	(32,1/3)	29.2214	11.9025	(32,1/3)	29.3379	15.0000	(48,1/2)	30.6941
	Total	**44.6280**		**193.9113**	**44.6280**		**193.9113**	**48.8290**		**193.3595**	**47.4994**		**190.3646**
Case 2	"Akiyo"	5.0000	(32,1/3)	36.1434	5.0000	(32,1/3)	35.3258	5.0000	(32,1/3)	35.2539	5.0000	(32,1/3)	35.8514
	"Mother&Daughter"	6.0360	(32,1/3)	34.0389	5.4467	(32,1/3)	32.5165	6.3586	(32,1/3)	33.5627	5.0000	(32,1/3)	32.4116
	"Salesman"	5.5710	(32,1/3)	32.5823	6.4488	(32,1/3)	32.7412	6.1069	(32,1/3)	32.4249	5.0000	(32,1/3)	31.7982
	"Hall"	6.5600	(32,1/3)	33.3179	7.5948	(32,1/3)	33.5278	7.0575	(32,1/3)	32.9887	5.2294	(32,1/3)	31.4334
	"Foreman"	10.8100	(32,1/3)	30.6672	15.0000	(48,1/2)	32.5214	15.0000	(48,1/2)	32.4018	12.6330	(32,1/3)	31.4334
	"Coastguard"	10.5830	(32,1/3)	29.5215	12.2136	(32,1/3)	29.6692	11.9233	(32,1/3)	29.5011	15.0000	(48,1/2)	31.4334
	Total	**44.5600**		**196.2712**	**51.7039**		**196.3019**	**51.4463**		**196.1331**	**47.8624**		**194.3614**
Case 3	"Akiyo"	5.0000	(32,1/3)	36.0155	5.5936	(32,1/3)	36.3045	5.0000	(32,1/3)	35.2806	5.0000	(32,1/3)	35.8273
	"Mother&Daughter"	6.0325	(32,1/3)	33.9130	6.7573	(32,1/3)	34.1980	6.4400	(32,1/3)	33.6732	5.0000	(32,1/3)	32.3854
	"Salesman"	5.5685	(32,1/3)	32.4877	5.0000	(32,1/3)	31.5356	6.1980	(32,1/3)	32.5171	5.0000	(32,1/3)	31.7793
	"Hall"	6.5560	(32,1/3)	33.1933	5.7320	(32,1/3)	31.7751	7.1535	(32,1/3)	33.1013	5.2272	(32,1/3)	31.4039
	"Foreman"	10.8230	(32,1/3)	30.5507	15.0000	(48,1/2)	32.8400	12.4530	(32,1/3)	30.8146	12.6201	(32,1/3)	31.4039
	"Coastguard"	10.5970	(32,1/3)	29.4348	11.8194	(32,1/3)	29.6321	12.1445	(32,1/3)	29.6109	15.0000	(48,1/2)	31.4039
	Total	**44.5770**		**195.5950**	**49.9023**		**196.2853**	**49.3890**		**194.9977**	**47.8473**		**194.2037**
Case 4	"Akiyo"	5.0000	(32,1/3)	34.9081	5.0000	(32,1/3)	35.8943	5.0000	(32,1/3)	34.3861	5.0000	(32,1/3)	33.7426
	"Mother&Daughter"	5.9965	(32,1/3)	32.8337	6.0290	(32,1/3)	33.7938	6.3065	(32,1/3)	32.7405	5.0000	(32,1/3)	30.1199
	"Salesman"	5.5440	(32,1/3)	31.6736	5.5665	(32,1/3)	32.3982	5.9745	(32,1/3)	31.7394	5.0000	(32,1/3)	30.1496
	"Hall"	6.5155	(32,1/3)	32.1320	6.5520	(32,1/3)	33.0756	6.9585	(32,1/3)	32.1522	5.5550	(32,1/3)	29.7558
	"Foreman"	10.9590	(32,1/3)	29.5999	8.8385	(32,1/3)	29.0024	11.9135	(32,1/3)	29.7447	12.8151	(32,1/3)	29.7558
	"Coastguard"	10.7140	(32,1/3)	28.7254	8.6335	(32,1/3)	28.2780	11.3330	(32,1/3)	28.6895	15.0000	(32,1/3)	29.7558
	Total	**44.7290**		**189.8727**	**40.6195**		**192.4423**	**47.4860**		**189.4522**	**48.3701**		**183.2795**

Table 18: Experimental Results using PSO for $R_k = 144$ kbps and $W_t = 30$ MHz.

		NNBS			CNBS			MAD			MMD		
	Sequences	**S**	$(\mathbf{R_s}, \mathbf{R_c})$	**PSNR**	**S**	$(\mathbf{R_s}, \mathbf{R_c})$	**PSNR**	**S**	$(\mathbf{R_s}, \mathbf{R_c})$	**PSNR**	**S**	$(\mathbf{R_s}, \mathbf{R_c})$	**PSNR**
Case 1	"Akiyo"	5.0000	(48,1/3)	36.4608	5.0000	(48,1/3)	36.4608	5.0000	(48,1/3)	35.9137	5.0000	(48,1/3)	34.5798
	"Mother&Daughter"	6.0859	(48,1/3)	34.5607	6.0889	(48,1/3)	34.5607	6.3540	(48,1/3)	34.5109	6.3054	(48,1/3)	33.2093
	"Salesman"	6.5475	(48,1/3)	33.6832	6.5475	(48,1/3)	33.6832	6.9400	(48,1/3)	33.7930	7.3095	(48,1/3)	33.2093
	"Hall"	6.2033	(48,1/3)	34.0215	6.2033	(48,1/3)	34.0215	6.5390	(48,1/3)	34.0764	6.7042	(32,1/3)	33.2093
	"Foreman"	10.9137	(72,1/2)	33.5108	10.9137	(72,1/2)	33.5108	11.5525	(72,1/2)	33.6666	12.5330	(48,1/3)	33.2093
	"Coastguard"	10.4261	(48,1/3)	30.9488	10.4261	(48,1/3)	30.9488	10.9800	(48,1/3)	30.9864	15.0000	(48,1/3)	33.2093
	Total	**45.1795**		**203.1858**	**45.1795**		**203.1858**	**47.3655**		**202.9470**	**52.8521**		**200.6263**
Case 2	"Akiyo"	5.0000	(48,1/3)	36.9372	5.0000	(48,1/3)	35.3652	5.0000	(48,1/3)	36.3332	5.0000	(48,1/3)	35.5691
	"Mother&Daughter"	6.0765	(48,1/3)	34.9906	6.1183	(48,1/3)	33.5877	6.3770	(48,1/3)	34.9365	6.4225	(48,1/3)	34.3115
	"Salesman"	6.5275	(48,1/3)	34.0740	8.1458	(48,1/3)	34.9117	6.9825	(48,1/3)	34.2124	7.5287	(48,1/3)	34.3115
	"Hall"	6.1895	(48,1/3)	34.4212	7.7352	(48,1/3)	35.2744	6.5760	(48,1/3)	34.4928	6.8920	(48,1/3)	34.3115
	"Foreman"	10.7665	(72,1/2)	33.9734	13.1513	(72,1/2)	34.9981	11.4865	(72,1/2)	34.1553	12.3809	(72,1/2)	34.3115
	"Coastguard"	11.8530	(72,1/2)	32.7052	14.4449	(72,1/2)	33.5649	12.8185	(72,1/2)	33.0510	15.0000	(72,1/2)	34.3115
	Total	**46.4130**		**207.1016**	**54.5955**		**207.7020**	**49.2405**		**207.1812**	**53.2241**		**207.1266**
Case 3	"Akiyo"	5.0000	(48,1/3)	36.9433	5.0000	(48,1/3)	37.6623	5.0000	(48,1/3)	35.9637	5.0000	(48,1/3)	35.1208
	"Mother&Daughter"	6.0765	(48,1/3)	34.9962	6.0590	(48,1/3)	35.6522	6.3570	(48,1/3)	34.5617	6.3659	(48,1/3)	33.8065
	"Salesman"	6.5275	(48,1/3)	34.0791	5.2935	(48,1/3)	32.6142	6.9450	(48,1/3)	33.8430	7.4243	(48,1/3)	33.8065
	"Hall"	6.1890	(48,1/3)	34.4263	5.0040	(48,1/3)	32.9227	6.5435	(48,1/3)	34.1261	6.8021	(48,1/3)	33.8065
	"Foreman"	10.7650	(72,1/2)	33.9795	10.5535	(72,1/2)	34.7077	11.5450	(72,1/2)	33.7248	12.4494	(72,1/2)	33.8065
	"Coastguard"	10.3110	(48,1/3)	31.2108	11.5990	(72,1/2)	33.3202	12.8355	(72,1/2)	32.6268	15.0000	(72,1/2)	33.8065
	Total	**44.8690**		**205.6352**	**43.5090**		**206.8793**	**49.2260**		**204.8461**	**53.0417**		**204.1533**
Case 4	"Akiyo"	5.0000	(48,1/3)	35.4595	5.0000	(48,1/3)	36.6970	5.0000	(48,1/3)	35.1774	5.0000	(48,1/3)	32.9847
	"Mother&Daughter"	6.1155	(48,1/3)	33.6705	6.0830	(48,1/3)	34.7734	6.3125	(48,1/3)	33.7643	6.2398	(48,1/3)	31.6621
	"Salesman"	6.5910	(48,1/3)	32.8784	6.5375	(48,1/3)	33.8763	6.8640	(48,1/3)	33.0576	7.1215	(48,1/3)	31.6621
	"Hall"	6.2340	(48,1/3)	33.1952	6.1965	(48,1/3)	34.2192	6.4740	(48,1/3)	33.3461	6.5542	(48,1/3)	31.6621
	"Foreman"	10.3350	(48,1/3)	31.6048	8.7005	(48,1/3)	30.8078	10.7305	(48,1/3)	31.7761	12.5792	(48,1/3)	31.6621
	"Coastguard"	10.6795	(48,1/3)	30.4360	9.0040	(48,1/3)	29.8923	10.7025	(48,1/3)	30.2586	15.0000	(48,1/3)	31.6621
	Total	**44.9550**		**197.24444**	**41.5215**		**200.2660**	**46.0835**		**197.3801**	**52.4947**		**191.2952**

Table 19: Experimental Results using PSO for $R_k = 144$ kbps and $W_t = 22.5$ MHz.

		NNBS			CNBS			MAD			MMD		
	Sequences	**S**	$(\mathbf{R_s}, \mathbf{R_c})$	**PSNR**	**S**	$(\mathbf{R_s}, \mathbf{R_c})$	**PSNR**	**S**	$(\mathbf{R_s}, \mathbf{R_c})$	**PSNR**	**S**	$(\mathbf{R_s}, \mathbf{R_c})$	**PSNR**
Case 1	"Akiyo"	5.0000	(48,1/3)	34.1645	5.0000	(48,1/3)	34.1645	5.0000	(48,1/3)	33.1807	5.0000	(48,1/3)	30.1623
	"Mother&Daughter"	5.8885	(48,1/3)	32.0453	5.8885	(48,1/3)	32.0453	6.1850	(48,1/3)	31.7519	6.6545	(48,1/3)	30.1623
	"Salesman"	6.1985	(48,1/3)	31.1217	6.1985	(48,1/3)	31.1217	6.6445	(48,1/3)	31.0805	7.4745	(48,1/3)	30.1623
	"Hall"	5.9185	(48,1/3)	31.5210	5.9185	(48,1/3)	31.5210	6.2885	(48,1/3)	31.3786	6.9120	(48,1/3)	30.1623
	"Foreman"	9.4195	(48,1/3)	29.2876	9.4195	(48,1/3)	29.2876	10.4010	(48,1/3)	29.6193	13.2165	(48,1/3)	30.1623
	"Coastguard"	8.8895	(48,1/3)	28.0057	8.8895	(48,1/3)	28.0057	9.9280	(48,1/3)	28.3462	14.8490	(48,1/3)	30.1623
	Total	**41.3145**		**186.1458**	**41.3145**		**186.1458**	**44.4470**		**185.3572**	**54.1065**		**180.9738**
Case 2	"Akiyo"	5.0000	(48,1/3)	34.8552	5.0000	(48,1/3)	33.1191	5.0000	(48,1/3)	33.8512	5.0000	(48,1/3)	31.7686
	"Mother&Daughter"	5.8840	(48,1/3)	32.6833	5.8950	(48,1/3)	31.0925	6.2265	(48,1/3)	32.4322	6.4705	(48,1/3)	31.0979
	"Salesman"	6.1905	(48,1/3)	31.7107	7.7055	(48,1/3)	32.6571	6.7150	(48,1/3)	31.7506	7.3337	(48,1/3)	31.0979
	"Hall"	5.9135	(48,1/3)	32.1199	7.3670	(48,1/3)	33.0788	6.3480	(48,1/3)	32.0442	6.7650	(48,1/3)	31.0979
	"Foreman"	9.3350	(48,1/3)	29.8588	11.4845	(48,1/3)	30.8089	10.5020	(48,1/3)	30.3640	12.8977	(48,1/3)	31.0979
	"Coastguard"	8.8210	(48,1/3)	28.4254	10.8730	(48,1/3)	29.1200	10.1715	(48,1/3)	29.0056	15.0000	(48,1/3)	31.0979
	Total	**41.1440**		**189.6533**	**48.2950**		**189.8764**	**44.9630**		**189.4478**	**53.4669**		**187.2581**
Case 3	"Akiyo"	5.0000	(48,1/3)	34.5609	5.2395	(48,1/3)	35.7362	5.0000	(48,1/3)	33.5194	5.0000	(48,1/3)	31.0367
	"Mother&Daughter"	5.8860	(48,1/3)	32.4107	6.1590	(48,1/3)	33.5056	6.2060	(48,1/3)	32.0955	6.5748	(48,1/3)	30.7007
	"Salesman"	6.1940	(48,1/3)	31.4588	5.2415	(48,1/3)	30.0895	6.6800	(48,1/3)	31.4189	7.4234	(48,1/3)	30.7007
	"Hall"	5.9155	(48,1/3)	31.8640	5.0000	(48,1/3)	30.4669	6.3185	(48,1/3)	31.7148	6.8547	(48,1/3)	30.7007
	"Foreman"	9.3705	(48,1/3)	29.6126	9.6730	(48,1/3)	30.6207	10.4530	(48,1/3)	29.9952	13.0894	(48,1/3)	30.7007
	"Coastguard"	8.8500	(48,1/3)	28.2447	8.7360	(48,1/3)	28.9827	10.0510	(48,1/3)	28.6790	15.0000	(48,1/3)	30.7007
	Total	**41.2160**		**188.1517**	**40.0490**		**189.4016**	**44.7085**		**187.4228**	**53.9423**		**184.5402**
Case 4	"Akiyo"	5.0000	(48,1/3)	33.0309	5.0000	(48,1/3)	34.4020	5.0000	(48,1/3)	32.2495	5.0000	(48,1/3)	28.7813
	"Mother&Daughter"	5.8955	(48,1/3)	31.0128	5.8870	(48,1/3)	32.2639	6.1265	(48,1/3)	30.8076	6.5060	(48,1/3)	28.7813
	"Salesman"	6.2120	(48,1/3)	30.1727	6.1960	(48,1/3)	31.3233	6.5465	(48,1/3)	30.1503	7.2135	(48,1/3)	28.7813
	"Hall"	5.9260	(48,1/3)	30.5520	5.9170	(48,1/3)	31.7262	6.2070	(48,1/3)	30.4547	6.6985	(48,1/3)	28.7813
	"Foreman"	9.5655	(48,1/3)	28.4022	8.0570	(48,1/3)	27.4835	10.2450	(48,1/3)	28.5880	12.8005	(48,1/3)	28.7813
	"Coastguard"	9.0075	(48,1/3)	27.3516	7.5680	(48,1/3)	26.6678	9.5950	(48,1/3)	27.4337	13.6900	(48,1/3)	28.7813
	Total	**41.6065**		**180.5222**	**38.6250**		**183.8667**	**43.7200**		**179.6838**	**51.9085**		**172.6878**

Nash product, thus contradicting the fact that the NBS maximizes the Nash product. Therefore, the solution provided by the NBS criterion is Pareto-optimal.

Similar reasoning applies also to the MAD criterion. If we assume that the solution given by the MAD is not Pareto-optimal, this means that there is another solution where at least one node receives lower distortion and no node increases its distortion. However, such a solution would lead to an even smaller average distortion, thus contradicting the fact that the MAD criterion minimizes the average distortion. Therefore, the solution provided by the MAD criterion is Pareto-optimal.

As mentioned earlier, the MMD solution occurs when an "equilibrium" is reached, i.e., when all nodes have the same distortion (except in some cases when a node, i.e., motion class, uses a power level at the lower end of the considered power level range), and, increasing a node's transmission power will increase the distortions of the other nodes, thus leading to a higher maximum distortion.

If the solution given by the MMD is not Pareto-optimal, this would mean that there exists another solution where at least one node receives a lower distortion and no node increases its distortion. Such a solution would result in a deviation from the "equilibrium". Thus, the lower distortion of one node would be a result of an increase of its transmission power. This would lead to an increase of the distortions of the other nodes. Therefore, an alternative solution where at least one node receives a lower distortion and no node increases its distortion cannot exist and the MMD leads to a Pareto-optimal solution.

For comparison reasons, each examined criterion, except for the PSO, it was also run using three competing optimization algorithms, for all cases of node distributions. Specifically, PSO's performance was compared with that of the deterministic algorithms AS [16, 17, 18, 77, 78], IP [20, 21] and TRR [22, 23]. Each of these methods was run for the same maximum number of function evaluations as PSO, i.e., 70000 function evaluations. Furthermore, 30 independent experiments were also conducted for each one of the aforementioned deterministic methods, starting from a different, random starting point at each experiment, within the range $[5.0, 15.0]$.

In the following, Tables 20-23 provided statistical information regarding the performance of all the aforementioned algorithms, over all independent trials. Specifically, each table presents the results for a particular bit rate and bandwidth combination. The column "Case" refers to a specific node distribution. The column "Success" shows how many times each algorithm succeeds in finding the optimal solution to a precision of six decimal digits, out of 30 independent trials. Columns "Min", "Mean", "Max" and "Median" report the min, mean, max and median value of the function, respectively, over the 30 experiments. The standard deviation of the 30 values of the function is presented under the column "Std". We should note that for the NNBS and CNBS criteria the objective function is the one given by Eq. (59), assuming different bargaining powers for each of them. Similarly, the objective functions of the MAD and MMD criteria can be found in [1].

The last column of the tables presents the results of the Wilcoxon rank sum hypothesis tests [79, 80], having set the significance level at 1%. More specifically, the obtained values of these tests can be either 1 or 0. A value equal to 1 indicates rejection of the null hypothesis at the 1% significance level, while a value equal to 0 indicates a failure to reject the null hypothesis at the 1% significance level. For each case of nodes' distribution, PSO was compared with the respective case of the AS, IP and TRR algorithms, and the results of the two-sided rank sum tests were reported under the "Ranksum" column, next to AS, IP and TRR algorithms, respectively. For example, for the case of $R_k = 96$ kbps and $W_t = 20$ MHz, for the NNBS criterion, having "1" under the "Ranksum" column to Case 1 of AS, this means that the test rejects the null hypothesis of equal medians for the 30 values of the NNBS function using the PSO and the 30 values of the NNBS function using the AS, at 1% significance level.

Observing the successes of each optimization method over the 30 experiments for all considered bit rate and bandwidth combinations, we saw that PSO far exceeds the other methods, where in many cases its success rate is 100%. The great advantage of PSO compared to the other methods is more obvious in the MMD criterion. While PSO's success rate is in many cases 100%, the other methods fail nearly always to reach the optimal solution. However, there are a few cases where PSO's successes are less than 30. In these cases, if we examine the other statistic values of the tables, we will observe that the min value of the function differs from the max value (of the 30 values) in the third, second or first decimal digit. This claim is also confirmed by the small values of the standard deviation or by the fact that the min function value is equal with the median function value or have a slight difference in the fourth or third decimal digit. However, even in cases where PSO achieves a near-optimal solution, this solution is acceptable in practice, since it has only a slight impact on the utilities achieved by the nodes. Thus, all these statistical information reinforced our view about the efficiency of PSO in solving such optimization tasks.

Also, PSO, AS and IP behaved better with the MAD criterion, noting better performance. As it was previously referred, PSO far exceeds the other competing methods, being able to nearly always reach the optimal solution. Among the benchmarks that we used for comparison with the PSO, the IP algorithm was the most efficient one, followed in performance by the AS, and finally, by the TRR, which fails always (in all examined cases) to reach the optimal solution.

The considerably low success rates of the deterministic algorithms can be probably attributed to the shape of the corresponding objective functions. Specifically, if they include steep hills as well as large flat areas, this can trap the deterministic approaches if they are initialized within these regions. This means that the selection of the starting point is very important for the performance of each method. For example, if the functions are flat in a large part, a starting point in this area does not lead any of the three above methods to find the optimal solution. This fact motivated us to use the PSO algorithm as the optimization solver in this paper.

Lastly, experimental results of the PSO's convergence speed were presented in Table 24. Specifically, this table shows the time that PSO requires to find the optimal solution with a precision of 6 decimal digits, in terms of the number of iterations that the swarm is updated. Thus, these statistics concern only the experiments where PSO reaches the optimal solution. In this table were included results for all node distributions of all considered bit rate and bandwidth combinations, and for all tested criteria. Due to the fact that PSO is a stochastic algorithm, we did not only cite the average performance, i.e., the mean number of iterations that the swarm is updated in order to reach the solution (Mean), but we also presented the best case, i.e., the minimum number of iterations (Min) and the worst case, i.e., the maximum number of iterations (Max).

The criterion that presented the fastest PSO's convergence, requiring less iterations on average

Table 20: Statistical Results for PSO, AS, IP, TRR, $R_k = 96$ kbps and $W_t = 20$ MHz

Criterion	Algorithm	Case	Success	Min	Mean	Max	Median	Std	Ranksum
NNBS	PSO	#1	30	-5.726552	-5.726552	-5.726552	-5.726552	0.00	–
		#2	30	-6.759974	-6.759974	-6.759974	-6.759974	0.00	–
		#3	29	-6.138522	-6.138506	-6.138032	-6.138522	0.00	–
		#4	24	-4.275103	-4.272522	-4.232132	-4.275103	0.01	–
	AS	#1	4	-5.726552	-0.121092	1.000000	1.000000	2.55	1
		#2	2	-6.759974	0.482668	1.000000	1.000000	1.97	1
		#3	4	-6.138522	0.048197	1.000000	1.000000	2.47	1
		#4	7	-4.275103	-0.582531	1.000000	1.000000	2.46	1
	IP	#1	6	-5.726552	-0.345310	1.000000	1.000000	2.74	1
		#2	1	-6.759974	0.482668	1.000000	1.000000	1.97	1
		#3	3	-6.138522	0.286148	1.000000	1.000000	2.18	1
		#4	9	-4.275103	-0.582531	1.000000	1.000000	2.46	1
	TRR	#1	0	-5.330930	-0.213350	1.000000	1.000000	2.28	1
		#2	0	-5.908247	0.565973	1.000000	1.000000	1.66	1
		#3	0	-4.873453	0.277376	1.000000	1.000000	1.88	1
		#4	0	-3.367513	-0.163746	1.000000	1.000000	1.82	1
CNBS	PSO	#1	30	-5.726552	-5.726552	-5.726552	-5.726552	0.00	–
		#2	30	-6.550393	-6.550393	-6.550393	-6.550393	0.00	–
		#3	30	-6.409900	-6.409900	-6.409900	-6.409900	0.00	–
		#4	30	-4.904941	-4.904941	-4.904941	-4.904941	0.00	–
	AS	#1	3	-5.726552	0.327345	1.000000	1.000000	2.05	1
		#2	2	-6.550393	0.496640	1.000000	1.000000	1.92	1
		#3	1	-6.409900	0.259011	1.000000	1.000000	2.26	1
		#4	7	-4.904941	-2.149301	1.000000	-4.904939	3.00	1
	IP	#1	4	-5.726552	0.103126	1.000000	1.000000	2.33	1
		#2	0	-6.550392	0.748320	1.000000	1.000000	1.38	1
		#3	1	-6.409900	0.259010	1.000000	1.000000	2.26	1
		#4	14	-4.904941	-1.755639	1.000000	1.000000	3.00	1
	TRR	#1	0	-4.964087	0.515564	1.000000	1.000000	1.51	1
		#2	0	1.000000	1.000000	1.000000	1.000000	0.00	1
		#3	0	-5.078231	0.442476	1.000000	1.000000	1.71	1
		#4	0	-4.420913	-0.777876	1.000000	1.000000	2.41	1
MAD	PSO	#1	29	27.877986	27.903443	28.641710	27.877986	0.14	–
		#2	30	22.105961	22.105961	22.105961	22.105961	0.00	–
		#3	30	25.335557	25.335557	25.335557	25.335557	0.00	–
		#4	28	38.152870	38.195643	38.921273	38.152872	0.17	–
	AS	#1	30	27.877986	27.877986	27.877986	27.877986	0.00	0
		#2	30	22.105961	22.105961	22.105961	22.105961	0.00	0
		#3	14	25.335557	27.840128	100.472675	25.335558	13.72	1
		#4	30	38.152872	38.152872	38.152872	38.152872	0.00	0
	IP	#1	27	27.877986	27.877986	27.877987	27.877986	0.00	0
		#2	30	22.105961	22.105961	22.105961	22.105961	0.00	0
		#3	14	25.335557	25.335558	25.335558	25.335558	0.00	1
		#4	30	38.152872	38.152872	38.152872	38.152872	0.00	0
	TRR	#1	0	35.459611	84.873294	590.658891	55.698445	105.48	1
		#2	0	29.444823	31922142.648722	957609654.693354	198.978964	174834459.25	1
		#3	0	29.759017	649.290198	13790.047768	66.250344	2528.78	1
		#4	0	45.894814	97.197020	428.296977	60.885126	103.30	1
MMD	PSO	#1	26	32.630183	32.681779	33.238361	32.630183	0.16	–
		#2	30	27.063638	27.063638	27.063638	27.063638	0.00	–
		#3	20	28.211844	28.375334	29.236985	28.211844	0.33	–
		#4	29	45.627729	45.673158	46.990611	45.627729	0.25	–
	AS	#1	0	32.630184	32.727708	33.837196	32.630313	0.28	1
		#2	0	27.063640	27.214074	28.781947	27.064162	0.40	1
		#3	0	28.211845	28.277313	29.324319	28.214876	0.21	1
		#4	1	45.627729	45.627799	45.628617	45.627735	0.00	1
	IP	#1	0	32.893982	32.921179	33.593664	32.894431	0.13	1
		#2	0	27.286547	27.343641	27.381377	27.346057	0.01	1
		#3	0	28.475167	28.483026	28.513347	28.482314	0.01	1
		#4	0	45.992175	46.004366	46.080940	46.001779	0.01	1
	TRR	#1	0	63.809690	1473.410378	11798.985887	735.239348	2557.98	1
		#2	0	50.968639	871.311987	3926.881004	561.712215	990.35	1
		#3	0	54.714794	5969.861550	162460.812440	324.760820	29562.79	1
		#4	0	63.999563	166.903248	491.288336	128.784483	96.83	1

over all 30 experiments per case, was the MAD, which behaves better than all the other competing schemes. On the contrary, PSO confronted the biggest challenge in convergence, using the MMD criterion. With an exception for the case of $R_k = 96$ kbps and $W_t = 15$ MHz, in all other bit rate and bandwidth combinations, the MMD required much more iterations on average compared to

Table 21: Statistical Results for PSO, AS, IP, TRR, $R_k = 96$ kbps and $W_t = 15$ MHz

Criterion	Algorithm	Case	Success	Min	Mean	Max	Median	Std	Ranksum
NNBS	PSO	#1	30	-5.931049	-5.931049	-5.931049	-5.931049	0.00	–
		#2	30	-6.884919	-6.884919	-6.884919	-6.884919	0.00	–
		#3	29	-6.357387	-6.357375	-6.357014	-6.357387	0.00	–
		#4	30	-4.644677	-4.644677	-4.644677	-4.644677	0.00	–
	AS	#1	10	-5.931049	-1.310350	1.000000	1.000000	3.32	1
		#2	11	-6.884919	-2.679628	1.000000	1.000000	4.00	1
		#3	2	-6.357387	-1.942954	1.000000	1.000000	3.67	1
		#4	2	-4.644677	-2.386805	1.000000	-4.644673	2.81	1
	IP	#1	14	-5.931049	-2.234490	1.000000	1.000000	3.52	1
		#2	13	-6.884919	-2.416798	1.000000	1.000000	3.97	1
		#3	18	-6.357387	-3.414432	1.000000	-6.357387	3.67	1
		#4	11	-4.644677	-1.069715	1.000000	1.000000	2.77	1
	TRR	#1	0	-5.622618	-2.655088	1.000000	-4.322057	2.89	1
		#2	0	-6.486487	-1.237290	1.000000	1.000000	3.24	1
		#3	0	-6.035897	-2.238168	1.000000	-3.305525	3.14	1
		#4	0	-4.130423	-1.386533	1.000000	-2.321361	2.17	1
CNBS	PSO	#1	30	-5.931049	-5.931049	-5.931049	-5.931049	0.00	–
		#2	19	-6.476440	-6.466387	-6.449022	-6.476440	0.01	–
		#3	16	-6.374505	-6.357740	-6.338579	-6.374505	0.02	–
		#4	30	-5.366147	-5.366147	-5.366147	-5.366147	0.00	–
	AS	#1	8	-5.931049	-1.541384	1.000000	1.000000	3.40	1
		#2	6	-6.476440	-0.744503	1.000000	1.000000	3.22	1
		#3	5	-6.374505	-0.229084	1.000000	1.000000	2.80	1
		#4	5	-5.366147	-1.970868	1.000000	1.000000	3.23	1
	IP	#1	16	-5.931049	-2.696559	1.000000	-5.931049	3.52	1
		#2	4	-6.476440	0.003141	1.000000	1.000000	2.58	1
		#3	9	-6.374505	-1.212352	1.000000	1.000000	3.44	1
		#4	14	-5.366147	-1.970869	1.000000	1.000000	3.23	1
	TRR	#1	0	-5.497558	-2.238326	1.000000	-3.878174	2.92	1
		#2	0	-5.926976	-0.693331	1.000000	1.000000	2.67	1
		#3	0	-5.030588	0.261632	1.000000	1.000000	1.92	1
		#4	0	-5.104637	-1.385651	1.000000	1.000000	2.80	1
MAD	PSO	#1	30	42.715334	42.715334	42.715334	42.715334	0.00	–
		#2	18	34.740266	34.741492	34.743331	34.740266	0.00	–
		#3	30	38.678888	38.678888	38.678888	38.678888	0.00	–
		#4	30	56.482854	56.482854	56.482854	56.482854	0.00	–
	AS	#1	8	42.715334	42.715335	42.715336	42.715335	0.00	1
		#2	27	34.740266	34.740266	34.740267	34.740266	0.00	1
		#3	17	38.678888	38.678888	38.678889	38.678888	0.00	1
		#4	8	56.482854	56.482855	56.482855	56.482855	0.00	1
	IP	#1	30	42.715334	42.715334	42.715334	42.715334	0.00	0
		#2	11	34.740266	34.740267	34.740267	34.740267	0.00	0
		#3	30	38.678888	38.678888	38.678888	38.678888	0.00	0
		#4	30	56.482854	56.482854	56.482854	56.482854	0.00	0
	TRR	#1	0	48.597923	67.903578	124.637931	59.695320	21.60	1
		#2	0	41.072661	2562336.995613	76818946.290372	69.551001	14024836.44	1
		#3	0	41.140134	55.932004	84.065159	55.987149	9.81	1
		#4	0	59.823066	84.709830	142.269987	81.943355	21.17	1
MMD	PSO	#1	26	55.420774	55.516563	56.139190	55.420774	0.25	–
		#2	30	46.745971	46.745971	46.745971	46.745971	0.00	–
		#3	27	47.064096	47.260824	50.356854	47.064096	0.67	–
		#4	30	68.786486	68.786486	68.786486	68.786486	0.00	–
	AS	#1	0	55.420775	213734.132136	6410416.730469	55.420789	1170366.50	1
		#2	2	46.745971	427404.773826	6410416.730469	46.746009	1626362.98	1
		#3	0	47.064097	47.076131	47.414143	47.064110	0.06	1
		#4	0	68.786488	68.954052	72.913638	68.786535	0.75	1
	IP	#1	0	55.788466	213734.511989	6410416.730469	55.809086	1170366.43	1
		#2	0	47.116362	47.135636	47.155817	47.136172	0.01	1
		#3	0	47.373010	47.450356	47.459722	47.452354	0.01	1
		#4	0	69.178991	69.180494	69.198662	69.179764	0.00	1
	TRR	#1	0	93.225285	214326.061791	6410416.730469	337.734698	1170255.19	1
		#2	0	78.373678	4090.934508	89078.591611	343.627444	16255.22	1
		#3	0	105.814688	433327.625626	6410416.730469	279.925460	1624953.58	1
		#4	0	96.411897	181.725259	339.864507	149.604006	71.05	1

the other criteria. Especially when the bit rate was equal to 144 kbps, the lowest average iteration number was equal to 684 out of 700 iterations.

Table 22: Statistical Results for PSO, AS, IP, TRR, $R_k = 144$ kbps and $W_t = 30$ MHz

Criterion	Algorithm	Case	Success	Min	Mean	Max	Median	Std	Ranksum
NNBS	PSO	#1	28	-5.600859	-5.599407	-5.579073	-5.600859	0.01	–
		#2	22	-6.723017	-6.719601	-6.710207	-6.723017	0.01	–
		#3	30	-6.062459	-6.062459	-6.062459	-6.062459	0.00	–
		#4	25	-4.144447	-4.121988	-3.845342	-4.144447	0.07	–
	AS	#1	5	-5.600859	-0.760229	1.000000	1.000000	2.97	1
		#2	0	-6.723015	0.742566	1.000000	1.000000	1.41	1
		#3	3	-6.062459	-0.177076	1.000000	1.000000	2.68	1
		#4	0	-4.144446	-0.200370	1.000000	1.000000	2.21	1
	IP	#1	10	-5.600859	-1.200286	1.000000	1.000000	3.16	1
		#2	1	-6.723017	0.742566	1.000000	1.000000	1.41	1
		#3	5	-6.062459	-0.177076	1.000000	1.000000	2.68	1
		#4	7	-4.144447	-0.200371	1.000000	1.000000	2.21	1
	TRR	#1	0	-5.020738	0.461282	1.000000	1.000000	1.65	1
		#2	0	-4.769009	0.807700	1.000000	1.000000	1.05	1
		#3	0	-5.326840	0.004166	1.000000	1.000000	2.27	1
		#4	0	-3.502565	0.078349	1.000000	1.000000	1.71	1
CNBS	PSO	#1	28	-5.600859	-5.599407	-5.579073	-5.600859	0.01	–
		#2	30	-6.572136	-6.572136	-6.572136	-6.572136	0.00	–
		#3	29	-6.255745	-6.253124	-6.177124	-6.255745	0.01	–
		#4	25	-4.746744	-4.729444	-4.584500	-4.746744	0.05	–
	AS	#1	5	-5.600859	-0.760229	1.000000	1.000000	2.97	1
		#2	1	-6.572136	0.747595	1.000000	1.000000	1.38	1
		#3	1	-6.255745	0.274426	1.000000	1.000000	2.21	1
		#4	4	-4.746744	-0.340907	1.000000	1.000000	2.47	1
	IP	#1	10	-5.600859	-1.200286	1.000000	1.000000	3.16	1
		#2	1	-6.572136	0.747595	1.000000	1.000000	1.38	1
		#3	3	-6.255745	0.274425	1.000000	1.000000	2.21	1
		#4	7	-4.746744	-0.340907	1.000000	1.000000	2.47	1
	TRR	#1	0	-5.020738	0.461282	1.000000	1.000000	1.65	1
		#2	0	-3.896261	0.836791	1.000000	1.000000	0.89	1
		#3	0	-4.803903	0.481003	1.000000	1.000000	1.59	1
		#4	0	-4.448528	-0.132917	1.000000	1.000000	2.10	1
MAD	PSO	#1	30	28.671136	28.671136	28.671136	28.671136	0.00	–
		#2	29	22.197505	22.203320	22.371955	22.197505	0.03	–
		#3	19	25.781431	25.795943	25.821008	25.781431	0.02	–
		#4	30	39.537574	39.537574	39.537574	39.537574	0.00	–
	AS	#1	29	28.671136	28.671136	28.671137	28.671136	0.00	0
		#2	30	22.197505	22.197505	22.197505	22.197505	0.00	0
		#3	23	25.781431	25.781431	25.781432	25.781431	0.00	0
		#4	2	39.537574	39.537575	39.537575	39.537575	0.00	1
	IP	#1	30	28.671136	28.671136	28.671136	28.671136	0.00	0
		#2	30	22.197505	22.197505	22.197505	22.197505	0.00	0
		#3	30	25.781431	25.781431	25.781431	25.781431	0.00	1
		#4	30	39.537574	39.537574	39.537574	39.537574	0.00	0
	TRR	#1	0	38.174917	80.084232	437.191990	54.975283	82.08	1
		#2	0	33.022878	115.806950	658.762104	61.160962	131.73	1
		#3	0	35.043037	136.701257	806.049917	74.006241	186.53	1
		#4	0	46.219864	65.138385	125.127617	59.559891	18.31	1
MMD	PSO	#1	14	31.056458	31.151369	31.355355	31.057992	0.13	–
		#2	26	24.095459	24.129881	24.612998	24.095459	0.12	–
		#3	15	27.066388	27.242809	28.630456	27.066426	0.40	–
		#4	29	44.347172	44.347172	44.347173	44.347172	0.00	–
	AS	#1	0	31.056462	31.078239	31.525284	31.056759	0.09	0
		#2	0	24.095463	24.135839	24.835710	24.095768	0.14	1
		#3	0	27.066398	27.224033	29.311025	27.072111	0.45	0
		#4	0	44.347187	44.419303	45.299474	44.352565	0.23	1
	IP	#1	0	31.241349	31.244034	31.245254	31.244358	0.00	1
		#2	0	24.279991	24.285232	24.287873	24.285217	0.00	1
		#3	0	27.228921	27.248421	27.259118	27.249201	0.00	1
		#4	0	44.524078	44.535475	44.598444	44.532140	0.01	1
	TRR	#1	0	94.109723	576.252212	3386.972994	288.327944	715.21	1
		#2	0	87.636164	605.994373	3050.645396	269.316773	740.79	1
		#3	0	45.631121	2812.207090	36087.939245	627.444041	6679.12	1
		#4	0	61.519355	208.647801	439.313149	185.546088	93.59	1

Table 23: Statistical Results for PSO, AS, IP, TRR, $R_k = 144$ kbps and $W_t = 22.5$ MHz

Criterion	Algorithm	Case	Success	Min	Mean	Max	Median	Std	Ranksum
NNBS	PSO	#1	26	-6.728280	-6.706684	-6.317561	-6.728280	0.08	–
		#2	28	-7.817586	-7.817496	-7.814898	-7.817586	0.00	–
		#3	27	-7.198682	-7.167147	-6.771945	-7.198682	0.11	–
		#4	20	-5.259108	-5.158823	-4.178432	-5.259108	0.24	–
	AS	#1	3	-6.728280	-2.348921	1.000000	1.000000	3.90	1
		#2	7	-7.817586	-2.820954	1.000000	1.000000	4.44	1
		#3	5	-7.198682	-3.372630	1.000000	-7.198680	4.16	1
		#4	13	-5.259108	-2.129554	1.000000	-2.129553	3.18	0
	IP	#1	13	-6.728280	-2.348921	1.000000	1.000000	3.90	1
		#2	13	-7.817586	-2.820954	1.000000	1.000000	4.44	1
		#3	16	-7.198682	-3.372630	1.000000	-7.198682	4.16	1
		#4	15	-5.259108	-2.129554	1.000000	-2.129554	3.18	0
	TRR	#1	0	-5.920830	-1.691694	1.000000	1.000000	3.03	1
		#2	0	-7.072670	-2.070224	1.000000	1.000000	3.61	1
		#3	0	-6.461379	-2.447709	1.000000	-4.086208	3.33	1
		#4	0	-4.428599	-1.096080	1.000000	-0.021107	2.28	1
CNBS	PSO	#1	26	-6.728280	-6.706684	-6.317561	-6.728280	0.08	–
		#2	29	-7.494610	-7.494609	-7.494581	-7.494610	0.00	–
		#3	30	-7.247564	-7.247564	-7.247564	-7.247564	0.00	–
		#4	24	-5.968381	-5.879394	-5.345384	-5.968381	0.18	–
	AS	#1	3	-6.728280	-2.348921	1.000000	1.000000	3.90	1
		#2	7	-7.494610	-2.680997	1.000000	1.000000	4.28	1
		#3	14	-7.247564	-3.398701	1.000000	-7.247563	4.18	1
		#4	2	-5.968381	-2.484190	1.000000	-2.484189	3.54	1
	IP	#1	13	-6.728280	-2.348921	1.000000	1.000000	3.90	1
		#2	13	-7.494610	-2.680998	1.000000	1.000000	4.28	1
		#3	16	-7.247564	-3.398701	1.000000	-7.247564	4.18	1
		#4	15	-5.968381	-2.484190	1.000000	-2.484191	3.54	0
	TRR	#1	0	-5.920830	-1.691694	1.000000	1.000000	3.03	1
		#2	0	-6.353936	-1.683354	1.000000	1.000000	3.18	1
		#3	0	-6.700017	-2.361050	1.000000	-3.812727	3.26	1
		#4	0	-5.471234	-1.591104	1.000000	-0.546628	2.75	1
MAD	PSO	#1	30	56.480888	56.480888	56.480888	56.480888	0.00	–
		#2	30	44.424576	44.424576	44.424576	44.424576	0.00	–
		#3	30	50.564936	50.564936	50.564936	50.564936	0.00	–
		#4	30	78.125561	78.125561	78.125561	78.125561	0.00	–
	AS	#1	28	56.480888	56.480888	56.480889	56.480888	0.00	0
		#2	28	44.424576	44.424576	44.424577	44.424576	0.00	0
		#3	25	50.564936	50.564936	50.564937	50.564936	0.00	0
		#4	29	78.125561	78.125561	78.125562	78.125561	0.00	0
	IP	#1	30	56.480888	56.480888	56.480888	56.480888	0.00	0
		#2	30	44.424576	44.424576	44.424576	44.424576	0.00	0
		#3	30	50.564936	50.564936	50.564936	50.564936	0.00	0
		#4	30	78.125561	78.125561	78.125561	78.125561	0.00	0
	TRR	#1	0	70.058420	114.105190	305.226320	100.026179	49.94	1
		#2	0	55.440766	95.548555	265.978810	83.776112	42.75	1
		#3	0	62.454791	102.904933	297.469295	87.282984	50.16	1
		#4	0	94.335021	142.020580	313.279410	126.272882	52.33	1
MMD	PSO	#1	26	62.640217	62.674556	63.670340	62.640217	0.19	–
		#2	30	50.499656	50.499656	50.499656	50.499656	0.00	–
		#3	29	55.336279	55.446682	58.648373	55.336279	0.60	–
		#4	25	86.090121	86.138088	86.839018	86.090121	0.16	–
	AS	#1	0	62.640227	62.709359	64.231017	62.641429	0.29	1
		#2	0	50.499664	50.597425	52.681553	50.501584	0.40	1
		#3	0	55.336303	55.451090	56.332457	55.337953	0.28	1
		#4	0	86.090138	86.298447	88.117830	86.106936	0.49	1
	IP	#1	0	62.667073	62.689967	62.702033	62.691908	0.01	1
		#2	0	50.666813	50.843280	55.099470	50.695189	0.80	1
		#3	0	55.484306	56.219901	76.256342	55.529304	3.78	1
		#4	0	86.090126	86.249038	90.661932	86.090335	0.83	1
	TRR	#1	0	105.389738	661.950070	1853.695807	472.654046	473.79	1
		#2	0	104.554625	684.388187	1739.286364	533.403263	513.81	1
		#3	0	88.154391	650.196306	2273.759910	411.834949	534.75	1
		#4	0	131.077527	515.742949	1396.314830	392.958246	297.15	1

Table 24: PSO's Convergence Speed in terms of Best (Min), Average (Mean) and Worst (Max) swarm update iterations.

	Case	NNBS			CNBS			MAD			MMD		
		Min	**Mean**	**Max**	**Min**	**Mean**	**Max**	**Min**	**Mean**	**Max**	**Min**	**Mean**	**Max**
$\mathbf{R_k = 96}$ **kbps** $\mathbf{W_t = 20}$ **MHz**	#1	465	559.4	696	443	561.4	682	366	482.7	650	518	611.7	700
	#2	336	558.6	700	302	523.3	686	288	437.8	547	497	587.7	660
	#3	437	552.6	700	385	503.1	666	307	402.1	646	536	620.6	699
	#4	500	588.8	692	404	582.3	700	294	405.6	694	373	429.6	498
$\mathbf{R_k = 96}$ **kbps** $\mathbf{W_t = 15}$ **MHz**	#1	490	660.9	700	470	597.9	697	310	421.9	695	389	463.8	561
	#2	391	593.5	700	405	576.6	700	281	401.2	641	323	390.2	522
	#3	414	605.7	694	495	563.9	681	361	532.1	680	364	424.9	546
	#4	447	621.9	700	374	598.6	699	318	390.5	471	364	413.8	498
$\mathbf{R_k = 144}$ **kbps** $\mathbf{W_t = 30}$ **MHz**	#1	461	630.5	700	518	625.1	700	383	505.3	679	687	697.6	700
	#2	433	599.7	697	442	606.0	689	414	548.0	694	636	684.0	700
	#3	426	594.1	700	420	604.7	697	418	592.2	700	691	698.4	700
	#4	500	659.8	700	421	592.5	700	322	488.4	672	677	695.2	700
$\mathbf{R_k = 144}$ **kbps** $\mathbf{W_t = 22.5}$ **MHz**	#1	437	649.2	700	427	627.2	699	376	506.3	681	691	697.9	700
	#2	454	636.4	700	393	616.0	700	386	552.5	700	645	691.8	700
	#3	454	626.1	700	482	619.0	700	396	560.0	686	667	693.5	700
	#4	509	658.2	700	453	652.8	700	366	540.2	690	692	698.2	700

5.3 Geometric Bargaining Approach for Optimizing Resource Allocation in Wireless Visual Sensor Networks

In this work, we assumed that the network consists of $K = 100$ nodes grouped into $C = 2$ motion classes based on the amount of motion in the detected scenes, while other values of C could also be used. Therefore, two motion classes were formed. A high-motion class consisting of the nodes that monitor scenes with high levels of motion, which was represented by the "Foreman" video sequence, and a low-motion class consisting of the nodes that image scenes with low levels of motion, which was represented by the "Akiyo" video sequence.

In cases where the nodes that record low motion suddenly record an event with high motion, a new node clustering is required to achieve a reliable and optimal resource allocation. The same also holds for the cases where the nodes that image high motion instantaneously image a scene with virtually no detected motion. The resolution for both video sequences was the QCIF, and the URDCs were obtained at a frame rate of 15 frames per second.

The RCPC codes used for channel coding had a mother code of rate 1/4 [14]. Given that the bit rate constraint was $R_k = 96$ kbps and considering a node clustering into two motion classes, it follows that the source-channel coding rate combinations per motion class could take the following values: $\{(R_{s,1}, R_{c,1}), (R_{s,2}, R_{c,2})\} \in \{(32, 1/3), (48, 1/2), (64, 2/3)\}$. The pair $(R_{s,1}, R_{c,1})$ was the combination of the source and channel coding rates for the high-motion class of nodes and the $(R_{s,2}, R_{c,2})$ corresponded to the same parameters for the low-motion class of nodes. The power levels took continuous values from the set $\mathbf{P} = [5.0, 15.0]$ W. For the bandwidth, we examined the values of $W_t = 20$ MHz and $W_t = 15$ MHz.

All the presented results obtained using simulations. The results of the KSBS were compared with the corresponding results of the NBS, MTU and w.MTU. The optimization tool that NBS, MTU and w.MTU used to solve the mixed-integer optimization problem that resulted from the discrete source and channel coding rate combinations and the continuous power levels was the PSO algorithm [81, 15], with the same parameter settings as in Section 4.1.3. In all conducted experiments, we assumed that the thermal and background noise could be modeled as AWGN with $N_0 = 10^{-7}$ W/Hz. For values of N_0 smaller than 10^{-7}, a marginal PSNR increase was anticipated, which is trivial and unperceivable by the human eye. Additionally, $PSNR_{cl}$, which corresponded to the utility U_{cl} for class of nodes cl, was used to assess the perceptual video quality of the "Foreman" and "Akiyo" video sequences.

Presentation and Discussion of Results

A large part of our experimental results were organized into tables. Each row of the tables refers to a specific node distribution, which is denoted as "$N_1 - N_2$", where $N_1, N_2 \in \{10, 30, 50, 70, 90\}$ and $N_1 + N_2 = K = 100$. This means that the high-motion class consisted of N_1 nodes and the low-motion class of N_2 nodes, respectively.

Table 25 explored the effect of assigning different dp values to the results of the KSBS. The terms $PSNR_1$ and $PSNR_2$ refered to the PSNR achieved by the high- and low-motion class, respectively. It can be seen that higher dp values favor the high-motion class and lower dp values favor the low-motion class. Videos with more intense motion activity are generally considered as more important compared to more stationary videos, since such videos image scenes of interest. Therefore, aiming at better video quality for the high-motion scenes, we chose to initialize dp with the highest values among the tested ones, for each bit rate and bandwidth combination. Specifically, for $R_k = 96$ kbps and $W_t = 20$ MHz, the selected dp value was $dp = (28, 28)^\top$ dB, while for $R_k = 96$ kbps and $W_t = 15$ MHz, the selected dp value was $dp = (26, 26)^\top$ dB. It is worth mentioning that it is not necessary for the dp to have the same value for both motion classes. However, we made this assumption in an effort to be equally fair to all of them.

Also, from Table 25, we inferred that the PSNR values for both motion classes are reduced when the bandwidth is reduced, while the bit rate, N_0 and the disagreement point remain the same. This is attributed to the fact that when the bandwidth W_t is reduced, the term I_0, which is equal to $I_0 = \sum_{j \neq k}^{K} S_j / W_t$, increases. Thus, the energy per bit to MAI and noise ratio of Eq. (8) becomes lower, which leads to reduced PSNR values.

Table 25: PSNR results for 3 different dp assignments per bit rate and bandwidth combination.

	$R_k = 96$ kbps, $W_t = 20$ MHz						$R_k = 96$ kbps, $W_t = 15$ MHz					
	$dp = (28, 28)^\top dB$		$dp = (26, 26)^\top dB$		$dp = (24, 24)^\top dB$		$dp = (26, 26)^\top dB$		$dp = (25, 25)^\top dB$		$dp = (24, 24)^\top dB$	
$N_1 - N_2$	$PSNR_1$	$PSNR_2$	$PSNR_1$	$PSNR_2$	$PSNR_1$	$PSNR_2$	$PSNR_1$	$PSNR_2$	$PSNR_1$	$PSNR_2$	$PSNR_1$	$PSNR_2$
$90 - 10$	28.2248	31.7811	27.6533	38.7737	27.4387	40.4599	26.3072	33.3874	26.0796	37.7415	25.9756	39.1441
$70 - 30$	29.0590	32.8873	28.3531	35.5374	28.0505	36.7516	26.7322	31.7317	26.3766	33.6255	26.1257	34.6615
$50 - 50$	30.3679	33.5810	29.5671	34.3620	29.2021	35.1549	27.6806	30.9220	27.2761	31.6966	27.0460	32.4253
$30 - 70$	32.0458	34.3732	31.5431	34.8620	31.2067	35.2058	29.5953	31.5920	29.2774	31.8243	29.0081	32.0654
$10 - 90$	34.9841	36.0284	34.7502	36.1288	34.5811	36.1992	32.9591	32.9897	32.8731	33.0132	32.7973	33.0311

Continuing, Table 26 included the results for the NBS, KSBS, MTU and w.MTU, when $R_k = 96$ kbps and $W_t = 20$ MHz, for all considered node distributions. In this case, NBS and KSBS assumed $dp = (28, 28)^\top$ dB. The same results for the aforementioned criteria were also depicted in Table 27, but for the case of $R_k = 96$ kbps and $W_t = 15$ MHz. In this case, NBS and KSBS assumed $dp = (26, 26)^\top$ dB. The combination of the source-channel coding rate, and the power level of the high-motion class were represented as $(R_{\mathrm{s},1}, R_{\mathrm{c},1})$, and S_1, respectively, while $(R_{\mathrm{s},2}, R_{\mathrm{c},2})$ and S_2 were the corresponding parameters for the low-motion class.

First of all, all four criteria gave a higher PSNR to the low-motion class of nodes compared to the high-motion class, with an exception observed for the MTU criterion, in cases where more nodes belong to the low-motion class. In such cases, the high-motion class achieves higher PSNR values than the low-motion class. The KSBS is a promising criterion, since it assigns close enough values to the PSNR of the two motion classes. Compared to the other schemes, the KSBS favors the high-motion class clearly more than the w.MTU and in many cases more than the NBS and MTU. This fact plays an important role, considering the significance of the scenes that include high levels of motion.

The MTU criterion guarantees the highest levels of total utility, cumulatively for both motion classes, compared to all other schemes. However, in cases where the cardinality of the low-motion class is smaller than this of the high-motion class, a large discrepancy between $PSNR_1$ and $PSNR_2$ was observed. Interpreting the results for the w.MTU, it favored eminently the low-motion class of nodes, offering clearly higher PSNR values compared to the NBS and KSBS, and even in some cases compared to the MTU. Interesting were the cases where the two motion classes included the same number of nodes. In such cases, both MTU and w.MTU offered exactly the same solution, i.e., the same PSNR values to both motion classes.

Regarding the power levels, for the NBS and KSBS we observed that the high-motion class of nodes requires higher power levels compared to the low-motion class, unlike w.MTU where the low-motion class maintains the highest power levels. For the MTU, we infered thatthe class that has the highest power level, achieved the highest PSNR. Also, for the source and channel coding rate combinations, since the total bit rate was assumed to be constant, a higher source coding rate means that fewer bits are available for channel coding, resulting in less error protection. Therefore, a higher power level was required in order to increase channel reliability, increasing at the same time the interference to the transmissions of the other nodes.

Table 26: Results for $R_k = 96\,\text{kbps}$, $W_t = 20\,\text{MHz}$. For the NBS and KSBS $dp = (28, 28)^\top dB$.

	NBS						KSBS					
$N_1 - N_2$	$(R_{s,1}, R_{c,1})$	S_1	$(R_{s,2}, R_{c,2})$	S_2	$PSNR_1$	$PSNR_2$	$(R_{s,1}, R_{c,1})$	S_1	$(R_{s,2}, R_{c,2})$	S_2	$PSNR_1$	$PSNR_2$
90 − 10	(48, 1/2)	15.0000	(32, 1/3)	6.1023	28.3548	29.1082	(48, 1/2)	11.7000	(32, 1/3)	6.3000	28.2248	31.7811
70 − 30	(64, 2/3)	15.0000	(32, 1/3)	6.3135	29.5326	30.8287	(48, 1/2)	9.5000	(32, 1/3)	5.3000	29.0590	32.8873
50 − 50	(64, 2/3)	15.0000	(32, 1/3)	6.9364	30.9757	32.7535	(64, 2/3)	9.8000	(32, 1/3)	5.3000	30.3679	33.5810
30 − 70	(64, 2/3)	15.0000	(64, 2/3)	8.9106	31.2109	35.2367	(64, 2/3)	9.7000	(32, 1/3)	5.0000	32.0458	34.3732
10 − 90	(64, 2/3)	15.0000	(64, 2/3)	9.1006	32.2861	36.9037	(64, 2/3)	15.0000	(64, 2/3)	6.3000	34.9841	36.0284

	MTU						w.MTU					
$N_1 - N_2$	$(R_{s,1}, R_{c,1})$	S_1	$(R_{s,2}, R_{c,2})$	S_2	$PSNR_1$	$PSNR_2$	$(R_{s,1}, R_{c,1})$	S_1	$(R_{s,2}, R_{c,2})$	S_2	$PSNR_1$	$PSNR_2$
90 − 10	(32, 1/3)	5.0000	(64, 2/3)	15.0000	26.7244	44.9688	(48, 1/2)	13.6537	(64, 2/3)	15.0000	27.6931	38.6067
70 − 30	(32, 1/3)	5.0246	(64, 2/3)	15.0000	25.3578	43.1664	(32, 1/3)	8.3514	(64, 2/3)	15.0000	26.5871	41.2879
50 − 50	(32, 1/3)	8.1044	(64, 2/3)	15.0000	25.9290	40.3410	(32, 1/3)	8.1044	(64, 2/3)	15.0000	25.9290	40.3410
30 − 70	(64, 2/3)	15.0000	(32, 1/3)	5.6892	33.5507	33.2252	(32, 1/3)	7.9229	(64, 2/3)	15.0000	25.2663	39.3116
10 − 90	(64, 2/3)	15.0000	(64, 2/3)	5.0000	36.3876	35.2762	(32, 1/3)	7.7983	(64, 2/3)	15.0000	24.6122	38.2269

Table 27: Results for $R_k = 96\,\text{kbps}$, $W_t = 15\,\text{MHz}$. For the NBS and KSBS $dp = (26, 26)^\top dB$.

	NBS						KSBS					
$N_1 - N_2$	$(R_{s,1}, R_{c,1})$	S_1	$(R_{s,2}, R_{c,2})$	S_2	$PSNR_1$	$PSNR_2$	$(R_{s,1}, R_{c,1})$	S_1	$(R_{s,2}, R_{c,2})$	S_2	$PSNR_1$	$PSNR_2$
90 − 10	(32, 1/3)	15.0000	(32, 1/3)	7.8222	26.4914	28.5181	(32, 1/3)	9.1000	(32, 1/3)	8.2000	26.3072	33.3874
70 − 30	(32, 1/3)	15.0000	(32, 1/3)	8.1418	26.9339	30.0794	(32, 1/3)	8.9000	(32, 1/3)	6.0000	26.7322	31.7317
50 − 50	(48, 1/2)	15.0000	(32, 1/3)	7.1911	27.9503	30.3836	(48, 1/2)	9.6000	(32, 1/3)	5.0000	27.6806	30.9220
30 − 70	(48, 1/2)	15.0000	(32, 1/3)	7.6311	29.0261	32.0622	(64, 2/3)	11.2000	(32, 1/3)	5.1000	29.5953	31.5920
10 − 90	(64, 2/3)	15.0000	(32, 1/3)	7.4228	31.0886	33.3624	(64, 2/3)	13.2000	(32, 1/3)	5.2000	32.9591	32.9897

	MTU						w.MTU					
$N_1 - N_2$	$(R_{s,1}, R_{c,1})$	S_1	$(R_{s,2}, R_{c,2})$	S_2	$PSNR_1$	$PSNR_2$	$(R_{s,1}, R_{c,1})$	S_1	$(R_{s,2}, R_{c,2})$	S_2	$PSNR_1$	$PSNR_2$
90 − 10	(32, 1/3)	5.0000	(64, 2/3)	15.0000	25.3543	43.2224	(32, 1/3)	8.1158	(64, 2/3)	15.0000	25.8689	40.2343
70 − 30	(32, 1/3)	5.0263	(64, 2/3)	15.0000	23.7017	41.0550	(32, 1/3)	7.8819	(64, 2/3)	15.0000	25.0542	38.9792
50 − 50	(32, 1/3)	7.7475	(64, 2/3)	15.0000	24.2297	37.5805	(32, 1/3)	7.7475	(64, 2/3)	15.0000	24.2297	37.5805
30 − 70	(64, 2/3)	15.0000	(32, 1/3)	5.5879	30.7752	30.6264	(32, 1/3)	7.6648	(64, 2/3)	15.0000	23.3987	36.0942
10 − 90	(64, 2/3)	15.0000	(32, 1/3)	5.0000	34.1215	32.6676	(32, 1/3)	11.1948	(32, 1/3)	15.0000	24.9082	34.3075

The PF values for the NBS, KSBS and w.MTU were included in Table 28. Since the MTU was used as the reference criterion in Eq. (35), the PF values for this criterion were not defined. Moreover, as it was previously implied, in cases where the nodes were equally assigned to both motion classes, the w.MTU solutions coincided with the solutions of the MTU. Hence, in such cases the PF values were not defined either for the w.MTU.

The obtained PF results can be explained as follows: For every unit of utility lost by a class of nodes using the MTU, there are PF units of utility gained cumulatively for both motion classes, using also the MTU. The tendency of PF values for each scheme was similar for both considered combinations of bit rate and bandwidth, from node distribution to node distribution. Specifically, as the cardinality of the high-motion class decreases against the cardinality of the low-motion class, a PF decrease is observed, except for the case of "$10-90$" where the PF value is increased. Additionally, no specific scheme offers the highest or the lowest PF values in all node distributions. This always depends on the achieved PSNR values in each case. However, the conclusion derived using this metric was that the lower the PF value for a scheme, the smaller the discrepancy between the total achieved PSNR by the considered scheme and the MTU. Therefore, when the number of nodes that belong to the high-motion class increases, the utility gained cumulatively for both motion classes decreases.

Table 28: PF values per bit rate and bandwidth combination.

	$R_k = 96$ kbps, $W_t = 20$ MHz			$R_k = 96$ kbps, $W_t = 15$ MHz		
$N_1 - N_2$	NBS	KSBS	w.MTU	NBS	KSBS	w.MTU
$90-10$	8.7280	7.7895	5.5677	11.9314	9.3211	4.8066
$70-30$	1.9553	1.7772	0.5281	2.3957	2.0765	0.5348
$50-50$	0.5035	0.5229	–	0.9343	0.9295	–
$30-70$	0.1632	0.3109	0.3611	0.2182	0.2219	0.3491
$10-90$	1.5201	0.8659	2.9907	3.3651	2.6088	4.6182

Additional pieces of information were also provided by the graphical illustration of the results. Figure 15 depicted the relation between the total achieved utility and the total consumed power, for all examined criteria. Each subfigure referred to a specific node distribution and presented the results, for both considered bit rate and bandwidth combinations. As we observed, the tendency of the total utility as well as that of the total power consumption is similar for both considered bit rate and bandwidth combinations. Specifically, the sum of the PSNR values is reduced in all criteria and node distributions, when the bandwidth is reduced (keeping the bit rate constant), since in such a case the value of Eq. (7) decreases. For the sum of the power levels, there is no noticeable difference between the two considerations for the bandwidth.

From Fig. 15, we also observed that no scheme simultaneously holds the desired features of achieving the highest levels of utility and consuming the lowest levels of power, cumulatively for both motion classes. Clearly, such a scheme would be a preferable scheme. Although the MTU assures the highest levels of utility, it is an unfair scheme if we consider the amounts of consumed power as well as the high discrepancy that is often observed in the PSNR values of the two motion classes. Alternatively, if we are interested in achieving similar PSNR values for both motion classes, we could say that in some cases the NBS is the most suitable criterion, while in some other cases the MTU meets this requirement. Despite all these, neither the NBS nor the MTU can be considered as equally fair criteria to both motion classes, if we also consider the power levels required by each motion class. In cases of similar PSNR values, the high-motion class is undoubtedly more demanding in resources.

The KSBS that was proposed in this paper is a compromise to all our requirements. The main strength of this method is that it guarantees the lowest power level values, cumulatively for both motion classes, far exceeding the other competing methods. Additionally, it assigns close PSNR values to both motion classes compared to the values assigned by the MTU and w.MTU and even by the NBS, in cases where the cardinality of the low-motion class is greater than that of the high-motion one. Also, the KSBS clearly outperforms the NBS in terms of the total utility gained by both motion classes, and in cases where more nodes belong to the low-motion class, it also outperforms the w.MTU.

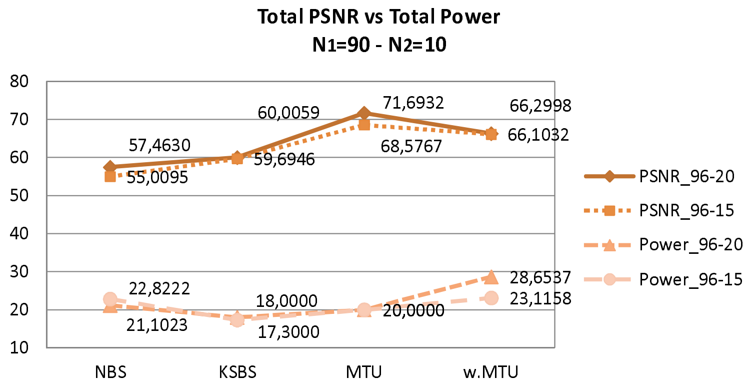

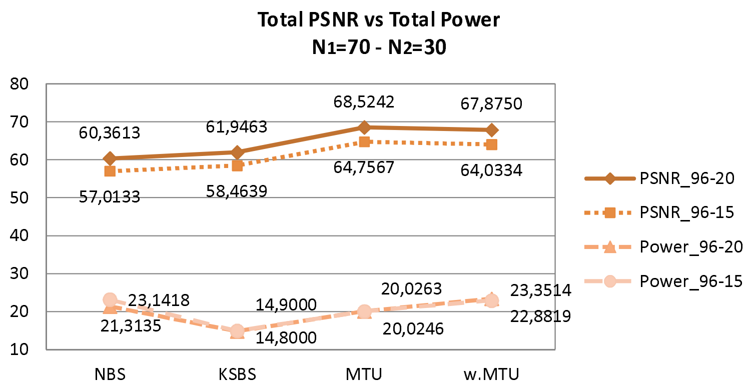

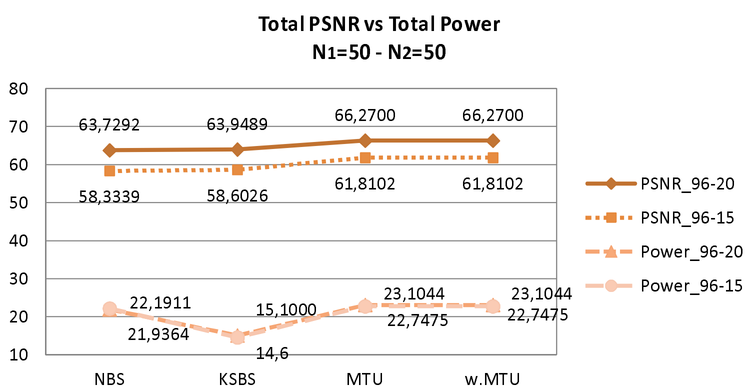

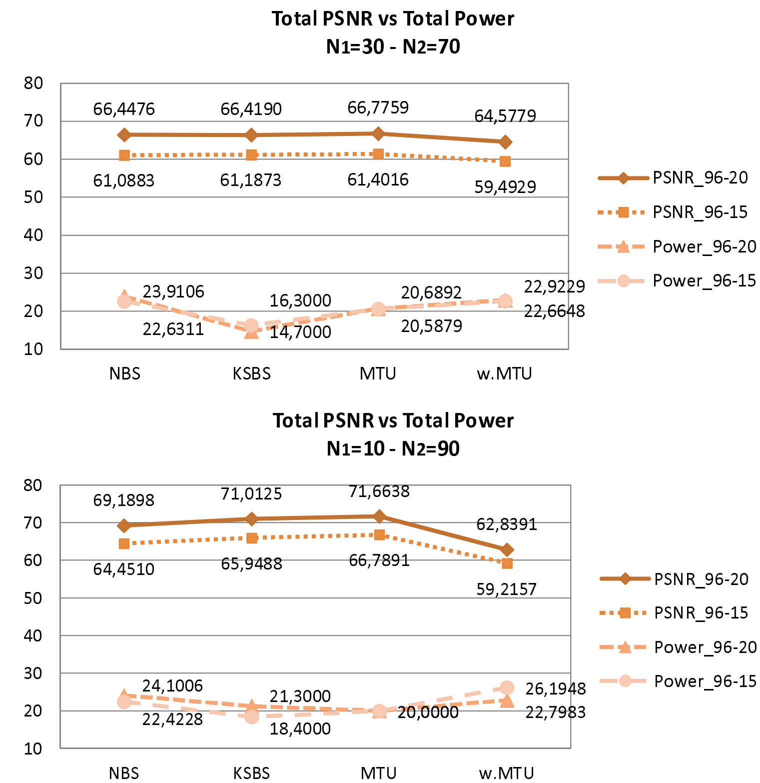

Figure 15: Total PSNR gain versus total power consumption.

5.4 Fairness Issues in Resource Allocation Schemes for Wireless Visual Sensor Networks

In this work, we clustered the $K = 100$ nodes of the network into $C = 2$ motion classes, based on the amount of motion included in the captured scenes. Thus, a high- and a low-motion class of nodes were formed, while the "Foreman" and "Akiyo" video sequences were used to represent each motion class, respectively. The bit rate was 96 kbps and the bandwidth 20 MHz. The source and channel coding rates were assumed to take discrete values from the set $\{(32, 1/3), (48, 1/2), (64, 2/3)\}$ and the power levels assumed continuous values from the set $\mathbf{S} = [5.0, 15.0]$ in Watts. Additionally, the PSNR metric was used for the measurement of the video quality. In all conducted experiments, we assumed that the thermal and background noise can be modeled as AWGN with $N_0 = 10^{-7}$ W/Hz.

Tables 40-33 presented the results for all fairness metrics considered in this work. Each of the tables refers to a different node distribution and each line of the tables refers to a specific scheme. The term N_1 declares the cardinality of the high-motion class of nodes and the N_2 the cardinality of the low-motion class of nodes. The first column of each table shows the schemes, the second column shows the PF values of each scheme and the third column cites the JI values of the nodes' utilities (expressed in terms of PSNR). The fourth column depicts the total utility achieved by each scheme, and the last column shows the total consumed power for each scheme. Since a fair and efficient scheme guarantees high amounts of total utility, is equally fair to both motion classes and is not demanding in resources (in our case power levels), we used bold type for the lowest PF value, the highest JI value, the highest total utility and the lowest total power among all schemes, for each considered node distribution. Moreover, in Tables 34-38, we presented the PSNR of the high-motion class, the PSNR of the low-motion class, the power level of the high-motion class and the power level of the low-motion class, respectively. Of course, each line of the tables refers to a specific scheme, while each of the tables refers to a different node distribution.

Regarding the results from Tables 40-33, one way to interpret the PF values obtained using Eq. (35) is that for every unit of utility lost by a class of nodes using the MTU instead of the considered scheme, there are PF units of utility gained cumulatively for both motion classes using also the MTU instead of the considered scheme. Additionally, the lower the PF value for a scheme, the smaller the discrepancy between the total achieved PSNR by the considered scheme and the MTU. Therefore, if we desire to have a high total utility, the scheme that offers the lowest PF value is the preferred one. However, no specific scheme holds the lowest PF values for all considered node distributions. This always depends on the achieved PSNR values in each case. Moreover, since the MTU criterion was considered as the reference criterion in Eq. (35), the PF values for this scheme are not defined. Additionally, in cases where both motion classes include the same number of nodes, the w.MTU solutions coincide with the solutions of the MTU. Hence, in such a case the PF values are not defined either for the w.MTU. From the JI values, we observed that all schemes promise quite fair utility allocations for both motion classes, since the JI values in all examined cases are greater than 0.93. However, the MMD criterion assures absolutely equal allocations for both motion classes, guaranteeing JI values equal to unity. This means that the MMD is fair to the 100% of the nodes, as it results from the definition of the Jain's index, and thus it is the most fair scheme among all as it regards the equality of the utility allocations.

Additionally, if we consider that a high-performance scheme provides high amounts of utility cumulatively for both motion classes, the MTU is the scheme that can assure this requirement, as it is declared by its name. Indeed, as we see from Tables 40-33, this scheme offers the highest total utility in all considered node distributions. Finally, if the system resources are limited (as it is usual in wireless VSNs), it is necessary to have a scheme that is able to optimally allocate the transmission parameters among the nodes, while spending low amounts of power for the video transmission over the network, and guaranteeing adequate levels of viewing quality. In such a case, our choice is the KSBS criterion, since in four out of five node distributions, it assures the lowest power consumption compared to all other schemes.

Generalizing, no scheme holds all desired characteristics of achieving the highest total utility, while assigning similar utilities to the two motion classes, and spending the lowest overall power, at the same time. Clearly, such a scheme would be a preferable scheme. Each proposed metric investigates fairness under a different perspective and it is rather impossible for a single metric to gather all aspects of fairness, at the same time. Specifically, if we are interested in a scheme that gathers the highest amounts of utility compared to all other schemes, our choice would be the MTU criterion. Although the MTU assures the highest levels of utility, it is an unfair scheme if we consider the amounts of consumed power as well as the high discrepancy that is often observed between the PSNR values of the motion classes. The PF values indicate the scheme that approaches in performance the MTU. However, no specific scheme keeps the lowest PF values in all considered node distributions. From another point of view, if our priority is a scheme that assigns as close utilities as possible to both motion classes, surely the MMD criterion would be our selection. However, the total utility gained by the MMD is quite low relative with the total utility gained by the MTU. From another aspect, we would select the KSBS criterion, if we were looking for a scheme that consumes low amounts of power, while guaranteeing adequate levels of video viewing quality, at the same time. Nevertheless, this criterion fails to gather high amounts of total utility compared to the MTU, and also there is a large discrepancy between the utilities of the two motion classes, up to approximately 4 dB.

Scheme	PF	JI	Total Utility	Total Power
MAD	7.9258	0.9974	59.5422	22.6210
MMD	9.0271	**1.0000**	56.7578	20.7257
n.NBS	8.7280	0.9998	57.4630	21.1023
c.NBS	7.7732	0.9965	59.9914	23.0548
KSBS	7.7895	0.9965	60.0059	**18.0000**
MTU	–	0.9392	**71.6932**	20.0000
w.MTU	**5.5677**	0.9736	66.2998	28.6537

Table 29: Fairness metrics for the case of $N_1 = 90 - N_2 = 10$.

Scheme	PF	JI	Total Utility	Total Power
MAD	1.8301	0.9976	61.4641	22.6110
MMD	2.0510	**1.0000**	59.5078	20.5814
n.NBS	1.9553	0.9995	60.3613	21.3135
c.NBS	1.7870	0.9967	61.8099	23.1208
KSBS	1.7772	0.9962	61.9463	**14.8000**
MTU	–	0.9365	**68.5241**	20.0000
w.MTU	**0.5281**	0.9552	67.8748	23.3521

Table 30: Fairness metrics for the case of $N_1 = 70 - N_2 = 30$.

Scheme	PF	JI	Total Utility	Total Power
MAD	**0.5027**	0.9991	63.7608	22.0445
MMD	0.5450	**1.0000**	63.1836	20.7300
n.NBS	0.5035	0.9992	63.7292	21.9364
c.NBS	0.5035	0.9992	63.7292	21.9364
KSBS	0.5229	0.9975	63.9489	**15.1000**
MTU	–	0.9548	**66.2700**	23.1044
w.MTU	–	0.9548	**66.2700**	23.1044

Table 31: Fairness metrics for the case of $N_1 = 50 - N_2 = 50$.

Scheme	PF	JI	Total Utility	Total Power
MAD	0.1749	0.9968	66.4491	23.7092
MMD	0.0331	**1.0000**	66.7706	20.9121
n.NBS	0.1632	0.9963	66.4476	23.9106
c.NBS	**0.0165**	0.9999	66.7746	20.7968
KSBS	0.3109	0.9988	66.4190	**14.7000**
MTU	–	0.9999	**66.7758**	20.6893
w.MTU	0.3611	0.9548	64.5780	22.9236

Table 32: Fairness metrics for the case of $N_1 = 30 - N_2 = 70$.

Scheme	PF	JI	Total Utility	Total Power
MAD	1.3567	0.9970	69.6722	23.4148
MMD	**0.7140**	**1.0000**	71.3714	20.6298
n.NBS	1.5201	0.9956	69.1898	24.1006
c.NBS	0.8418	0.9999	71.4211	21.9862
KSBS	0.8659	0.9998	71.0125	21.3000
MTU	–	0.9998	**71.6638**	**20.0000**
w.MTU	2.9907	0.9552	62.8391	22.7983

Table 33: Fairness metrics for the case of $N_1 = 10 - N_2 = 90$.

Scheme	PSNR	Power
MAD	$[28.2575, 31.2847]$	$[15.0000, 7.6210]$
MMD	$[28.3789, 28.3789]$	$[15.0000, 5.7257]$
n.NBS	$[28.3548, 29.1082]$	$[15.0000, 6.1023]$
c.NBS	$[28.2298, 31.7616]$	$[15.0000, 8.0548]$
KSBS	$[28.2248, 31.7811]$	$[11.7000, 6.3000]$
MTU	$[26.7244, 44.9688]$	$[5.0000, 15.0000]$
w.MTU	$[27.6931, 38.6067]$	$[13.6537, 15.0000]$

Table 34: PSNR values and power level values for the case of $N_1 = 90 - N_2 = 10$.

Scheme	PSNR	Power
MAD	[29.2156, 32.2485]	[15.0000, 7.6110]
MMD	[29.7539, 29.7539]	[15.0000, 5.5814]
n.NBS	[29.5326, 30.8287]	[15.0000, 6.3135]
c.NBS	[29.1152, 32.6947]	[15.0000, 8.1208]
KSBS	[29.0590, 32.8873]	[9.5000, 5.3000]
MTU	[25.3434, 43.1807]	[5.0000, 15.0000]
w.MTU	[26.5873, 41.2875]	[8.3521, 15.0000]

Table 35: PSNR values and power level values for the case of $N_1 = 70 - N_2 = 30$.

Scheme	PSNR	Power
MAD	[30.9207, 32.8401]	[15.0000, 7.0445]
MMD	[31.5918, 31.5918]	[15.0000, 5.7300]
n.NBS	[30.9757, 32.7535]	[15.0000, 6.9364]
c.NBS	[30.9757, 32.7535]	[15.0000, 6.9364]
KSBS	[30.3679, 33.5810]	[9.8000, 5.3000]
MTU	[25.9290, 40.3410]	[8.1044, 15.0000]
w.MTU	[25.9290, 40.3410]	[8.1044, 15.0000]

Table 36: PSNR values and power level values for the case of $N_1 = 50 - N_2 = 50$.

Scheme	PSNR	Power
MAD	[31.3549, 35.0942]	[15.0000, 8.7092]
MMD	[33.3853, 33.3853]	[15.0000, 5.9121]
n.NBS	[31.2109, 35.2367]	[15.0000, 8.9106]
c.NBS	[33.4708, 33.3038]	[15.0000, 5.7968]
KSBS	[32.0458, 34.3732]	[9.7000, 5.0000]
MTU	[33.5506, 33.2252]	[15.0000, 5.6893]
w.MTU	[25.2666, 39.3114]	[7.9236, 15.0000]

Table 37: PSNR values and power level values for the case of $N_1 = 30 - N_2 = 70$.

Scheme	PSNR	Power
MAD	[32.9280, 36.7442]	[15.0000, 8.4148]
MMD	[35.6857, 35.6857]	[15.0000, 5.6298]
n.NBS	[32.2861, 36.9037]	[15.0000, 9.1006]
c.NBS	[35.8566, 35.5645]	[15.0000, 6.9862]
KSBS	[34.9841, 36.0284]	[15.0000, 6.3000]
MTU	[36.3876, 35.2762]	[15.0000, 5.0000]
w.MTU	[24.6122, 38.2269]	[7.7983, 15.0000]

Table 38: PSNR values and power level values for the case of $N_1 = 10 - N_2 = 90$.

5.5 Distortion-Aware Joint Scheduling and Resource Allocation for Wireless Video Transmission

For the evaluation of our proposed approaches presented in this work, a number of experiments were conducted. We considered a single hop wireless VSN topology, where each node is equidistant and has clear line of sight with its base station. Each node could record a scene of different motion. Specifically, the nine YUV QCIF sequences listed in Table 39 (with 15 fps frame rate) were used. The available bandwidth was $W_t = 1$ MHz and the total transmission rate for the HTCDMA system was $R_{\text{total}} = 288$ kbps.Moreover, we assumed that a time frame was divided in $N = 3$ time slots with $ts = 10$ ms duration each, and that three nodes were allowed to simultaneously transmit during each time slot. We presented the results of the evaluation that is based on comparing the proposed HTCDMA system to a DS-CDMA with the same bandwidth, but with lower bit rate, i.e. 96 kbps, in order for each node to experience the same bit rate in both systems. For the NBS, the disagreement point for both systems and for all transmitting nodes was set to 24 dB.

In the proposed scheme, the transmit powers assumed continuous values within the range $[0.0500, 0.5000]$ W. On the other hand, the selected subset of transmitting nodes per time slot and the source and channel coding rates of each node were selected from a discrete set, i.e. Coding Set $CS \in \{1 : (32\,\text{kbps}, 1/3), 2 : (48\,\text{kbps}, 1/2), 3 : (64\,\text{kbps}, 2/3)\}$. Hence, the formulated optimization problems were mixed-integer problems. In order to efficiently solve the formulated problem, we employed the PSO optimization technique [46]. PSO has been used before in similar resource allocation problems over wireless VSNs as in [1, 2]. Considering the stochastic nature of the PSO algorithm, 30 independent experiments were executed for each problem instance to ensure the validity of the results [46].

The different node subset selection for the two criteria in the proposed HTCDMA system is illustrated in Fig. 16. For both criteria, the scheduled nodes per ts had different rate-distortion characteristics. For example, the "Mother-Daughter" video, which is of low motion, is transmitted in the same time slot with "Suzie" and "Salesman", which are considered videos of medium motion. This is a result of the employed distortion-aware functions and is important for the video quality enhancement during each ts.

Table 39 reported the obtained results for the network resource allocation using the proposed method for the considered HTCDMA and the DS-CDMA system. A close inspection of the results revealed that strong channel coding is selected for the majority of the nodes in all cases. Only for some medium or high motion nodes we had the selection of weaker channel coding rate. Besides this, the total power that is required for the video transmission is slightly lower for the NBS than the MAD criterion for both systems (1.76% for HTCDMA and 7.16% for DS-CDMA).

Regarding the resulting quality gain of the proposed HTCDMA over DS-CDMA, we considered the PSNR difference ($PSNR_k^{\text{HTCDMA}} - PSNR_k^{\text{DS-CDMA}}$), for each node k and for the two different criteria. This is depicted in Fig. 17. For both optimization criteria, the average PSNR gain is greater than 3 dB (particularly 3.47 dB for MAD and 3.11 dB for NBS), which is a considerable quality enhancement. Furthermore, it is remarkable that the quality gain is higher for the videos with higher amount of motion. This is due to the fact that HTCDMA reduces the interference among the transmitting nodes. Moreover, the scheduling is performed with regard to the resulting

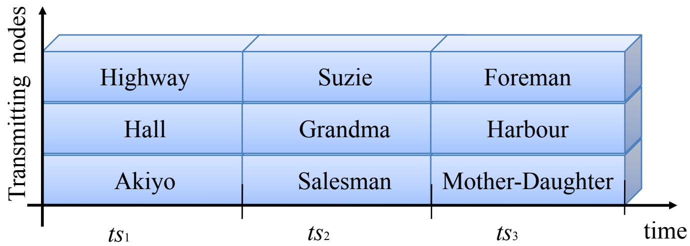

(a) Scheduled nodes per ts using MAD.

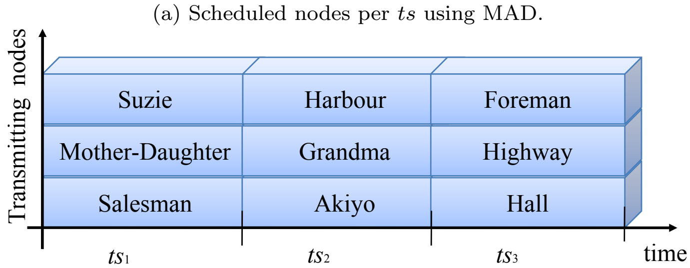

(b) Scheduled nodes per ts using NBS.

Figure 16: Scheduled nodes for transmission in a time frame.

Table 39: Results for HTCDMA and DS-CDMA.

Proposed HTCDMA						
	MAD			**NBS**		
Nodes	PSNR	CS	S	PSNR	CS	S
1.Akiyo	33.4457	1	0.0500	32.2730	1	0.0523
2.Salesman	32.0021	2	0.0781	31.5022	2	0.0707
3.Grandma	32.9401	1	0.0500	32.5180	1	0.0500
4.Mother-Daughter	32.2943	1	0.0500	33.1749	1	0.0500
5.Harbour	31.2454	3	0.0983	31.0477	3	0.0954
6.Hall	33.6395	1	0.0597	33.7675	1	0.0500
7.Highway	33.3946	1	0.0604	33.9298	1	0.0632
8.Suzie	32.8205	1	0.0625	32.6780	1	0.0580
9.Foreman	32.4454	1	0.0533	33.5102	1	0.0632
DS-CDMA						
	MAD			**NBS**		
Nodes	PSNR	CS	S	PSNR	CS	S
1.Akiyo	30.4438	1	0.0528	31.0597	1	0.0523
2.Salesman	27.8555	1	0.0670	27.1846	1	0.0589
3.Grandma	30.7121	1	0.0500	31.4448	1	0.0500
4.Mother-Daughter	30.6904	1	0.0539	31.4871	1	0.0538
5.Harbour	26.5457	2	0.0980	26.9821	2	0.0868
6.Hall	29.9832	1	0.0651	30.4413	1	0.0630
7.Highway	29.7705	1	0.0653	30.0973	1	0.0627
8.Suzie	29.9789	1	0.0640	30.4265	1	0.0620
9.Foreman	26.9850	1	0.0736	27.3091	1	0.0609

video distortion; thus the optimal combination of nodes is selected for transmission.

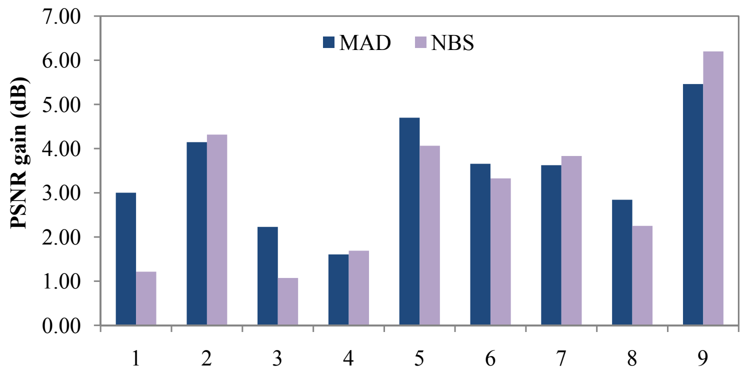

Figure 17: PSNR gain per node of HTCDMA over DS-CDMA for both criteria.

5.6 Resource Allocation in Visual Sensor Networks Using a Reinforcement Learning Framework

In this work, the $K = 100$ nodes of the network were clustered into $M = 4$ motion classes, with each class consisting of 25 nodes. All video sequences (Fig. 7) were at QCIF resolution and the H.264/AVC High profile for 4:2:0 color format video was selected to compress each of them. The RCPC codes had mother rate 1/4 [14], the total bandwidth was $W_t = 20$ MHz and the target bit rate $R_k = 96$ kbps. The tested GoP lengths were $\{3, 5, 10, 30\}$. The set of admissible source and channel coding rate combinations was $\mathbf{C} \in \{1 : (32, 1/3), 2 : (48, 1/2), 3 : (64, 2/3)\}$ and the power levels assumed values from the set $\mathbf{S} = \{5, 7, 9, 11, 13, 15\}$ mW. The disagreement point was $dp = (25, 25, 25, 25)^\top$ dB. In order to encourage exploration in the adopted RL scheme, the initial state-action value functions were selected optimistically [31]. The specific optimization problem was treated as a continuous task, where the optimal solution was reached, when the controller remained in the same state for a maximum number of steps (stopping criterion).

In the following, Table 40 presents the optimal determination of the transmission parameters for all considered criteria. Although all possible combinations for the GoP length for each video sequence were tested, we cited only three cases. Case 1: all video sequences were compressed with GoP length 30 (relatively infrequent IDR-frame placement), Case 2: all video sequences were compressed with GoP length 3 (relatively frequent IDR-frame placement) and Case 3: each motion class selected the optimal GoP length.

Let index 1 denote the high motion class, index 2 the medium-high motion class, index 3 the low-medium motion class and index 4 the low motion class. Thus, GoP_{cl}, S_{cl} and C_{cl} refered to the GoP, power level and source-channel coding rate combination for the class cl, $cl = \{1, \ldots, 4\}$. From the obtained results, we observed that when the optimal GoP length was selected for each motion class, we received an increase in the total PSNR (sum of the PSNRs) of all motion classes up to 4.2 dB compared to the case when GoP length was 30 and up to 9.6 dB when GoP length was 3.

Table 40: Resource allocation for all considered criteria.

Case	GoP_1	GoP_2	GoP_3	GoP_4	S_1	S_2	S_3	S_4	C_1	C_2	C_3	C_4	Total PSNR
MAD													
1	30	30	30	30	15	15	5	5	3	3	1	1	118.3214
2	3	3	3	3	15	11	5	5	1	1	1	1	112.9643
3	30	3	30	30	15	13	5	5	3	1	1	1	122.5263
NBS													
1	30	30	30	30	11	11	7	5	3	3	1	1	120.4887
2	3	3	3	3	15	9	13	7	1	1	1	1	118.9107
3	30	3	30	30	15	11	13	7	3	1	2	1	124.4835
MTU													
1	30	30	30	30	5	7	15	13	1	1	3	3	125.2693
2	3	3	3	3	11	11	13	11	1	1	1	1	121.2006
3	30	3	30	30	5	11	15	13	1	1	3	3	129.0177

Furthermore, as Fig. 18 shows, for the MAD and NBS criteria, when optimal GoP length was selected, all video sequences increased their own utilities compared to the other two GoP length considerations. For the MTU criterion, only the "Foreman" video sequence augmented its utility compared to the other two GoP length considerations. However, the total PSNR increase achieved using the optimal GoP length was 7.8 dB compared to Case 2, and 3.7 dB compared to Case 1, which is a considerable PSNR increase.

In the following, Fig. 19 compared the PSNR values achieved by each considered criterion, for all tested video sequences. The MAD favors the video sequences including high and medium-high amounts of motion, while the MTU is preferred by the nodes that capture low and low-medium amounts of motion. Regarding the NBS, it is the criterion that presents the smallest discrepancy between the PSNR values of all video sequences, being a compromise between the values of MAD and MTU, for all video sequences.

Last but not least, Fig. 20 depicted the mean number of steps that the SARSA algorithm required compared to the ES algorithm. It is obvious that SARSA needs a significantly smaller number of steps and hence less time, in order to discover the optimal combination of nodes' transmission parameters, for all considered criteria. This is attributed to the efficient way that the particular algorithm uses the received information from the environment. These two approaches, i.e., SARSA and ES, will become non comparable in the case of online processing.

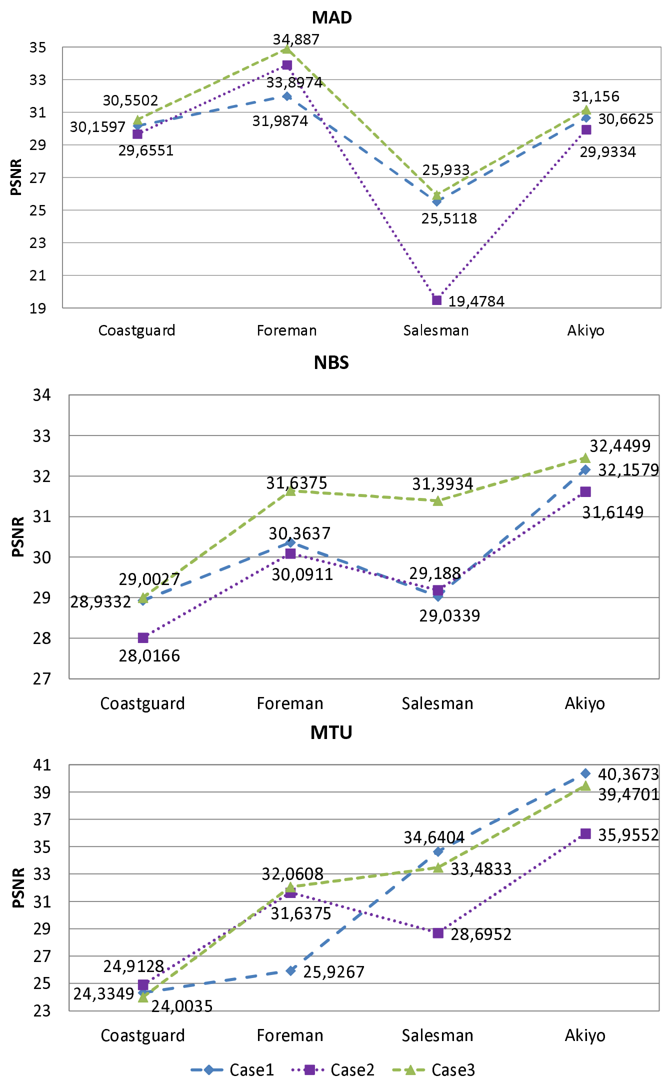

Figure 18: PSNR achieved for all video sequences for 3 different GoP lengths.

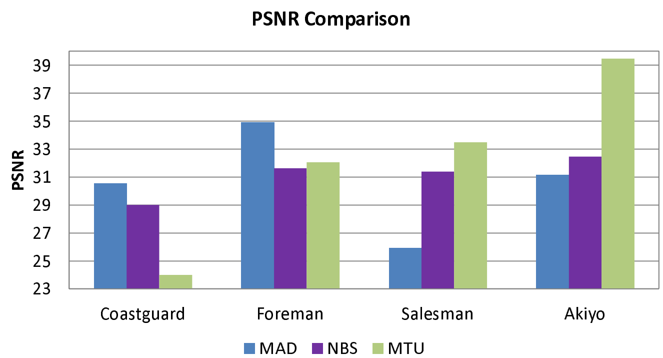

Figure 19: PSNR achieved by each criterion for all video sequences.

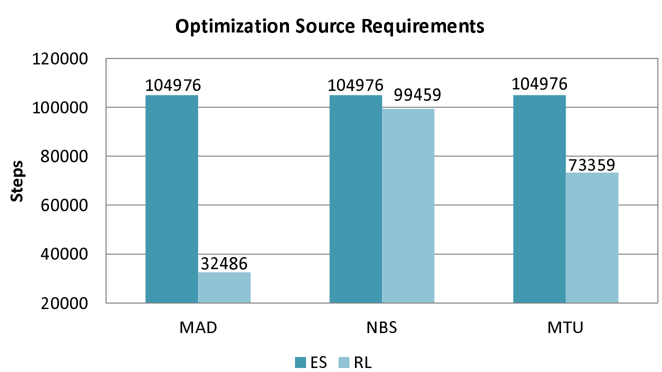

Figure 20: Steps required by ES and RL to reach to the solution.

5.7 Priority-Based Cross-Layer Optimization for Multihop DS-CDMA Visual Sensor Networks

In the considered WVSN, we assumed that neighboring visual sensors monitor the same area. Due to this assumption, the 20 nodes are organized in four clusters of the same cardinality $\{C1, C2, C3, C4\}$. As the CCU is out of the transmission range of the source nodes, four relay nodes $\{R1, R2, R3, R4\}$ retransmit the received videos of each cluster to the CCU as shown in Fig. 2. Interference exists among the nodes in the clusters as they transmit their videos to their corresponding relay node. Moreover, the relay nodes interfere with each other when they retransmit videos to the CCU. The five nodes of each cluster transmit video sequences of the same motion level, thus the (α_k,β_k) parameters within a cluster's nodes are assumed to be equal and invariant in time. In order to evaluate the performance of our method, several cases with different motion amounts per cluster and various levels of power spectral density of background noise N_0 were tested. Two of them were presented as they distinctly demonstrate the effectiveness of the priority-based criteria for different visual sensors resource requirements. In Test Case 1, N_0 was equal to 0 pW/Hz, while in Test Case 2 it was equal to 1 pW/Hz. In both test cases, the nodes of cluster $C1$ transmit high motion videos while the nodes of cluster $C2$ transmit low motion videos and the nodes of clusters $C3$ and $C4$ transmit different medium motion videos. The notions "low", "medium" and "high" motion were used for video sequences of similar motion levels with "Akiyo", "Salesman" and "Foreman" QCIF video sequences of 15 fps, respectively.

The range of $[100, 500]$ mW was used for the transmission powers of all source nodes and the range $[100, 5000]$ mW for the relay nodes. For all links, the total bandwidth W_t was 5 MHz. For the source nodes in clusters, the valid source and channel coding rate set was $CS \in \{1 : (32\text{kbps}, 1/3), 2 : (48\text{kbps}, 1/2), 3 : (64\text{kbps}, 2/3)\}$ and the transmission bit rate R_k was equal to 96 kbps. For the relay nodes the transmission bit rate R_m was 480 kbps and the channel coding rate was set to 2/3. RCPC codes with mother rate 1/4 were used and the size of the link layer packets was 400 bits. A number of 30 independent experiments were conducted for each criterion. Our experiments showed that the PSO algorithm performs efficiently for all employed criteria and both test cases using a number of parameters equal to 12, a number of particles equal to 80 and a maximum number of iterations equal to 500.

Table 42 depicts the achieved PSNRs and the allocated CS of all the optimization criteria in each test case. In both test cases, e.NBS offers the lowest PSNR to high motion nodes whereas the low motion nodes have the highest PSNR. Both w.NBS and MWAD generally achieve to enhance the PSNRs according to the motion level, i.e. they offer better quality to nodes that transmit high motion video. Nonetheless, MWAD treats more fairly the low and medium motion nodes as it offers higher PSNR than w.NBS can achieve. More specifically, in the first test case, if w.NBS is used, the high motion nodes have a gain of 2.4418 dB in comparison with the case that MWAD is used; the low and medium motion nodes have a gain of 1.4590-2.8713 dB when MWAD is employed. In the second test case, low and medium motion nodes have a gain of 0.2781-0.6471 dB if MWAD is used. This criterion achieves higher average PSNR compared to w.NBS. Also, observing Table 42, it can be pointed out, that in both test cases, w.NBS and MWAD choose the source and channel coding rate combination that offers the highest available source coding rate to the high motion nodes. On the contrary, a higher channel coding rate is preferred for the low and medium motion nodes.

Test Case 1								
	C1		**C2**		**C3**		**C4**	
Criterion	PSNR(dB)	CS	PSNR(dB)	CS	PSNR(dB)	CS	PSNR(dB)	CS
e.NBS	32.5422	3	40.5000	3	33.7773	2	33.8292	2
w.NBS	39.1853	3	28.9987	1	29.8229	1	30.1971	1
MWAD	36.7435	3	30.4577	1	32.6942	2	32.9295	2
Test Case 2								
	C1		**C2**		**C3**		**C4**	
Criterion	PSNR(dB)	CS	PSNR(dB)	CS	PSNR(dB)	CS	PSNR(dB)	CS
e.NBS	30.2792	3	39.1806	3	32.8663	2	32.9030	2
w.NBS	33.6779	3	28.9038	1	31.3255	2	31.6311	2
MWAD	33.4342	3	29.5509	1	31.6767	2	31.9092	2

Table 41: PSNR and source and channel coding rates per test case.

As far as the transmission power allocation is concerned (Fig. 21), in both test cases and with every criterion, the transmission powers of the relay nodes were in accordance with the motion level of the transmitted video sequences. Namely, the transmission powers for the relay nodes of the clusters with high motion nodes are higher than the transmission powers of the relays of low and medium motion clusters. Moreover, the background noise results in higher transmission power demand for all nodes in order to keep the bit error rate probability per hop low and maintain high quality.

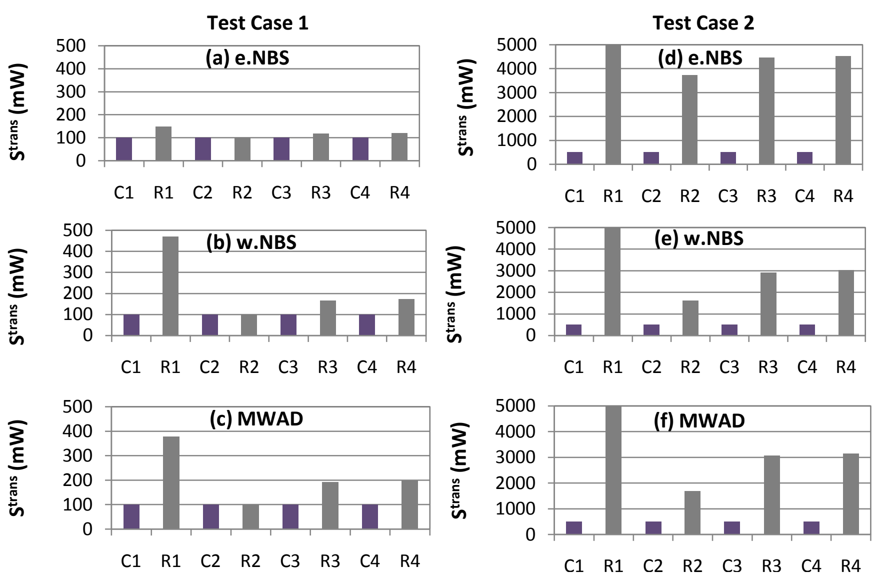

Figure 21: Allocated transmission power per test case.

5.8 Power-Aware QoS Enhancement in Multihop DS-CDMA Visual Sensor Networks

We assumed that neighboring visual sensors monitor the same area. Due to this assumption, the neighboring nodes are organized with respect to their location in clusters. We considered a wirelss VSN topology similar to the example of Fig. 2. We assumed that 20 source nodes are organized in four clusters of the same cardinality. Taking into account that the base station is out of the transmission range of the source nodes, a relay node is committed to each cluster in order to channel-decode-and-forward the video data to the base station. The enumeration of the relays corresponds to the enumeration of the cluster they are committed to (e.g. relay node 1 forwards the video data from cluster 1). Interference exists among the source nodes within a cluster as they transmit their videos to their corresponding relay node. Moreover, the four relay nodes interfere with each other when they retransmit videos to the base station.

Since the five source nodes of each cluster monitor the same area, we assumed that they transmit the same video sequences, thus the (α_k,β_k) parameters of nodes in a cluster are assumed to be equal and invariant in time. In order to evaluate the performance of our method, several cases with different motion levels per cluster were considered. In the presented results, cluster 1 nodes transmit high motion videos while the nodes of cluster 2 transmit low motion videos and the nodes of clusters 3 and 4 transmit different medium motion videos. The notions "low", "medium" and "high" motion were used for video sequences of similar motion levels with the "Akiyo", "Salesman" and "Foreman" QCIF video sequences of 15 fps, respectively.

The range of $[0.100, 0.500]$ W was used for the transmission powers of all source nodes and the range $[0.100, 5.000]$ W was used for the relay nodes. For all links, the total bandwidth W_t was 5 MHz. The background noise N_0 was equal to 1 pW/Hz, although various levels of power spectral density of background noise N_0 were also tested, providing similar results. For the source nodes in clusters, the set of possible source and channel coding rate choices was

$$\{(32\text{kbps}, 1/3), (48\text{kbps}, 1/2), (64\text{kbps}, 2/3)\}$$

and the total transmission bit rate R_k was the same for all cluster nodes and equal to 96 kbps. For the relay nodes, the transmission bit rate R_m was the same for all and equal to 480 kbps. The channel coding rates for the relay nodes were selected from the set $\{1/3, 1/2, 2/3\}$. RCPC codes with mother rate 1/4 were used.

As far as the values of (γ, δ) were concerned, we considered the range $[0.50, 1.00]$ for γ and $[0.00, 0.50]$ for δ. In order to reduce the infinite number of points in these ranges, we assumed that γ and δ can take values within the following sets (using a step size equal to 0.05): $\gamma \in \{0.50, 0.55, ..., 0.95, 1.00\} \subset [0.50, 1.00]$ and $\delta \in \{0.00, 0.05, ..., 0.45, 0.50\} \subset [0.00, 0.50]$, so that $\gamma + \delta = 1$. The conducted experiments per case (a number of 30 independent experiments) demonstrate that PSO optimization performs efficiently for the number of problem parameters to be determined (using a number of swarm particles equal to 80 and a maximum number of PSO iterations for convergence equal to 1200).

The allocated source and channel coding rates for each cluster as well as the channel coding rates for the relay nodes for the different values of (γ, δ) were reported in Table 42. Regarding the resulting channel coding rates for the relay nodes, the weakest channel coding rate was selected in all cases for all relays, i.e. 2/3. Furthermore, we observed that in all cases, using the highest source coding rate is preferred for the high motion source nodes. On the other hand, for the nodes of medium and low amount of motion, stronger channel coding rate is employed.

Table 42: Source and channel coding rates per cluster and relay for the various values of γ.

	EWAD				**MWAD**			
Cluster	1	2	3	4	1	2	3	4
Motion level	high	low	medium	medium	high	low	medium	medium
$\gamma = 0.50$	(64kbps,2/3)	(48kbps,1/2)	(48kbps,1/2)	(48kbps,1/2)	(64kbps,2/3)	(32kbps,1/3)	(32kbps,1/3)	(48kbps,1/2)
$\gamma \in [0.55, 1.00]$	(64kbps,2/3)	(48kbps,1/2)	(48kbps,1/2)	(48kbps,1/2)	(64kbps,2/3)	(32kbps,1/3)	(48kbps,1/2)	(48kbps,1/2)
Relay	1	2	3	4	1	2	3	4
$\gamma \in [0.50, 1.00]$	2/3	2/3	2/3	2/3	2/3	2/3	2/3	2/3

For the video quality assessment we used the PSNR that is directly related to the expected video distortion $E\{D_{\text{s+c}}\}$, as given by Eq. (27). Figure 22 illustrates the resulting video quality in terms of PSNR in respect with the total transmitted power in the considered wireless VSN for the different values (γ, δ). As anticipated, EWAD favors the low motion nodes in terms of PSNR, while MWAD offers considerably higher PSNR to the high motion nodes for all values of γ. Using MWAD, we achieved to deliver videos with qualities proportional to their amount of motion.

To better demonstrate the impact of power control on the delivered video quality, we compared the PSNR for $\gamma < 1.00$ with the PSNR for $\gamma = 1.00$ (when no power control is applied). It is remarkable that using EWAD results in almost the same PSNR for the different (γ, δ) values. Particularly, the highest PSNR difference is 0.4179 dB and is observed for the high motion nodes (cluster 1) for $\gamma = 0.50$. Comparing the PSNR for $\gamma = 0.50$ for the nodes of cluster 2 with the PSNR for $\gamma = 1.00$, we observed that in order to achieve the highest video quality improvement that is equal to 0.3266 dB, we need to consume 20.24% more transmission power in total. Although MWAD achieves lower PSNR values on average, it allocates lower total transmission power compared to EWAD for the same (γ, δ) values, as depicted in Fig. 22(a). It is also important to point out that we achieved almost the same PSNR for $\gamma = 0.95$ and $\gamma = 1.00$ (the average PSNR difference for all clusters is 0.0188 dB) and at the same time we used 20.01% less total transmission power (see Fig. 22(b)). Considering these observations, we concluded that when power control is omitted ($\gamma = 1.00, \delta = 0.00$), excessive transmission power in total is consumed for a rather small video quality gain.

In Fig. 23, we depict the transmission power per cluster node for the different γ values, while in Fig. 24 we illustrate the allocated transmission powers per relay node. In Fig. 23 the effect of power control is clear, since the transmission power increases along with the increase of γ value (which means that the weighting factor for power in our problem formulation δ decreases). Moreover, in the case of ($\gamma = 1.00, \delta = 0.00$), when no power control is applied, all source nodes transmit using the maximum admissible power for both EWAD and MWAD.

Besides these, Fig. 23 and Fig. 24 reveal that the allocated transmission powers for each cluster and for each relay are in line with the motion levels of the recorded scenes. However, EWAD assigns

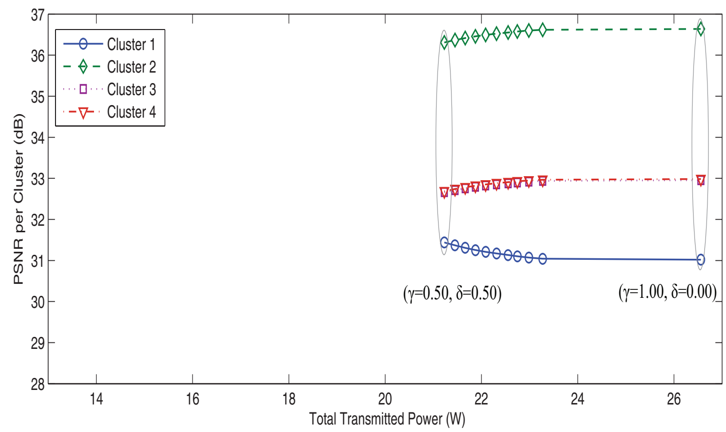

(a) Results for EWAD.

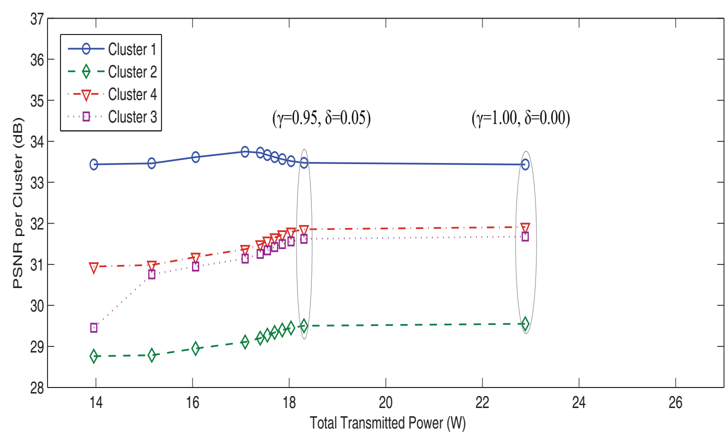

(b) Results for MWAD.

Figure 22: Resulting PSNR per cluster vs the total transmission power for all (γ, δ) values.

higher transmission power than MWAD, especially for the clusters of low and medium motion. For example, using EWAD the transmission power for the low motion nodes for $\gamma < 1.00$ ranges from 0.1560 W to 0.2141 W, whilst using MWAD the range is 0.1000-0.1039 W. This is explained from the fact that using MWAD we intend to favor the clusters in proportion to the amount of motion. So, in order to enhance the video quality of the high motion nodes, MWAD increases their transmission power and at the same time reduces the transmission power of all other clusters and relays. This increases the energy-per-bit to MAI and noise ratio for the high motion nodes and the corresponding relay, while at the same time it reduces for the other clusters and their relays. Hence, the reduction of the transmission power of the low and medium nodes is the main reason of their quality degradation.

Another observation from Fig. 24 is that in the case of EWAD the transmission power increases slightly as the γ value increases. Moreover, EWAD assigns higher transmission power than MWAD to all the relay nodes for the different γ as well. For example, for relay 3 EWAD assigns on average 1.5 W higher transmission power than MWAD. Considering this, it is inferred that using MWAD the battery-constrained nodes prolong their lifetime compared to the case that EWAD is utilized.

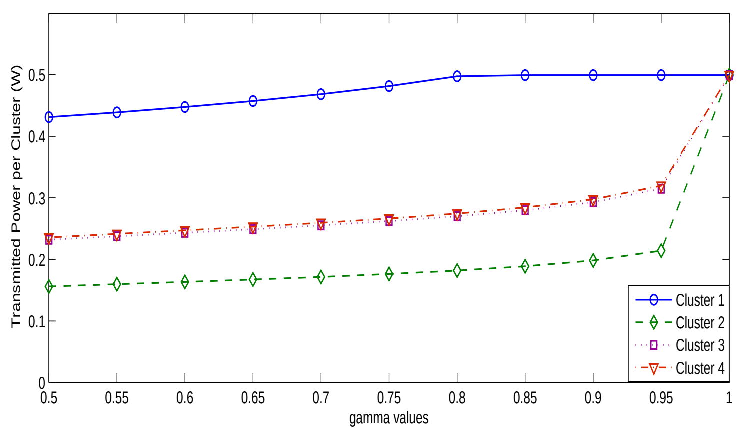

(a) Results for EWAD.

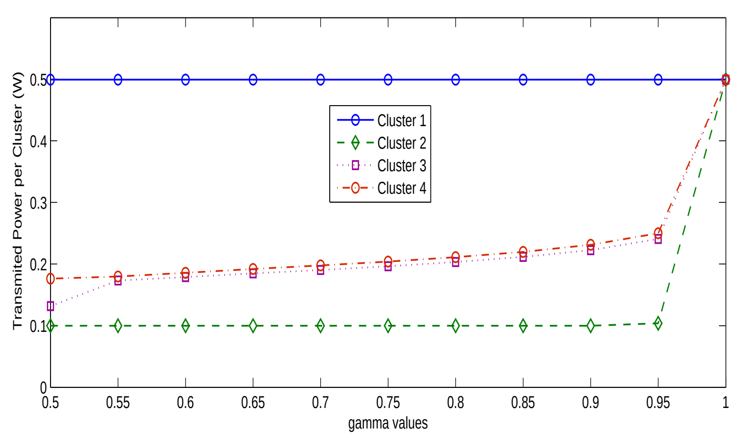

(b) Results for MWAD.

Figure 23: Transmission power per cluster node for the different γ values.

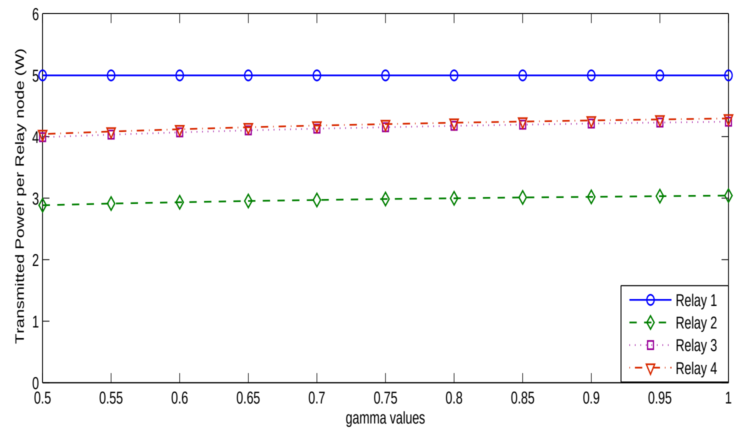

(a) Results for EWAD.

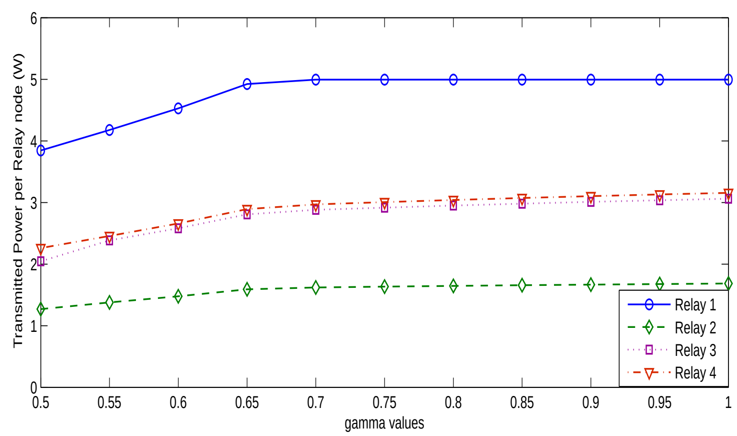

(b) Results for MWAD.

Figure 24: Transmission power per relay node for the different γ values.

5.9 A No-Reference Bitstream-Based Perceptual Model for Video Quality Estimation of Videos Affected by Coding Artifacts and Packet Losses

In this work, we used a publicly available database, which was formed with the goal of supporting reproducible research in the field of quality assessment algorithms [33]. Particularly, the test material used in our experiments included the "Foreman", "Mother" and "Paris" video sequences at CIF resolution (352x288 pixels) and "Ice", "Harbour" and "Parkjoy" video sequences at 4CIF resolution (704x576 pixels). All CIF sequences as well as "Harbour" consisted of 298 frames, while "Ice" and "Parkjoy" comprised of 238 and 250 frames, respectively. The GoP structure was IBBP with a GoP size of 16 frames. All sources were encoded using the JM 14.2 version of H.264/AVC reference software using the High profile, where a full row of MBs was coded as a separate slice and each of the sequences was corrupted with a Packet Loss Rate (PLR) of $0.1\%, 0.4\%, 1\%, 3\%$ and 5%. The video sequences used for the model training were the "Foreman", "Mother", "Paris", "Harbour" and "Parkjoy", for all the PLRs considered in this work, and the "Ice" video sequences for the five different PLRs were used for testing the performance of our model.

In Table 43 we present performance statistics for the MOS, SSIM and VQM quality metrics, as well as we assess the prediction error of our models using the NRMSE and MAE. Additionally, the row "Number of Used Features" presents the number of features used by LASSO (out of the 46 total features as described in Table 2) for making predictions, while the row "λ" depicts the λ values per case, used in Eq. (58).

Table 43: Performance results for "Ice" video sequences for all PLRs.

Performance Statistics	**MOS**	**SSIM**	**VQM**
PCC	0.9173	0.9982	0.8800
SROCC	1.0000	1.0000	1.0000
OR	0.0000	0.2000	0.0000
NRMSE	0.1476	3.1699	0.2720
MAE	0.4287	0.0951	0.8066
Number of Used Features	13	15	12
λ	9.9335×10^{-5}	4.3801×10^{-6}	1.2340×10^{-4}

Furthermore, the regression coefficient values assigned to each feature for the prediction of each quality metric are depicted in Table 44. From the obtained results we inferred that using the LASSO regression method, only a few features are eventually used for the prediction of subjective ratings as well as of the SSIM and VQM. The high performance statistics verified the suitability of the features indicated by LASSO in capturing the various types of video impairments and the effectiveness of LASSO in making accurate predictions, based on sparse models.

Table 44: Regression Coefficients.

Features	MOS	SSIM	VQM
0) Intercept	2.6052	0.0832	-0.1886
1) Intra[%]	**0.0000**	**0.0000**	**0.0000**
2) I4 $\times$ 4inIslice[%]	**0.0000**	2.1534×10^{-4}	0.2482
3) I16 $\times$ 16inIslice[%]	-0.0831	-0.0044	**0.0000**
4) IinPslice[%]	**0.0000**	**0.0000**	**0.0000**
5) P[%]	**0.0000**	**0.0000**	**0.0000**
6) PSkip[%]	**0.0000**	**0.0000**	**0.0000**
7) P16 $\times$ 16[%]	**0.0000**	**0.0000**	**0.0000**
8) P8 $\times$ 16[%]	**0.0000**	0.0047	**0.0000**
9) P8 $\times$ 8[%]	**0.0000**	**0.0000**	**0.0000**
10) P8 $\times$ 8Sub[%]	**0.0000**	**0.0000**	**0.0000**
11) P4 $\times$ 8[%]	**0.0000**	**0.0000**	**0.0000**
12) P4 $\times$ 4[%]	**0.0000**	**0.0000**	1.9112
13) B[%]	**0.0000**	0.0124	**0.0000**
14) BSkip[%]	**0.0000**	**0.0000**	**0.0000**
15) B16 $\times$ 16[%]	**0.0000**	**0.0000**	**0.0000**
16) B8 $\times$ 16[%]	**0.0000**	**0.0000**	**0.0000**
17) B8 $\times$ 8[%]	**0.0000**	**0.0000**	**0.0000**
18) B8 $\times$ 8Sub[%]	**0.0000**	**0.0000**	**0.0000**
19) B4 $\times$ 8[%]	**0.0000**	**0.0000**	**0.0000**
20) B4 $\times$ 4[%]	**0.0000**	**0.0000**	**0.0000**
21) $\Delta\mathrm{MV_x}$	**0.0000**	**0.0000**	**0.0000**
22) $\Delta\mathrm{MV_y}$	**0.0000**	**0.0000**	2.7188
23) $\mathrm{avg(MV_x)}$	**0.0000**	**0.0000**	**0.0000**
24) $\mathrm{avg(MV_y)}$	**0.0000**	**0.0000**	**0.0000**
25) $\mathrm{MV_0}$[%]	**0.0000**	**0.0000**	**0.0000**
26) $\Delta\mathrm{MV_0}$[%]	2.4405	**0.0000**	2.1070
27) Motion Intensity 1	**0.0000**	**0.0000**	**0.0000**
28) Motion Intensity 2	**0.0000**	-1.3768×10^{-6}	**0.0000**
29) $\mathrm{\|avg(MV_x)\|}$	**0.0000**	**0.0000**	**0.0000**
30) $\mathrm{\|avg(MV_y)\|}$	**0.0000**	**0.0000**	**0.0000**
31) Motion Intensity 3	**0.0000**	**0.0000**	**0.0000**
32) Motion Intensity 4	**0.0000**	**0.0000**	**0.0000**
33) NotStill	-1.1180	-0.2925	**0.0000**
34) HighMot	**0.0000**	**0.0000**	**0.0000**
35) MaxResEngy	3.0031×10^{-9}	**0.0000**	**0.0000**
36) MeanResEngy	-7.3627×10^{-9}	-7.6440×10^{-11}	-2.8375×10^{-8}
37) LR	-400.7000	-0.1382	951.9403
38) LostSinFrm	-8.1379	**0.0000**	1.3923
39) Height	16.4351	-0.0525	**0.0000**
40) TMDR	-14.3535	-0.5829	-19.2934
41) SpatialExtend	13.9946	-0.2504	-3.8692
42) SpatialExtend2	115.6684	1.6991	109.4864
43) SpatialExtendFrm	**0.0000**	**0.0000**	**0.0000**
44) Error1Frm	325.8795	1.8654	-985.2688
45) DistToRef	**0.0000**	0.0604	**0.0000**
46) FarConceal	452.2033	5.2607	-792.4988

6 Conclusions

In this research, we studied the problem of optimal resource allocation among the nodes of a wireless DS-CDMA VSN. More specifically, we optimally allocated the source coding rates, channel coding rates, and power levels to all nodes, based on the detected amount of motion per node. For the source and channel coding rates, discrete values were considered, while for the power levels, we assumed continuous values within a predetermined range.

The MAD criterion that minimizes the average network distortion and the MMD criterion that minimizes the maximum distortion among all nodes of the network, both aiming at achieving the highest possible video quality, were employed. In order to solve the underlying mixed integer optimization problems, the established PSO algorithm was employed, motivated by preliminary results in previous works. The performance of this algorithm was assessed in comparison with the performance of the AS method, justifying its capability in tackling such problems. Additionally, we developed a hybrid optimization method that is based on PSO, using the AS as a local optimizer. The experimental results using all optimization methods highlighted the superiority of HPSOAS over both AS and PSO, under various aspects.

Having clustered the nodes into two motion classes based on the amount of the detected motion per node, extensive experimentation showed that the MAD criterion works favorably for the nodes that image low motion, since they are offered considerably higher PSNR values. On the other hand, the MMD assigns equal PSNR values to both motion classes. Nevertheless, it is not sufficiently clear how fair the MMD can be for the nodes that record low motion, taking into consideration the significant PSNR reduction observed in this case, for this class of nodes. Furthermore, our results confirmed that the CCU receives less power with the MAD than with the MMD, implying that MAD requires less power for data transmission.

Experiments conducted under the presence of thermal and background noise, verified the conclusions derived for the noiseless case. The main impact of noise was a marginal reduction of the PSNR of both motion classes and optimization criteria, with only a minor exception. Also, the nodes that detected high levels of motion required considerably higher power levels than the nodes that detected low levels of motion, to accomplish data transmission.

Additionally, the problem of optimal resource allocation in a wireless visual sensor networks was tackled using the NBS. Our setup assumed that the nodes negotiate with the help of a CCU, and the result of the negotiation is the NBS, which aims at a fair distribution of system resources among the nodes. The NBS utilizes a disagreement point, which corresponds to the minimum acceptable video quality for each node.

Particularly, we proposed two optimization criteria based on the NBS, which differ in the way that the bargaining powers are determined for the nodes. The first approach treated each node as advantaged equally, while the second one assumed the same advantage for each class of nodes. The PSO algorithm was proved the best choice among other conventional optimization methods for solving the mixed-integer problems.

The performance of our proposed criteria was compared with the performance of the MAD and

MMD. The MAD criterion minimizes the average video distortion of the nodes without regard to fairness. The MMD criterion typically results in the same video distortion for all nodes, at the cost of a very high power consumption compared with the other schemes. This is a significant drawback of the MMD that could prohibit its use in practical applications. On the contrary, we confirmed that the NNBS and CNBS keep low computational complexity and can be used to any wireless VSN with a centralized topology that uses DS–CDMA. Additionally, a wise selection between NNBS and CNBS according to the needs of each application and the node distribution, produces worthwhile results that are preferable to those of MAD and MMD.

Furthermore, the Kalai-Smorodinsky bargaining solution was invoked to deal with the aforementioned problem. This solution, based on its fairness axioms, provides a fair and efficient rule that assigns the transmission parameters to each node. In our problem, this solution was derived geometrically, based on the graphical representation of each considered feasible set, implying low running complexity. The performance of the KSBS was assessed in comparison with three competing criteria: the Nash bargaining solution and two other methods that attempt to maximize an unweighted and a weighted version of the total system utility, respectively.

For the quality evaluation of the methods, we used a metric that captures both fairness and performance issues. This metric expresses the total utility gain achieved by all nodes using the MTU, that is attributed to every unit of utility lost by an isolated node, using also the MTU. Additionally, we studied the total utility achieved cumulatively from all nodes in combination with the total power consumption, for each scheme. No scheme gathers all desired features of being equally fair to all nodes, assuring the highest total utility, and requiring the lowest levels of power, at the same time. Nevertheless, comparisons led us to the conclusion that the KSBS is the criterion that is closer to our demands. The main strength of this method is that it assures quite low levels of power consumption, while assigning close enough PSNR values to all nodes and having low running complexity at the same time.

Another aspect of our research focused on the behavior modeling and analysis of the employed resource allocation schemes. We explored the performance and fairness of each examined scheme, by studying four different metrics that examine fairness under a different point of view: i) the PF metric which quantifies the relationship between fairness and performance, ii) the Jain's index which measures how "equal" is an allocation for all users, using the same scheme, iii) the utility gained cumulatively by all nodes of the same scheme and iv) the total consumed power by all nodes, also under the same scheme. All the solutions provided by the examined schemes were Pareto-optimal and thus, the choice about the most fair and efficient scheme was not evident. There was no scheme that holds all desired characteristics of achieving the highest total utility, while being equally fair to all nodes (equal utility allocations for the nodes), and spending the lowest total power, at the same time. Therefore, our investigation aligns with the general feeling that the most appropriate approach for tackling resource allocation problems in wireless VSNs, is rather problem-dependent. The application's special characteristics and requirements as well as the users' desires shall dictate the methodology to use, inhibiting the possibility of a panacea that would simultaneously favor all nodes.

In the same context, we considered the problem of the quality–driven joint node scheduling and resource allocation in a hybrid DS–CDMA over a TDMA system. In the proposed system, we used the NBS and MAD optimization criteria in order to decide on which nodes should transmit per time slot as well as what power level, source and channel coding rates should be used in order to enhance the delivered video quality. For the formulated mixed–integer optimization problem, the PSO was employed. The evaluation of the proposed approach showed that our approach offered the benefit of enhanced end-to–end video quality at the receiver compared to a similar DS–CDMA system that allows simultaneous transmissions of all nodes.

Also, we dealt with the problem of cross-layer resource allocation among the nodes of a wireless DS-CDMA VSN, considering the optimal GoP structure for the encoding of each video sequence captured by the nodes, at the same time. For the determination of the nodes' transmission parameters the MAD, NBS and MTU optimization criteria were used. Allowing the nodes to select among various GoP lengths for the encoding of the video they capture, considering the motion level included in those scenes, video quality enhancement was observed compared to fixed GoP length considerations. Furthermore, the RL approach adopted in order to tackle the discrete optimization problem (discrete transmission powers and discrete source-channel coding rates) was proven extremely efficient compared to the brute-force ES algorithm. Although both ES and SARSA algorithms are able to reach to the optimal solution, SARSA requires far less steps, making the proposed methodology applicable in online form.

A cross–layer resource allocation scheme for multihop DS-CDMA wirelss VSN was also proposed in our study. Two priority–based criteria that allocate the resources with respect to the motion level of the recorded video scenes were proposed and compared. w.NBS maximizes the distortion–related Nash product by using motion–based bargaining powers, while MWAD minimizes the weighted aggregation of the expected end–to–end video distortions by using motion–based weights. The e.NBS criterion is the NBS with equal bargaining powers. The conducted experiments illustrated that both priority–based criteria achieved their goal even in the case that the background noise was considered, resulting in higher video quality (in terms of PSNR) for the source nodes that view scenes of high motion compared to e.NBS. However, MWAD achieved higher average PSNR, whereas w.NBS demanded lower transmission power.

A method for effective joint end–to–end video quality enhancement and transmission power control in a multihop DS–CDMA based wirelss VSN was also considered. In this bi–objective problem formulation, we used weighting factors that regulate the tradeoff between these two objectives. Furthermore, we defined different weights for the aggregation function of the video distortion of the source nodes (EWAD and MWAD), that achieve to favor specific nodes according to the assigned weights. The conducted simulations demonstrated the tradeoff among the delivered video quality and the utilized transmission power. An important conclusion drawn was that excessive transmission power in total is consumed for a rather small video quality gain for certain nodes. Finally, by utilizing MWAD the low and medium motion nodes may experience longer lifetime, while on the other hand the high motion nodes deliver higher video quality.

At last, we proposed a novel NR objective video quality metric, which takes into account the compression artifacts as well as the impairments due to packet losses, during wireless video transmissions. Particularly, we extracted a large set of bitstream-based features that relate to perceptual video quality, and we exploited the LASSO regression method, for both feature selection and video quality estimation. The experimental results proved the efficiency of LASSO in producing estimated video quality values that correlate extremely well with MOS and two FR objective metrics. Also, it was shown that LASSO achieves high performance statistics, promising a sparse model representation, by keeping only the features that incur the strongest effects on perceptual video quality.

References

[1] K. Pandremmenou, L. P. Kondi, and K. E. Parsopoulos, "A study on visual sensor network cross-layer resource allocation using quality-based criteria and metaheuristic optimization algorithms," *Applied Soft Computing*, vol. 26, no. 0, pp. 149–165, 2015.

[2] K. Pandremmenou, L. P. Kondi, K. E. Parsopoulos, and E. S. Bentley, "Game-theoretic solutions through intelligent optimization for efficient resource management in wireless visual sensor networks," *Signal Processing: Image Communication*, vol. 29, no. 4, pp. 472–493, 2014.

[3] K. Pandremmenou, L. P. Kondi, and K. E. Parsopoulos, "Geometric bargaining approach for optimizing resource allocation in wireless visual sensor networks," *IEEE Transactions on Circuits and Systems for Video Technology*, vol. 23, pp. 1388–1401, Aug. 2013.

[4] K. Pandremmenou, L. P. Kondi, and K. E. Parsopoulos, "Fairness issues in resource allocation schemes for wireless visual sensor networks," in *Proceedings of the SPIE Electronic Imaging Symposium (Visual Information Processing and Communication III)*, (San Francisco, CA), Feb. 2013.

[5] A. V. Katsenou, L. P. Kondi, and E. Papapetrou, "Distortion-aware joint scheduling and resource allocation for wireless video transmission," in *Proceedings of the 21st European Signal Processing Conference (EUSIPCO), 2013*, pp. 1–5, Sept. 2013.

[6] K. Pandremmenou, N. Tziortziotis, L. P. Kondi, and K. Blekas, "Resource allocation in visual sensor networks using a reinforcement learning framework," in *18th International Conference on Digital Signal Processing (DSP), 2013*, pp. 1–6, Jul. 2013.

[7] E. G. Datsika, A. V. Katsenou, L. P. Kondi, E. Papapetrou, and K. E. Parsopoulos, "Priority-based cross-layer optimization for multihop DS-CDMA visual sensor networks," in *19th IEEE International Conference on Image Processing (ICIP), 2012*, pp. 1101–1104, Sept. 2012.

[8] A. V. Katsenou, E. G. Datsika, L. P. Kondi, E. Papapetrou, and K. E. Parsopoulos, "Power-aware QoS enhancement in multihop DS-CDMA visual sensor networks," in *18th International Conference on Digital Signal Processing (DSP), 2013*, pp. 1–6, Jul. 2013.

[9] K. Pandremmenou, M. Shahid, L. P. Kondi, and B. Lövström, "A no-reference bitstream-based perceptual model for video quality estimation of videos affected by coding artifacts and packet losses," in *Proceedings of the SPIE Electronic Imaging Symposium (Human Vision and Electronic Imaging XX)*, (San Francisco, CA), Feb. 2015. (to appear).

[10] J. Suris, L. Dasilva, Z. Han, A. Mackenzie, and R. Komali, "Asymptotic optimality for distributed spectrum sharing using bargaining solutions," *IEEE Transactions on Wireless Communications*, vol. 8, pp. 5225–5237, Oct. 2009.

[11] J. Wang, T. Korhonen, and Y. Zhao, "Weighted network utility maximization aided by combined queueing priority in OFDMA systems," in *IEEE International Conference on Communications, ICC '08*, pp. 3323–3327, May 2008.

[12] G. Tan, *Improving aggregate user utilities and providing fairness in multi–rate wireless LANs.* PhD thesis, Massachusetts Institute of Technology (MIT), Cambridge, MA, USA, 2006.

[13] R. K. Jain, D.-M. W. Chiu, and W. R. Hawe, "A quantitative measure of fairness and discrimination for resource allocation in shared computer systems," Tech. Rep. TR-301, Digital Equipment Corporation, Sept. 1984.

[14] J. Hagenauer, "Rate–compatible punctured convolutional codes (RCPC codes) and their applications," *IEEE Transactions on Communications*, vol. 36, pp. 389–400, Apr. 1988.

[15] R. C. Eberhart and J. Kennedy, "A new optimizer using particle swarm theory," in *Proceedings of the Sixth Symposium on Micro Machine and Human Science*, (Piscataway, NJ), pp. 39–43, IEEE Service Center, 1995.

[16] P. E. Gill, W. Murray, and M. H. Wright, *Practical optimization.* Academic Press, 1981.

[17] D. G. Luenberger and Y. Ye, *Linear and Nonlinear Programming.* New York: Springer, 2008.

[18] K. G. Murty, *Linear Complementarity, Linear and Nonlinear Programming.* Berlin: Heldermann Verlag: Sigma Series in Applied Mathematics 3, 1988.

[19] F. Neri, C. Cotta, and P. Moscato, *Handbook of Memetic Algorithms.* Berlin Heidelberg: Springer-Verlag, 2012.

[20] R. H. Byrd, J. C. Gilbert, and J. Nocedal, "A trust region method based on interior point techniques for nonlinear programming," *Mathematical Programming*, vol. 89, no. 1, pp. 149–185, 2000.

[21] R. H. Byrd, M. E. Hribar, and J. Nocedal, "An interior point algorithm for large scale nonlinear programming," *SIAM Journal on Optimization*, vol. 9, pp. 877–900, 1997.

[22] T. F. Coleman and Y. Li, "An interior trust region approach for nonlinear minimization subject to bounds," tech. rep., Cornell University, Ithaca, NY, USA, 1993.

[23] T. F. Coleman and Y. Li, "On the convergence of reflective Newton methods for large-scale nonlinear minimization subject to bounds," vol. 7 of *Mathematical Programming*, pp. 189–224, 1994.

[24] E. S. Bentley, L. P. Kondi, J. D. Matyjas, M. J. Medley, and B. W. Suter, "Spread spectrum visual sensor network resource management using an end-to-end cross-layer design," *IEEE Transactions on Multimedia*, vol. 13, no. 1, pp. 125–131, 2011.

[25] L. P. Kondi and E. S. Bentley, "Game-theory-based cross-layer optimization for wireless DS-CDMA visual sensor networks," in *Proceedings of the 17th IEEE International Conference on Image Processing (ICIP)*, pp. 4485–4488, Sept. 2010.

[26] J. Yuan and W. Yu, "Joint source coding, routing and power allocation in wireless sensor networks," *IEEE Transactions on Communications*, vol. 56, no. 6, pp. 886–896, 2008.

[27] W. Wang, D. Peng, H. Wang, H. Sharif, and H.-H. Chen, "Energy-constrained distortion reduction optimization for wavelet–based coded image transmission in wireless sensor networks," *IEEE Transactions on Multimedia*, vol. 10, pp. 1169–1180, Oct. 2008.

[28] Y. S. Chan and J. Modestino, "A joint source coding-power control approach for video transmission over CDMA networks," *IEEE Journal on Selected Areas in Communications*, vol. 21, pp. 1516–1525, Dec. 2003.

[29] B. Zatt, M. Porto, J. Scharcanski, and S. Bampi, "GoP structure adaptive to the video content for efficient H.264/AVC encoding," in *17th IEEE International Conference on Image Processing (ICIP)*, pp. 3053–3056, Sept. 2010.

[30] J. Lee, I. Shin, and H. Park, "Adaptive intra-frame assignment and bit-rate estimation for variable GoP length in H.264," *IEEE Transactions on Circuits and Systems for Video Technology*, vol. 16, pp. 1271–1279, Oct. 2006.

[31] R. Sutton and A. Barto, *Reinforcement Learning: An Introduction.* MIT Press Cambridge, USA, 1998.

[32] M. L. Puterman, *Markov Decision Processes: Discrete Stochastic Dynamic Programming.* John Wiley & Sons, Inc., 1994.

[33] F. De Simone, M. Naccari, M. Tagliasacchi, F. Dufaux, S. Tubaro, and T. Ebrahimi, "Subjective quality assessment of H.264/AVC video streaming with packet losses," *Eurasip Journal on Image and Video Processing*, vol. 2011 Article ID 190431, 2011.

[34] Z. Wang, A. C. Bovik, H. R. Sheikh, and E. P. Simoncelli, "Image quality assessment: from error visibility to structural similarity," *IEEE Transactions on Image Processing*, vol. 13, pp. 600–612, Apr. 2004.

[35] `http://www.its.bldrdoc.gov/resources/video-quality-research/software.aspx.` last checked: 2014-05-05.

[36] H. Wang, L. P. Kondi, A. Luthra, and S. Ci, *4G Wireless Video Communications.* Wiley Publishing, 2009.

[37] T. Wiegand, G. Sullivan, G. Bjontegaard, and A. Luthra, "Overview of the H.264/AVC video coding standard," *IEEE Transactions on Circuits and Systems for Video Technology*, vol. 13, pp. 560–576, July 2003.

[38] T. S. Rappaport, *Wireless Communications: Principles and Practice.* Upper Saddle River, NJ, USA: Prentice Hall PTR, 2nd ed., 2001.

[39] L. P. Kondi, F. Ishtiaq, and A. K. Katsaggelos, "Joint source–channel coding for motion–compensated DCT–based SNR scalable video," *IEEE Transactions on Image Processing*, vol. 11, pp. 1043–1052, 2002.

[40] K. S. Gilhousen, I. M. Jacobs, R. Padovani, A. J. Viterbi, L. A. Weaver, and C. E. Wheatley, "On the capacity of a cellular CDMA system," *IEEE Transactions on Vehicular Technology*, vol. 40, pp. 303–312, May 1991.

[41] K. Pandremmenou, L. P. Kondi, and K. E. Parsopoulos, "Optimal power allocation and joint source–channel coding for wireless DS–CDMA visual sensor networks," in *Visual Information Processing and Communication II*, vol. 7882, SPIE, Jan. 2011.

[42] L. P. Kondi and A. K. Katsaggelos, "Joint source–channel coding for scalable video using models of rate–distortion functions," in *Proceedings of the IEEE International Conference on Acoustics, Speech, and Signal Processing*, pp. 1377–1380, 2001.

[43] M. Bystrom and T. Stockhammer, "Modeling of operational distortion–rate characteristics for joint source–channel coding of video," in *Proceedings of the International Conference on Image Processing*, vol. 1, pp. 359–362, 2000.

[44] A. V. Katsenou, L. P. Kondi, and K. E. Parsopoulos, "Motion-related resource allocation in dynamic wireless visual sensor network environments," *IEEE Transactions on Image Processing*, vol. 23, pp. 56–68, Jan. 2014.

[45] G. Minati and E. Pessa, *Collective Beings*. New York: Springer, 2010.

[46] K. E. Parsopoulos and M. N. Vrahatis, *Particle Swarm Optimization and Intelligence: Advances and Applications*. Information Science Publishing (IGI Global), 2010.

[47] A. P. Engelbrecht, *Fundamentals of Computational Swarm Intelligence*. Wiley, 2006.

[48] J. Kennedy, "Small worlds and mega–minds: Effects of neighborhood topology on particle swarm performance," in *Proceedings of the IEEE Congress on Evolutionary Computation*, (Washington, D.C., USA), pp. 1931–1938, IEEE Press, 1999.

[49] P. N. Suganthan, "Particle swarm optimizer with neighborhood operator," in *Proceedings of the IEEE Congress on Evolutionary Computation*, (Washington, D.C., USA), pp. 1958–1961, 1999.

[50] M. Clerc and J. Kennedy, "The particle swarm-explosion, stability, and convergence in a multidimensional complex space," *IEEE Transactions on Evolutionary Computation*, vol. 6, pp. 58–73, Feb. 2002.

[51] R. C. Eberhart and Y. Shi, "Comparing inertia weights and constriction factors in particle swarm optimization," in *Proceedings of the IEEE Congress on Evolutionary Computation*, (Piscataway, NJ), pp. 84–88, 2000.

[52] I. C. Trelea, "The particle swarm optimization algorithm: convergence analysis and parameter selection," *Information Processing Letters*, vol. 85, no. 6, pp. 317–325, 2003.

[53] F. Van den Bergh and A. P. Engelbrecht, "A study of particle swarm optimization particle trajectories," *Information Sciences*, vol. 176, no. 8, p. 937–971, 2006.

[54] M. Jiang, Y. P. Luo, and S. Y. Yang, "Stochastic convergence analysis and parameter selection of the standard particle swarm optimization algorithm," *Information Sciences*, vol. 102, no. 1, p. 8–16, 2007.

[55] M. Schmitt and R. Wanka, "Particle swarm optimization almost surely finds local optima," in *Proceedings of the 15th Annual Conference on Genetic and Evolutionary Computation*, GECCO '13, (New York, NY, USA), pp. 1629–1636, ACM, 2013.

[56] K. Pandremmenou, L. P. Kondi, and K. E. Parsopoulos, "Optimal power allocation and joint source-channel coding for wireless DS-CDMA visual sensor networks using the Nash bargaining solution," in *IEEE International Conference on Acoustics, Speech and Signal Processing (ICASSP)*, pp. 2340–2343, May 2011.

[57] A. V. Katsenou, L. P. Kondi, and K. E. Parsopoulos, "Resource management for wireless visual sensor networks based on individual video characteristics," in *18th IEEE International Conference on Image Processing (ICIP)*, pp. 149–152, Sept. 2011.

[58] A. V. Katsenou, L. P. Kondi, K. E. Parsopoulos, and E. S. Bentley, "Quality-driven power control and resource allocation in wireless multi-rate visual sensor networks," in *19th IEEE International Conference on Image Processing (ICIP)*, pp. 1117–1120, Sept. 2012.

[59] A. V. Katsenou, L. P. Kondi, and K. E. Parsopoulos, "On the use of clustering for resource allocation in wireless visual sensor networks," in *Visual Information Processing and Communication III*, vol. 8305, pp. 83050S–83050S–13, SPIE, 2012.

[60] J. Kennedy and R. C. Eberhart, "A discrete binary version of the particle swarm algorithm," in *Proceedings of the Conference on Systems, Man and Cybernetics*, pp. 4104–4109, 1997.

[61] A. Farmahini-Farahani, S. Vakili, S. M. Fakhraie, S. Safari, and C. Lucas, "Parallel scalable hardware implementation of asynchronous discrete particle swarm optimization," *Engineering Applications of Artificial Intelligence*, vol. 23, no. 2, pp. 177–187, 2010.

[62] K. E. Parsopoulos and M. N. Vrahatis, "Recent approaches to global optimization problems through particle swarm optimization," *Natural Computing*, vol. 1, no. 2–3, pp. 235–306, 2002.

[63] K. E. Parsopoulos and M. N. Vrahatis, "Studying the performance of unified particle swarm optimization on the single machine total weighted tardiness problem," in *Lecture Notes in Artificial Intelligence (LNAI)* (A. Sattar and B. H. Kang, eds.), vol. 4304, pp. 760–769, Springer, 2006.

[64] E. C. Laskari, K. E. Parsopoulos, and M. N. Vrahatis, "Particle swarm optimization for integer programming," in *Proceedings of the IEEE Congress on Evolutionary Computation*, (Hawaii (HI), USA), pp. 1582–1587, IEEE Press, 2002.

[65] "MathWorks: Constrained non-linear optimization algorithms: R2012a documentation." http://www.mathworks.de/de/help/optim/ug/ constrained-nonlinear-optimization-algorithms.html, 2014. [accessed on 2-Jul-2014].

[66] K. Binmore, *Playing for Real: A Text on Game Theory.* Oxford University Press, 2007.

[67] K. Pandremmenou, L. P. Kondi, and K. E. Parsopoulos, "Kalai–Smorodinsky bargaining solution for optimal resource allocation over wireless DS–CDMA visual sensor networks," in *Proceedings of the SPIE Electronic Imaging Symposium (Visual Information Processing and Communication III)*, vol. 8305, SPIE, 2012.

[68] J. P. Conley and S. Wilkie, "The bargaining problem without convexity: extending the egalitarian and Kalai–Smorodinsky solutions," *Economic Letters*, vol. 36, pp. 365–369, Aug. 1991.

[69] E. Kalai and M. Smorodinsky, "Other solutions to Nash's bargaining problem," *Econometrica*, vol. 43, no. 3, pp. 513–518, 1975.

[70] G. A. Rummery and M. Niranjan, "On–line Q–learning using connectionist systems," tech. rep., 1994.

[71] P. Dayan, "The convergence of TD(λ) for general lambda," *Machine Learning*, vol. 8, pp. 341–362, 1992.

[72] R. Zhang, S. L. Regunathan, and K. Rose, "Video coding with optimal inter/intra-mode switching for packet loss resilience," *IEEE Journ. on Selected Areas in Communications*, vol. 18, no. 6, pp. 966–976, 2000.

[73] R. Tibshirani, "Regression shrinkage and selection via the Lasso," *Journal of the Royal Statistical Society, Series B*, vol. 58, pp. 267–288, 1994.

[74] R. Tibshirani, "The LASSO method for variable selection in the Cox model," *Statist. Med.*, vol. 16, no. 4, pp. 385–395, 1997.

[75] "Full reference television phase II subjective test plans," 2002. Objective Quality Model Evaluation Criteria.

[76] http://trace.eas.asu.edu/yuv/, 2013. [Online; accessed 19-Oct-2013].

[77] P. E. Gill, W. Murray, and M. H. Wright, *Practical optimization.* Academic Press, 1981.

[78] K. Schittkowski, "An active set strategy for solving optimization problems with up to 200,000,000 nonlinear constraints," *Appl. Numer. Math.*, vol. 59, pp. 2999–3007, Dec. 2009.

[79] J. D. Gibbons and S. Chakraborti, *Nonparametric Statistical Inference (Statistics: a Series of Textbooks and Monogrphs).* CRC, 4 ed., May 2003.

[80] M. Hollander and D. A. Wolfe, *Nonparametric Statistical Methods.* Wiley-Interscience, 2 ed., Jan. 1999.

[81] J. Kennedy and R. C. Eberhart, "Particle swarm optimization," in *Proc. IEEE Int. Conf. Neural Networks*, vol. IV, (Piscataway, NJ), pp. 1942–1948, IEEE Service Center, 1995.